GEOLOGY AND FRACTURE GEOMETRY IN SOURCE REGION OF HOG BACK LANDSLIDE, EASTERN SAN GABRIEL MOUNTAINS, WITH IMPLICATIONS FOR FAILURE MECHANISMS

A Thesis

Presented to the

Faculty of

California State Polytechnic University, Pomona

In Partial Fulfillment

Of the Requirements for the Degree

Master of Science

In

Geology

By

Reginald I. Agunwah

2020

SIGNATURE PAGE

THESIS:	**GEOLOGY AND FRACTURE GEOMETRY IN SOURCE REGION OF HOGBACK LANDSLIDE, EASTERN SAN GABRIEL MOUNTAINS, WITH IMPLICATIONS FOR FAILURE MECHANISMS**
AUTHOR:	Reginald I. Agunwah
DATE SUBMITTED:	Fall 2020
	Department of Geological Sciences

Dr. Jonathan A. Nourse
Thesis Committee Chair
Geological Sciences _____

Dr. Nicholas Van Buer
Geological Sciences _____

Dr. Jeffrey S. Marshall
Geological Sciences _____

ACKNOWLEDGEMENTS

I can finally say that after 20 years, my academic journey with California State University Polytechnic, Pomona is coming to a close. It is with great pleasure and honor that I am able present this thesis to the Cal Poly Pomona Department of Geological Sciences. The process of undertaking this project was figuratively and literally an uphill battle. More of a battle between my personal commitments than a battle waged in the field of geology. To physically march up and down the same terrain while earning cuts, bumps, bruises for the past decade was a humbling experience. In those words, I am incredibly proud of the finished product and pleased to be able to earn this Master's.

I would first like to thank the faculty and staff of Cal Poly Pomona's Geological Sciences department. I have learned so much from all of you. The various teaching styles of the classroom and the field contributed a wealth of knowledge that I use in my current employment today. I also appreciate the vast knowledge and passion of from the different fields of geology. The classes that I was able to attend were incredible and have strengthened my personal passion for geology.

I could not have completed this project without the guidance of Dr. Jonathan Nourse who has been my advisor for my Bachelor's Degree and now my Master's Degree. He helped me refine my Brunton work which allowed me to collect foliation, joint, fracture, dike, lineation, and fault measurements for the past 15 years of various field projects. I do not feel that I would have learned more about San Gabriel Mountain geology without working with Dr. Nourse. I am honored to add my work to the catalog of San Gabriel Mountain geological research under your study.

A vital part of the thesis process, for me, has revolved around finding places that I can review my data and write in peace. Also, having the opportunity to be around my fellow Master's and undergraduate colleagues was so refreshing because they are just as interested in the geology as I am. I could also speak with them without having to over-explain geological processes. Through this, I have developed friendships and networks that I will always treasure.

Finally, I would like to thank those that are the closest to me. To my wife Jane, thank you for being there since the beginning of this journey, starting in 2002 with my undergraduate studies. Thank you or pushing me to start and to finish this process. Most of all, thank you for never allowing me to quit. I would like to say thank you to my various geological field assistants, Breeanna Copeland Curts (GIT), Phuong Schmitt-Kallas (PG CEG), and Jessika Valenciano. Big thanks goes to Richard Mendoza for leading me through the bush on multiple field excursions and collecting the same cuts, scrapes, bumps and bruises as I did.

ABSTRACT

The Hog Back slide is a large rockslide in the southern foothills of the San Gabriel Mountains, located approximately five miles north of San Antonio Heights. This broad mound of translated slide boulders produced a natural dam across San Antonio Canyon in late Pleistocene time. The purpose my study is to investigate the fracture geometry that led to the failure of the Hog Back slide by the means of field mapping and stereonet analysis. This investigation builds on my previous senior thesis work that addressed the disturbed and/or displaced slide blocks. I completed a series of ten mapping traverses to acquire new rock observations and structural measurements, and constrain their locations with a GPS receiver. A synthesis of this research is used to develop a mechanical model for the failure of the Hog Back Slide.

Through the new rock observations and structural measurements, the displaced contact that was found within the Hogback slide remained relatively intact, even after the slide mass had translated 1,300 feet to the southeast. The distribution of clast sizes that were observed show that part of the felsic gneiss was emplaced as a megaclast. The clast sizes seen with the quartz diorite were more distributed and widespread. A mechanical analysis of the clasts and the in-place rock show that there may have been many factors that could have caused the failure, such as tectonic events, mechanical weathering, and chemical weathering.

Wherever the rock is exposed, it consistently shows the same kind of geometry in the planar structures contained therein. The foliations of the in-place rock generally strike northwest, with dips to the southwest. The foliations of the transported felsic gneiss clasts strike northwest and dip to the southwest. The foliations of the transported

quartz diorite clasts strike in all directions with no preferred dip angle. The most logical conclusion to be derived from this information is that the toe of the slide acted as a cushion for the head of the slide, allowing the felsic gneiss slide mass to retain an orientation similar to the bedrock measurements in the source area.

TABLE OF CONTENTS

LIST OF TABLES

LIST OF FIGURES

CHAPTER 1: INTRODUCTION

1.1 Purpose and Objectives:

The purpose my study is to investigate the fracture geometry that led to the failure of the Hog Back Slide by the means of field mapping, stereonet analysis, and safety factor calculations. This investigation builds on my previous senior thesis work that presented a reconnaissance investigation of the disturbed and/or displaced slide blocks. A primary aim is to understand the three-dimensional instabilities of rock slides involving two different crystalline units. Combined, this research intends to develop a mechanical model for the Hog Back Slide. A thorough understanding of Hog Back landslide will be accomplished through completion of the following objectives:

A. Mapping the geologic units of the in-place rock units above the Hog Back landslide deposit using a handheld geographic positioning system (GPS),
B. Measurement of foliations, fractures, joint sets, fault surfaces, and striations in the bedrock source area using a Brunton compass,
C. Compiling the data onto a detailed geologic map
D. Generating stereonets to resolve statistical orientations of measured structures.
E. Use of photographs to document key field relations in the study area.
F. Construction of a series of cross sections to illustrate fracture geometry.
G. Back-Calculation of Safety Factors to assess a range of operative cohesion and friction angles at failure for various scenarios
H. Development of three-dimensional models and drawings to illustrate likely failure mechanisms.

Through synthesis of all available field data, my thesis will deduce the degree of coherent translation versus chaotic jumbling of the slide mass. Such information from this data will be useful for exploring possible failure models.

1.2 Location and Access

My project study area is located in the eastern San Gabriel Mountains of Southern California, approximately 30 miles to the east of downtown Los Angeles (**Figure 1**). The area is characterized as a complex of highly fractured igneous and metamorphic rocks with a number of large landslides that can be seen in the topography by both aerial and surficial survey. The study area is focused in southern half of Section 25, the northern half of Section 36 of Township 2 North, Range 8 West within the Mount Baldy USGS 7.5 minute quadrangle, with a total area of almost 9,477,690 square feet (218 acres). The limits of the area are bounded in the southwest and west by the extent of the Sunset Peak landslide (Rodgers 1992), in the east by the San Antonio Creek, and in the north by Glendora Ridge Road and the Cow Canyon Landslide.

Due to the high degree of topographic relief throughout most of the San Gabriel Mountains, access to my field area is completely dependent upon major roads (active, seasonal, and abandoned), established dirt trails (by humans and/or wildlife), and un-improved trails.

Major roads within the study area include New Mount Baldy Road, Glendora Ridge Road, and Old Mount Baldy Road Trail. In addition to limited road access, there is a key area within the study area that is limited to foot traffic, specifically the Mount Baldy Wilderness Preserve which encompasses the Hog Back Slide and the Old Mount Baldy Road Trail. In the summer months, the dry climate of the San Gabriel Mountains is

prone to forest fire activity. In July and August of 2015 and 2016, fires forced the closure of major roads and inhibited my ability to access sites that I planned to investigate. In October of 2014, the federal government decreed the San Gabriel Mountains a national monument under the Forest Service. This may greatly inhibit admission to inaccessible locations in future studies.

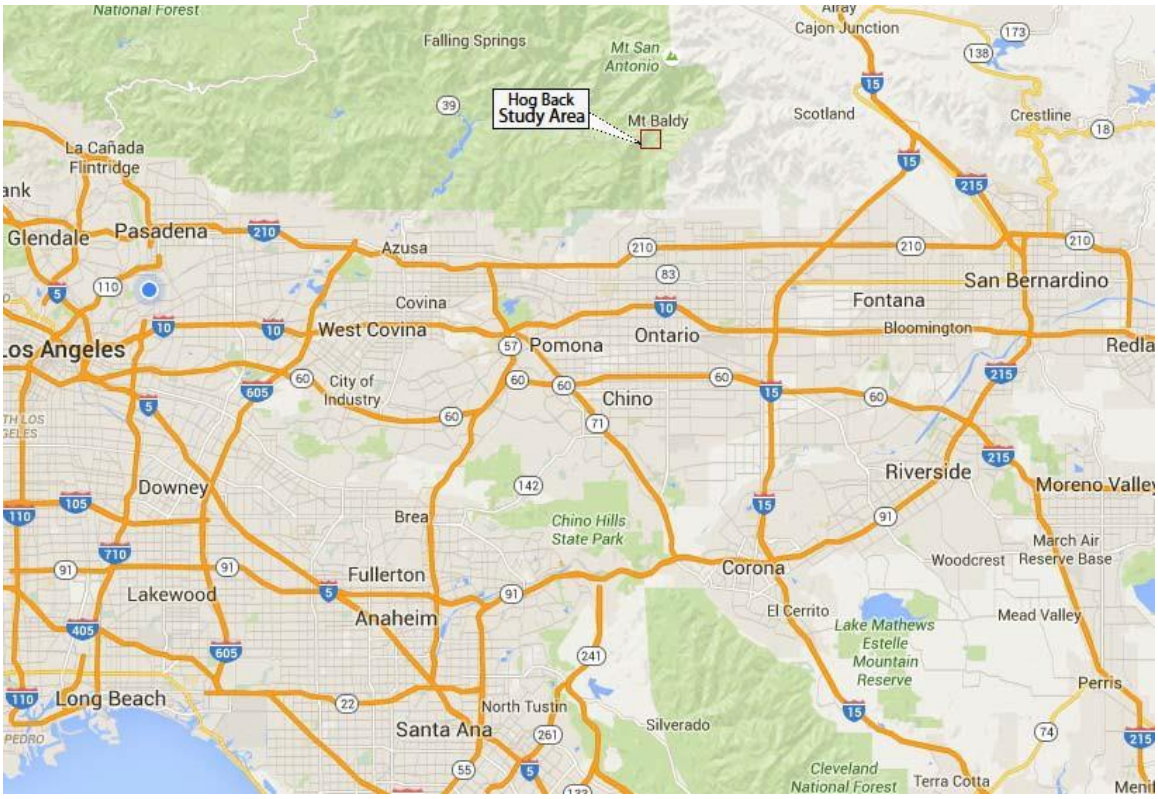

Figure 1. Vicinity Map of the Los Angeles Area showing the location of the Hog Back landslide.

1.3 Regional Geologic Setting

The study area is located in San Antonio Canyon within the Eastern San Gabriel Mountains structural block (**Figure 2**; Morton and Miller, 2003). The San Gabriel Mountains are part of the Transverse Ranges, a group of east- west trending mountains that extend from the Pacific Ocean near Point Conception in Santa Barbara County on the west to the San Bernardino Mountains on the east. The Transverse Range geomorphic province is characterized by the compressive stresses at a restraining bend in the San

Andreas Fault. These mountain ranges continue to rise through folding and faulting of rocks compressed between the North American and the Pacific tectonic plates. Through this process, the steepness of the canyons can cause instability within the rock masses which can produce landslides. Also, there is an abundance of NW, NE, and EW striking faults that pervade the study area. The intense shattering of the bedrock throughout the San Gabriel Mountains reduces the stability of mountainsides in general.

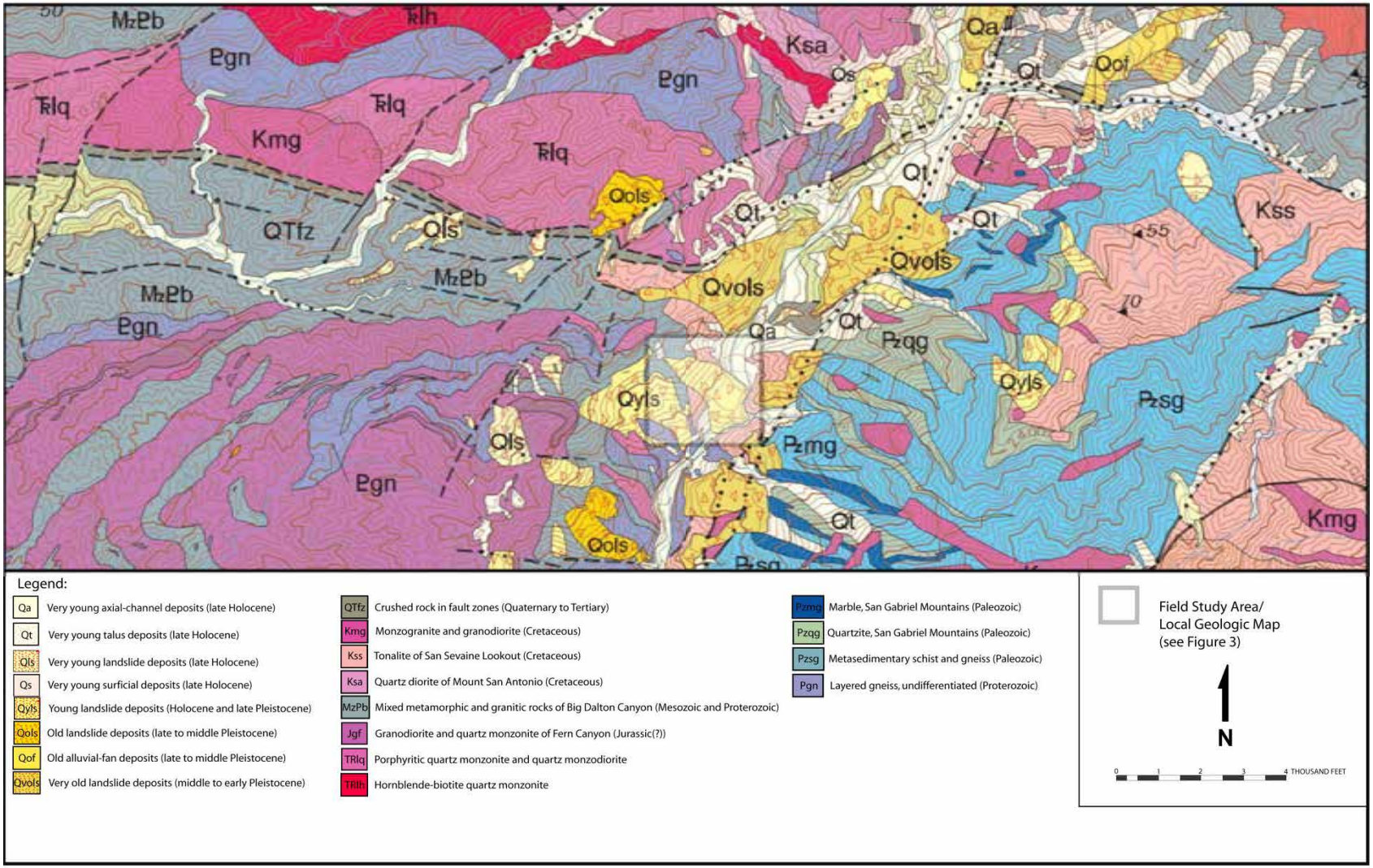

Figure 2: Regional Geological Map of the Central San Antonio Canyon Area. There are multiple slope failures present in the immediate vicinity of the Hog Back Slide. There is also an inset which depicts the thesis mapping area of Figure 3. (Morton et al, 2003)

1.4 Landslides in San Antonio Canyon

Landslides are movements of relatively large landmasses, either as nearly intact blocks or as jumbled mixes of bedrock, debris, and soil. They occur when there is a steepness of slope accompanied by the planes of weakness within a rock mass. San Antonio Canyon has a history of these multiple slide masses of enormous size which occurred between the early Pleistocene to early Holocene (Morton et al., 1987; Rogers et al., 1993; Morton and Miller, 2003; Barth 2020). Large catastrophic landslides present not only the immediate hazard of the landslide itself, but also can have effects lasting hundreds of years (drainage impoundment, lakes, dam-break floods, heightened erosion/aggradation, etc.) or longer (drainage reorganization, epigenetic gorge formation). New mapping in San Antonio Canyon reveals three times as many landslides as previously mapped and that landslides cover twice the surface area previously mapped (Barth 2020).

One important landslide in San Antonio Canyon is named the Hog Back Slide (**Figure 3**). It originated from the western wall of the canyon. Surficial Quaternary units, described by Morton and Miller, are:

- **Qa - Very young axial-channel deposits (late Holocene) -** Unconsolidated deposits of silty, sandy and cobbly alluvium deposited by streams in through-going stream valleys.
- **Qt -** Unconsolidated to slightly consolidated deposits of angular pebble-, cobble-, and boulder-size material that form scree and rubble on hill slopes and at base of slopes. In places, loose and hazardous to walk on.
- **Qyls** - **Young landslide deposits (Holocene and late Pleistocene) -** Slope-failure

deposits that consist of displaced bedrock blocks and (or) chaotically mixed rubble. Slightly dissected or modified surfaces. Deposits may or may not be active under current range of climatic conditions.

- **Qvols - Very old landslide deposits (middle to early Pleistocene) -**Slope-failure deposits that consist of displaced bedrock blocks and (or) chaotically mixed rubble. Geomorphic form of landslides poorly, or not at all, preserved. Inferred to have accumulated late in main uplift history of Transverse Ranges.

Hog Back landslide (**Figures 3 and 4**) is located on Mount Baldy Road between San Antonio Heights and Mount Baldy Village. The area of the Hog Back scar west of the Baldy Road is accessible by foot with very limited access by vehicle. There were areas of the scar that are steep covered by light vegetation. The good exposures of outcrop were in the areas inaccessible by vehicles. These areas can be accessed by foot. Most published reports focused on the rock slide's scar (Morton et al 1987, Herber 1987, Rogers et al 1992 (**Figure 4**), Nourse 1998, Barth 2020). The Hog Back scar area has been studied, but not in great detail.

My preliminary visit to the Hog Back scar in the winter of 2014 was mainly for information gathering about the areas surrounding the slide scar. This was the first time that Dr. Nourse and I had walked up along the ridge to the west of the scar. The ridge to the west of the scar is accessible only by foot. The canyons and outcrops near the slide and scar are accessible via the roadcuts made by Mt Baldy Road within the mass were as small as cobbles to as large as an automobile. Some blocks were as large as 14 feet across and larger. . There is also a rock body in the slide that is being classified as a megaclast in which its true volume cannot be determined at this time.

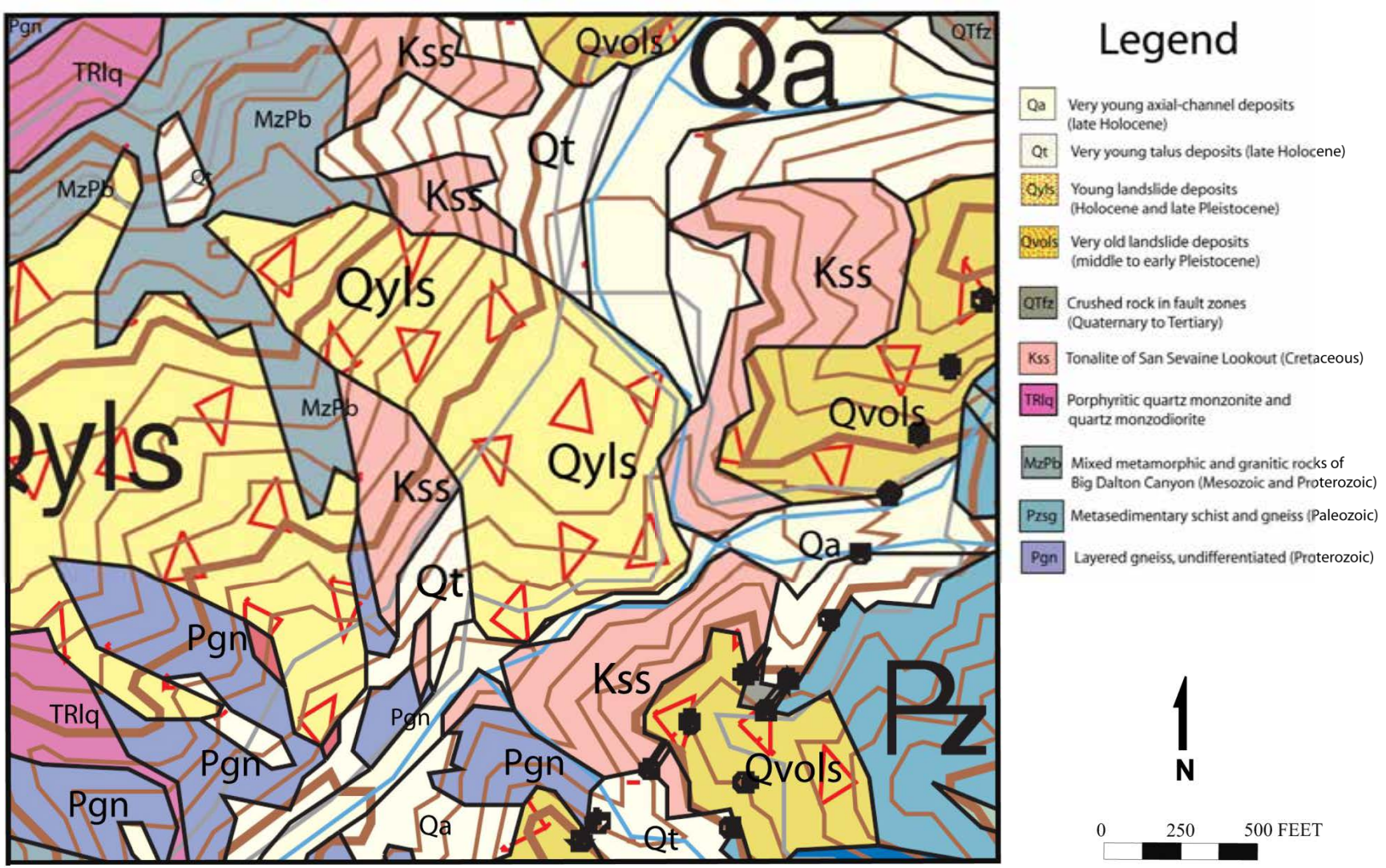

Figure 3: Map clip of the study area from Figure 2. Field area geology (Morton and Miller, 2003)

1.5 Previous Studies

As mentioned above, previous works by other authors identify the Hog Back landslide and show the geologic mapping of the surrounding rockslides and regional tectonism (Herber,1987, Morton et al., 1987, Rogers et al., 1992, Nourse et al., 1998; Morton and Miller, 2003). In 2008, Reginald Agunwah, an undergraduate student at Cal Poly Pomona, mapped a series of clast foliations within the Hog Back slide mass. It has been concluded that the slide was a mass failure that created a natural dam across San Antonio Canyon. (Herber 1987; Barth 2020)

Herber (1987), produced a field trip guidebook on the Hog Back landslide. This guide described the Hog Back as a well-preserved translator rock block slide in crystalline rock with good exposures of a thick shear zone across its toe and intact rock at its head. It also uses a cross section to show and describe different zones within the slide. This cross section increased in detail and was later used for the work produced by Rogers et al. (1992).

Morton et al., (1987), produced a report on the large rock avalanche deposits in the central and eastern San Gabriel Mountains. This report discussed the Mt. San Antonio Landslide, Cow Canyon Landslide, and the Hog Back Landslide. The map produced for this area also showed the smaller landslides. The team also mapped out the Crystal Lake Slide, Cloudburst Canyon Slide, and the Alpine Canyon Slide in the central San Gabriels.

Rogers et al. (1992) produced a report on the Paleolandslides in San Antonio Canyon. Their work focused on the Sunset Peak Slide and the Hog Back Slide in which they mapped the western wall of the canyon that produced these slides (**Figure 4**). They

then constructed cross sections of both slides and developed a series of diagrams to show in detail how the two areas failed and produced two large slides. A key observation described by Rogers et al. (1992) is that clasts within Hog Back Slide were derived from the contact zone between two major clast types ("hornblende-plagioclase gneiss" and "banded gneiss" metamorphic and granitic rocks) exposed on the west wall of San Antonio Canyon (Figure 4). My current study reinforces this observation.

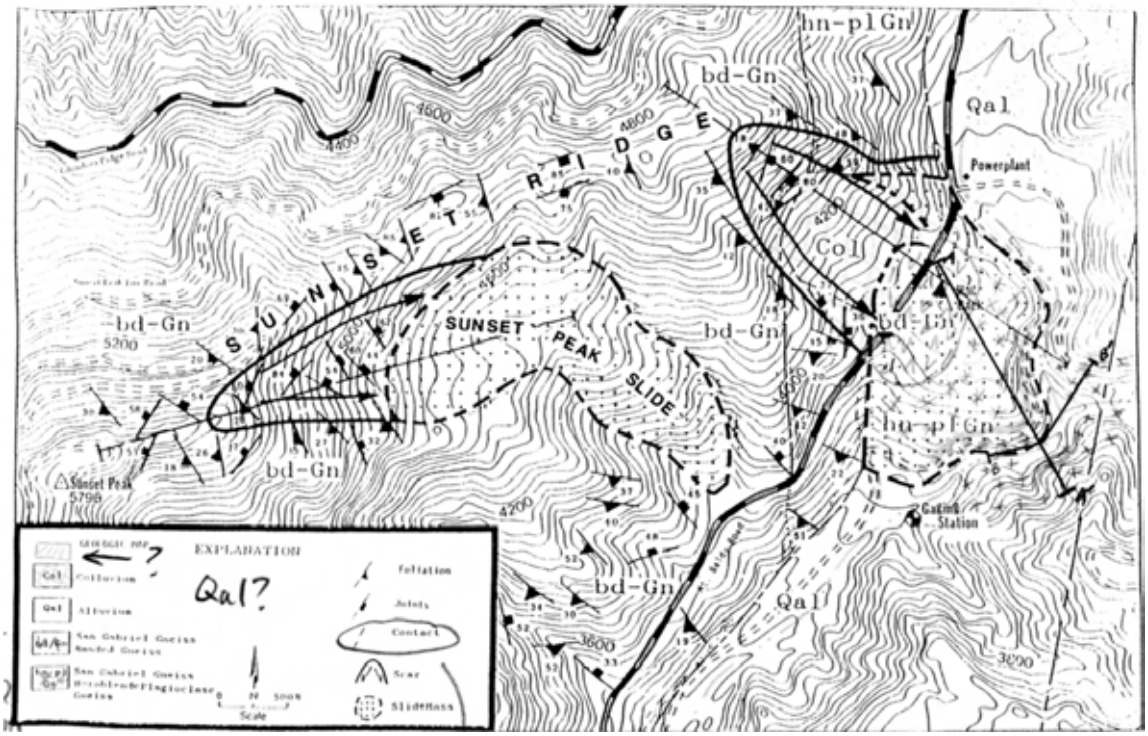

Figure 4 Map of Sunset Peak and Hog Back Slide areas. (Rogers et al., 1992)

Professor Jonathan Nourse of the Geologic Sciences Department at Cal Poly Pomona has performed varying degrees of work in the San Antonio Canyon area. This includes a geologic map of the Mount Baldy quadrangle that includes landslides (Nourse et al., 1998) and a Middle Miocene reconstruction of the central and eastern San Gabriel Mountains (Nourse, 2002). In this later work, Dr. Nourse discusses the fault system that affected the San Gabriel Mountains from the mid Miocene to the present.

Agunwah (2008), investigated the Hog Back Slide debris in order to map out clast lithologies and to find out if the degree of translation versus chaotic jumbling of the slide mass. The senior thesis was used also to see if the slide mass rocks remained in similar orientation during emplacement. Key findings from that paper were:

- The available landslide clasts showed that both the felsic gneiss and the quartz diorite have the same consistent orientation. The strikes were to the northwest and the dips were to the southwest. Upon analysis of the data together, it was observed that the felsic gneiss portion of the slide maintained a very uniform orientation, striking northwest and dipping to the southwest. The quartz diorite clasts had somewhat similar measurements to the felsic gneiss clasts, however, planes of strike and dip varied significantly with location and clast size.
- These results suggested that the Hog Back Slide deposit was both semi-coherent and incoherent at the same time. On the western half, it was semi coherent to the point where only one block orientation fell out of normal orientation of the bedrock source area; i.e., northwest- striking and southwest-dipping. On the eastern half, however, the slide was somewhat jumbled such that groups of slide blocks were out of place from the normal orientation of the field study area.

In 2016, Jon Marshak, a graduate student at Cal Poly Pomona, researched and mapped the distribution of the Middle Miocene dike swarms in the Eastern San Gabriel Mountains. In the area concerning the Hog Back Slide, his data indicated that the majority of the strikes of the associated dikes were trending to the Southwest and the Northeast. He concluded in his thesis that the Northeast trending dike populations,

prominently displayed in blocks south of the modern-day North San Gabriel Fault (NSGF), were intruded into fractures produced by a strike- slip stress environment that predated the middle Miocene magmatic event. Ancestral left-lateral movements on the San Antonio Canyon Fault, Sunset Ridge Fault and San Dimas Canyon Fault, suggest that these fractures represent the structural anisotropies developed in the early Miocene.

In 2017, Anselm Krause, an undergraduate student at the University of California at Riverside, concluded that the Hog Back Landslide was a rock avalanche with the capacity to transport large amounts of debris that are capable of affecting fluvial processes for hundreds of years after. Based off the dates, attained via dendrochronology, the Hog Back landslide was a very recent event and is potentially related to a generation of other large landslides within the SGM (Scherler et. al 2016). The large volume that was moved and its relation to the stream, has affected the current fluvial processes in the area. Physical characteristics of the toe exhibit risk as the steep scree slopes are easily moved onto active sites for tourists and the stream below. The stream profile exhibits a shallow decent towards the south, but the channel is still capable of turbulent activity. Overall, the Hog Back Landslide is a key example of a large event that has a great impact on a small area and continues to generate risk for the area.

In 2020, Nicolas Barth, a professor at the University of California at Riverside, revealed through new mapping in San Antonio Canyon that there could be at least three times as many landslides than previously mapped and that the landslides cover twice the surface area. He concluded in his article section that the best approach to mapping landslides in this landscape is to take a two-prong approach: (1) GIS mapping with lidar data to provide the most detailed view of geomorphology, and (2) field mapping with a structural geology focus to characterize rock textures and map contacts. He also

concluded that Early Holocene landslides may already have their geomorphic expression removed through erosional and weathering processes. Once sufficient soil has developed and vegetation has colonized a rock avalanche surface, wildfires are highly effective at degrading the geomorphic surface. Older surfaces may look similar to gravel fill deposits.

1.6 Hypothesis and Research Questions

The intent of my Master's Thesis is to address two hypotheses: (1) Hog Back landslide failed as a semi-coherent mass, preserving –pre- slide stratigraphy and structural orientations, and (2) A translatory mode of failure aided in the preservation of the contacts between rock units, and consistently oriented structures, both of which can be observed in the field. Important research questions include:

1. What are the geologic and structural characteristics of the slide scar region?
2. How much translation of marker units and contacts occurred during slide emplacement? How much rotation?
3. Are there chaotic vs. ordered clast orientations?
4. Are there statistical differences in orientation between small vs. large clasts?
5. How does intact bedrock structure compare with that of the clasts?
6. How did the slide fail? What were the most likely mechanisms?
7. Can various safety factor parameters be resolved or constrained?

CHAPTER 2: METHODS

To address the questions outlined in this thesis, I needed to organize and catalog the previous data from all the existing foliation orientation measurements and add them to the newer field measurements where they can be compared and contrasted to each other.

Some measurements were located on the previous maps from others that visited the Hog Back Slide without any GPS data (Rodgers and Herber, 1991; Nourse 1998). The more recent data from the Hog Back area provided much more abundant and detailed information, along with precise GPS coordinates. Finally, additional field work was conducted for underrepresented regions of the study area to fortify the database. These areas included the top of Sunset Ridge, the areas near the scar of the Hog Back Slide, and a canyon that was to the south of the Hog Back Slide scar.

2.1 Compilation of Field Data

Measurements taken by Nourse (1998), Cal Poly Pomona students, and myself (Agunwah, 2008) in the San Antonio Canyon area south of Mount Baldy Village, were augmented by my measurements from 2014 to 2018 acquired during a series of a geology field visits (GSC 415, GSC 491, CE 538, GSC 694). Recorded measurements included foliation orientations of clasts and intact bedrock, along with joints, epidote surfaces, dikes, fault traces, geologic contacts, folds and slickenside surfaces. Features mapped prior to 2008 were located qualitatively in field notes and marked onto topographic base maps. Beginning in 2008, feature locations were tightly constrained with the aid of a GPS device. Shortly after these field observations were taken, foliations and some dikes were

entered into OziExplorer so that the GPS points could be placed on a digital topographic map of the area. From here, a screenshot was taken and imported into Adobe Photoshop to trim the mapping area. After the mapping area was adjusted to a proper fit, it was further imported to Adobe Illustrator, where layers of information could be added.

I assigned Universal Transverse Mercator (UTM) coordinates to all locatable measurements on the map. These data points, however, were regularly intermingled with detailed information. Few of the measurements were standalone. For instance, the recorded field notes commonly observed the bedrock of the area, along with the foliations, joints, epidote surfaces, dikes, contacts and other data. This information would at times be recorded in a single GPS data point. Details are tabulated in Appendix A.

2.2 Geological Map Production

A primary objective in this study was to produce a geologic map of the bedrock, foliation, and other structural measurements. A compact version of my map product is presented later in Figure 6, and included at full size in Appendix B.

The first step to achieving this goal was to create a large topographic map of the study area, which exists within the Mount Baldy USGS 7.5 minute quadrangle. The quadrangle file was already in a .tiff format from USGS. Next, I used OziExplorer to georeference the GPS data points onto the map. The map was saved and edited in Adobe Photoshop to get the correct size. Once the size was obtained, the file was moved into Adobe Illustrator where maps could be created and data layers could be added. From there, geologic data that represented those data points were projected onto the proper layer.

The waypoint measurements with UTM coordinates were plotted as individual points within the 1927 North American Datum UTM zone 11 N. I produced a strike and dip symbol within Adobe Illustrator, along with the strike/dip/rake, joints, and dike symbols to represent my data. With the symbol property designed, I rotated each data point based upon the azimuth strike from the field notes. Finally, the color of these data points was defined by the different measurements.

My geologic and structural map includes a compilation of all my observation and measurements acquired since 2008 plus a few data points from other workers (Rogers et al, 1992, Nourse et al, 1998, Marshak, 2016). A color-coding system explained in the map legend of **Figure 6** distinguishes data from different sources.

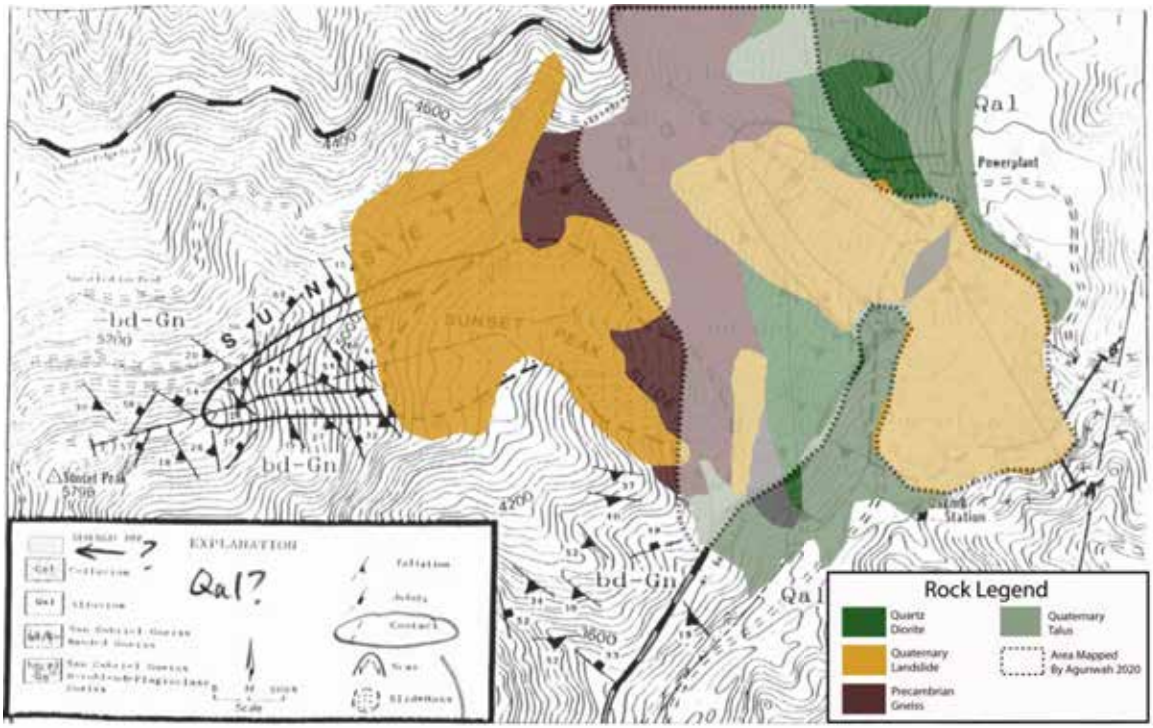

Figure 5. Index map showing general geology sources of data described in my thesis. Observations and measurements from Nourse (1998) and Rogers et al., 1992 allowed extrapolation of rock units to the west and east of my study area. Semi-transparent area (enclosed by dotted line) is overlaid onto Geology of Nourse and Rogers.

2.3 Stereonet Analysis

Stereonet projections allowed me to visualize three dimensional measurements in a two dimensional plot. Individual measurements, such as foliations, joints, epidote surfaces, dikes, were plotted as planes by inputting azimuth strike, with dip direction 90° clockwise from the strike direction. The measurement planes display a decreasing arc curvature with increasing amount dip with purely vertical dikes as straight lines parallel to the strike, and purely horizontal dikes intersecting with the outer edge of the circle. Poles are linear features perpendicular to the dike planes which plot as dots where the lines intersect the lower hemisphere of the sphere. I used a program called Stereonet 9 version 9.2.0 developed by Dr. Rick Allmendinger from Cornell University to plot my orientation measurements into multiple stereonet projections (Allmendinger, 2014). Stereonet 9 is a program that is more user-friendly than a previously software that I used in 2008. The previous program, Dipsdemo 5.1, produced stereonets plots that came out too dark to be read properly in a paper report. In-place rock planes are denoted by the solid bold color line (Brown for felsic gneiss, Green for quartz diorite). Rock planes in the slide blocks are denoted by the same color scheme as the in-place rock, with the plane line being dashed instead of solid. The “Inspector” feature within the Stereonet program generates contours based on “1% area method”. This method generates contours by calculating density of pole data within a circle 1/10th the radius of the stereonet (i.e. 1% of the area of the stereonet), which is useful for analyzing and dissecting major strike and dip patterns.

After compiling the previous field measurements from earlier work, I noticed that the data set lacked points in the surrounding areas next to the scar of the slide,

specifically to the north and south. The terrain around the Hog Back Slide is not as easily accessible. There is only the Sunset Ridge Trail that runs above the scar. There is no direct road access that would allow for measurements in the scar area. I pinpointed several locations which did not have previously collected measurements and are accessible by going off the trails. To collect foliations, joints, fractures, epidote surfaces, mafic dike, and other orientations, I noted the location via GPS, which is set on the NAD 1927 datum. Then, I used a brunton compass to measure the strike and dip of the features in question.

CHAPTER 3: RESULTS

In this section, I am presenting new field observations in the form of photographs and geologic mapping. **Figure 6** (reproduced at a higher resolution in Appendix B) is the main product of my recent field mapping. Several parts of the field map were clipped and expanded to highlight specific areas and features described in detail below. Also, there are a series of stereonet plots that present structural data by bedrock and feature type.

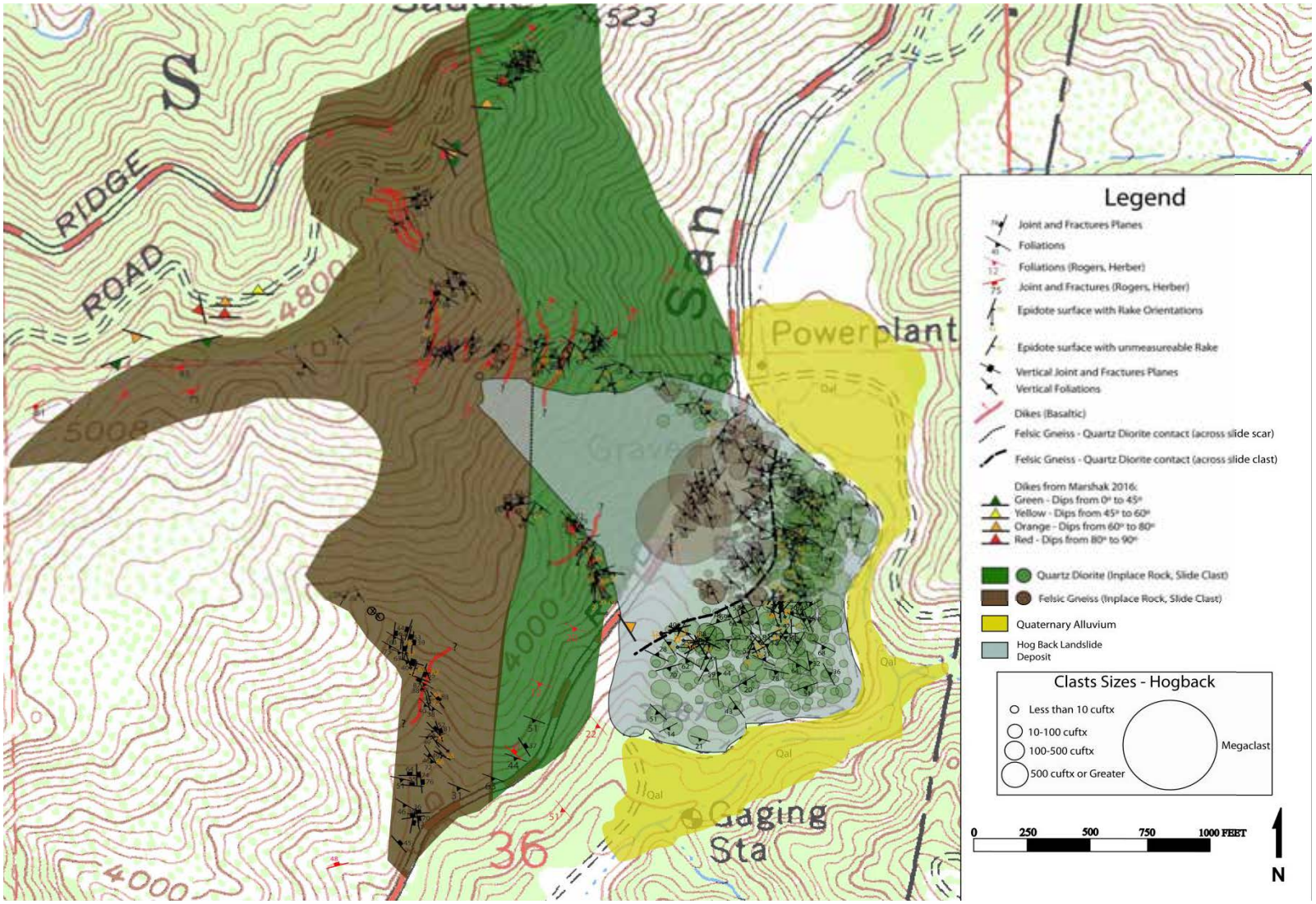

Figure 6. Composite geologic map of the Hog Back Landslide study area, showing all measurements taken during my thesis investigation. Higher Resolution Version appears in Appendix B.

3.1 Personal Field Work (Geological Mapping Traverses and Photography)

The first area I mapped in winter and spring of 2015 was along Mt Baldy Road directly southwest of the Hog Back Slide, where there were exposures of the in-place felsic gneiss in the western canyon wall (**Figures 7 and 8**). I parked at a turnout that was southeast of Sunset Peak, where I walked on the western side of the road for approximately 3,000 feet recording measurements. Later, I went into the canyon that was between the Sunset Peak slide and the scar of the Hog Back Slide to find more in-place rock while avoiding the debris of the Sunset Slide. I proceeded into this canyon until I was unable to continue further, due to the slide blocks that made the canyon too hazardous. I collected 29 total waypoints that included 59 measurements in the canyon (**Figure 7**). Foliations dipped consistently southwest, whereas joints and fractures displayed variable strikes with moderate to steep dips.

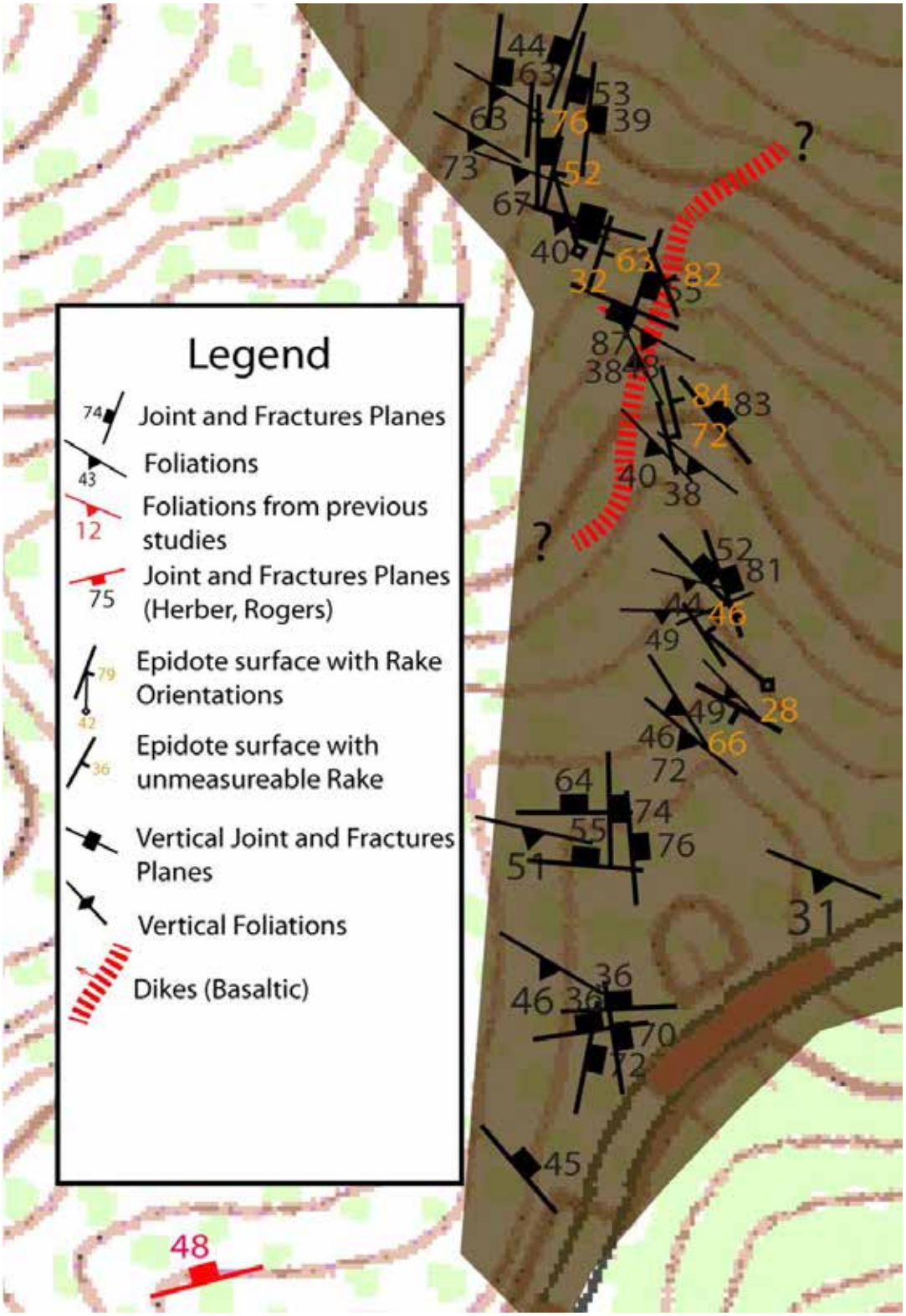

Figure 7: First traverse measurements through the western canyon, recording strike and dip, epidote surfaces, joints, and mafic dikes. The rock type is entirely Precambrian felsic gneiss. This is a clip from the main geologic map of Figure 6.

Figure 8. Photo of the western canyon, facing northwest.

The second traverse, in fall of 2015, was to the north of the Hog Back Slide scar. The rock was in-place in some areas, loose in other areas. The map unit was entirely quartz diorite. I walked in the up-slope direction to collect foliations and/or joints on the rock faces. In previous works (Rogers et al., 1992), there were a few recorded measurements in this area near the scar. I was able to get halfway up the slope when the weather changed from partly cloudy to a thunderstorm with moderate rain. I got off of the slope to measure some slide clasts that were felsic gneiss. I collected 20 total waypoints that included 26 measurements on the slope and the northern end of the Hog Back slide road cut. (**Figures 9 and 10**)

The west side of **Figure 9** includes an important data acquired by Dr. Nourse and myself in February 2014. We were able to pinpoint the location of the felsic gneiss-

quartz diorite contact high on a spur ridge north of the Hog Back scar. This contact projects southward to an excellent exposure that crosses the Mount Baldy Road.

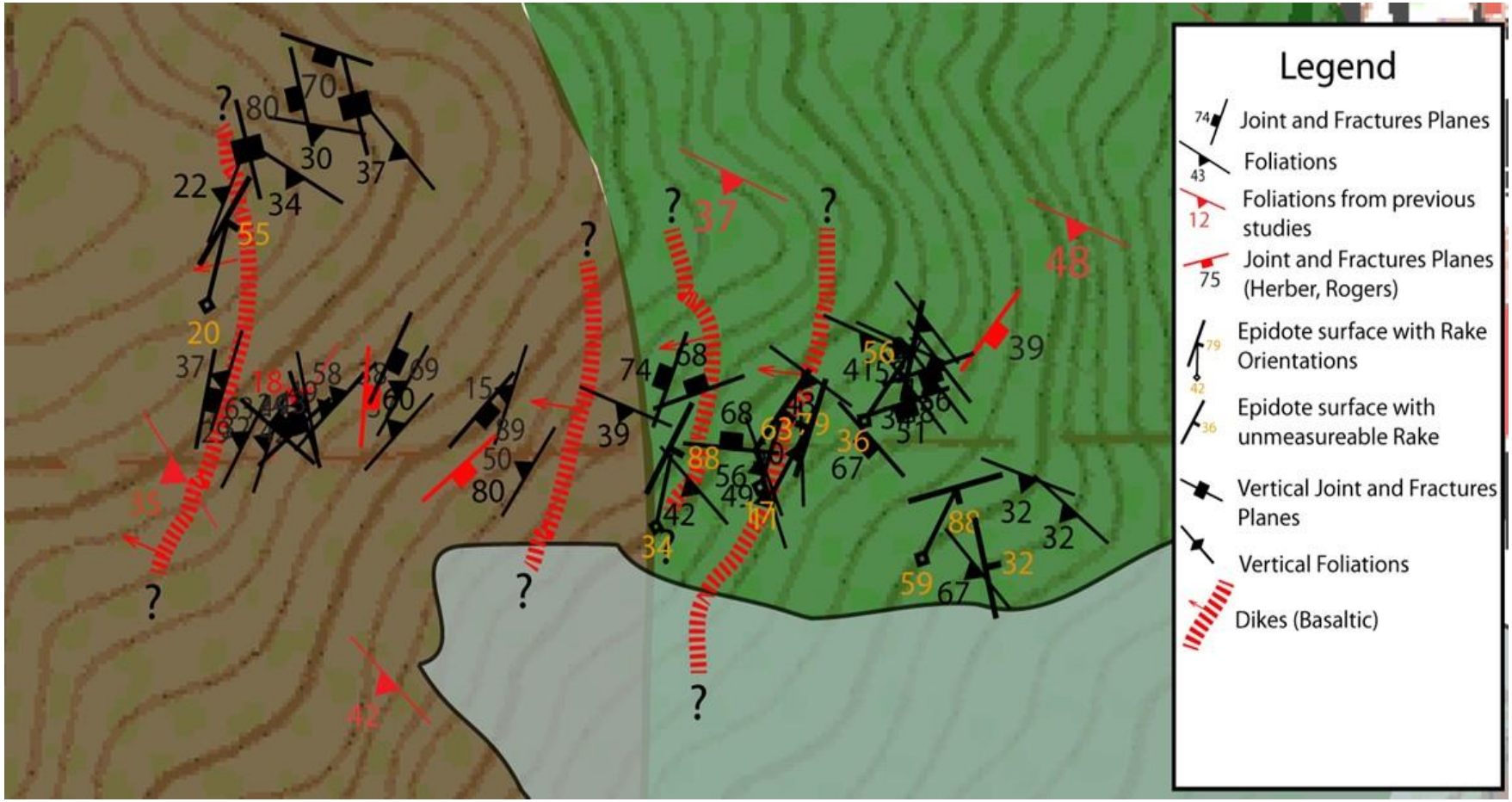

Figure 9. Second traverse measurements north of the Hog Back Slide scar, recording strike and dip, epidote surfaces, joints, rock contacts, and mafic dikes.

Figure 10. Photo of the descent from the northern area of the Hog Back Slide scar. The boulders are mainly quartz diorite.

The third and fourth traverses I walked, also in Spring 2016, were on the central area of the Hog Back Slide mass (**Figure 11**), where structural features in the clasts as well as clast size were measured. The mapped units were mostly quartz diorite clasts with some small boulders of felsic gneiss. Along this traverse, there were clasts that had slickenside surfaces. I associated each measurement of the clast's foliation with diameter, which ranged from medium to large (10 feet to 20 feet) in size. There were a few measurements taken on the southern end of the Mt Baldy Road cut through the Hog Back Slide. Also there were two measurements taken from the northeast area of the Hog Back Slide. In all, I collected 32 total waypoints that included 47 measurements.

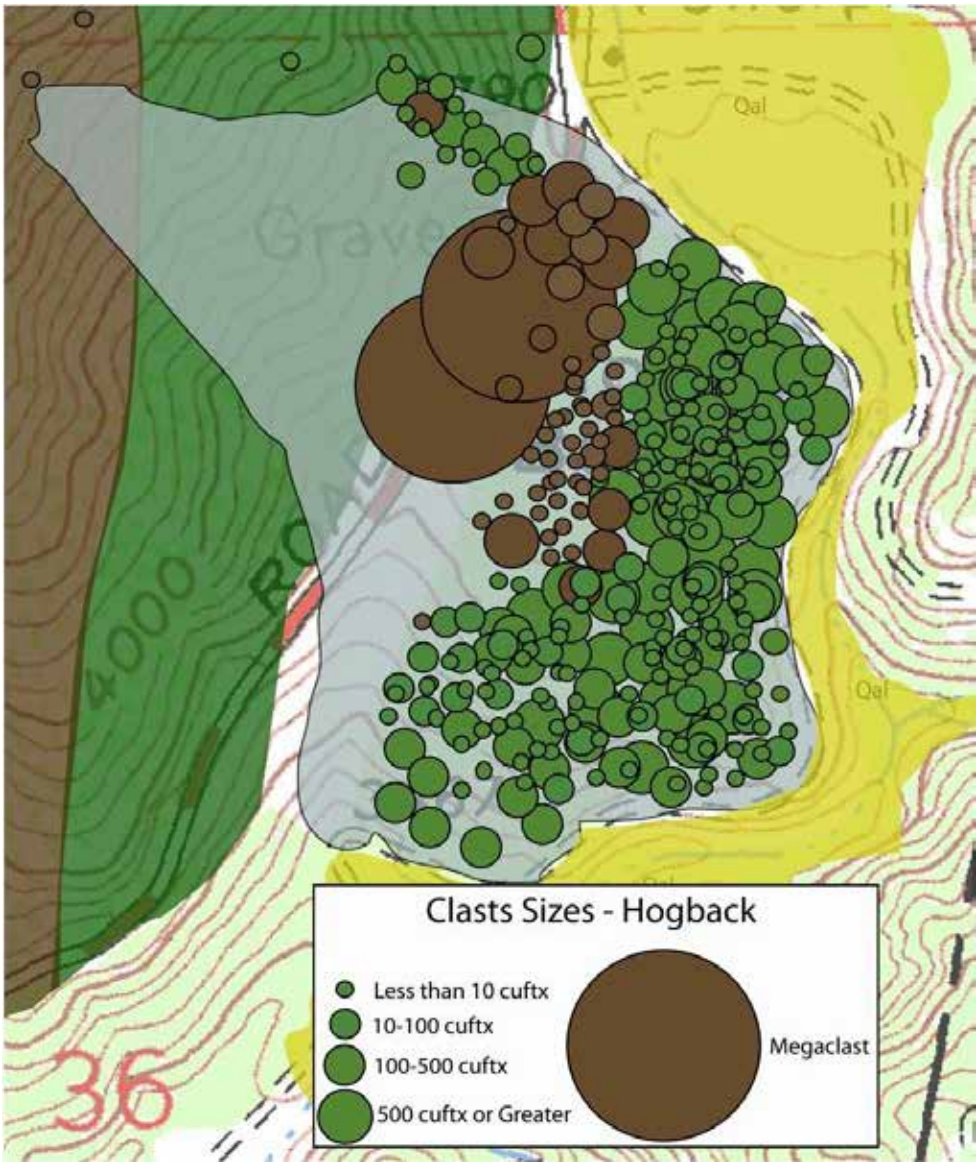

Figure 11. Clasts measured in my 3rd , 4th , and 5th traverses through the main part of Hog Back landslide. This map includes measurements taken during my Senior Thesis investigation (Agunwah, 2008).

The fifth traverse I walked, in December of 2016, was on the northern area of the Hog Back Slide area. The map units were mostly quartz diorite clasts with some boulders of felsic gneiss. Along this traverse, there were clasts that had slickenside surfaces like the third and fourth traverses. The major observation in this area was that a distinct contact between the felsic gneiss and quartz diorite clast types (**Figure 11**) was much more pinpointed than shown in the Rogers et al., (1992) mapping work. As in previous

traverses through the slide mass, each observation station noted the clast's foliation and mean diameter. There were a few measurements taken on the southern end of the Mt Baldy Road cut through the Hog Back Slide. These measurements are related to the megaclast (**Figure 12**). The megaclast is the part of the slide mass that separated from the in-place rock. The orientations with in this megaclast did not shift out of alignment with the in-place rock (**Figure 13**). Also, this megaclast is composed of felsic gneiss with some visible faulting occurring Also there were two measurements taken from the northeast area of the Hog Back Slide. In all, I collected 21 total waypoints that included 41 measurements.

Figure 12. Photo of the New Mt Baldy Road cut facing southeast, within the felsic gneiss Megaclast

Figure 13. Photo of the New Mt Baldy Road cut facing west, viewing the in-place felsic gneiss in the rock face. Megaclast is to the North of this area..

The sixth traverse I walked, in spring of 2017, was on the southern and eastern areas of the Hog Back Slide area (**Figure 11**). The clast types were mostly quartz diorite with some small boulders of felsic gneiss. Also there were a few measurements taken from the northeast area of the Hog Back Slide and used to close a data gap. In all, I collected 12 total waypoints that included 46 measurements.

The seventh traverse I walked in the fall of 2017, was on the northeastern part of Sunset Ridge area (**Figure 14**). The marker units included both quartz diorite and felsic gneiss, with a well-located marker unit contact (**Figure 15**). Along this traverse, there were areas that had slickenside surfaces. There were also mafic dikes that appeared to cause moderate weathering to the host rock. Along this traverse, the rocks appeared to be

much more fractured than the rocks from the southern canyon. In all, I collected 6 total waypoints that included 18 measurements.

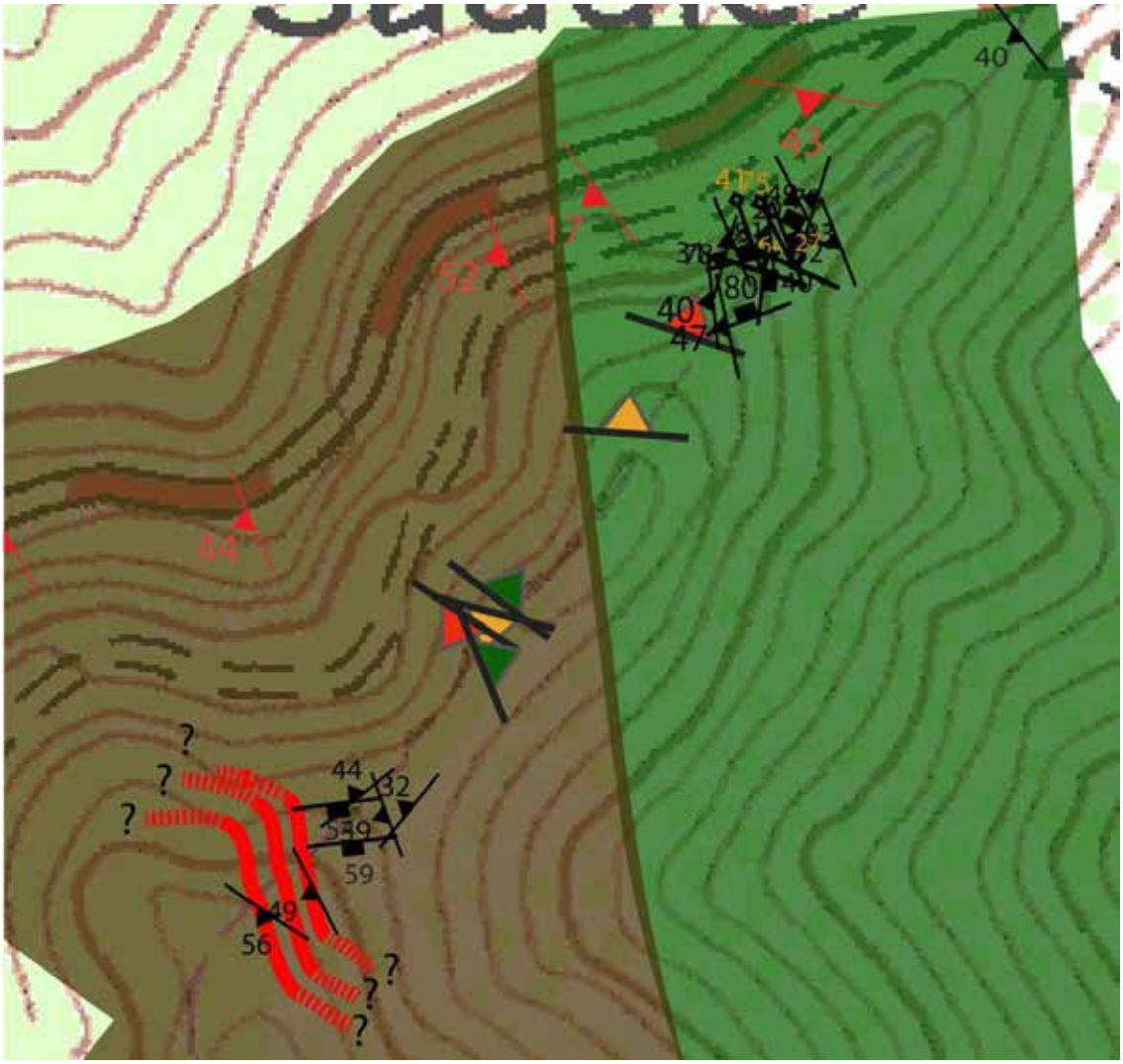

Figure 14: Traverse #7 along Sunset Ridge, recording strike and dip, epidote surfaces, joints, rock contacts, and mafic dikes. Larger colored strike and dip symbols are for previously measured dikes from Marshak 2016. (see legend on Figure 6)

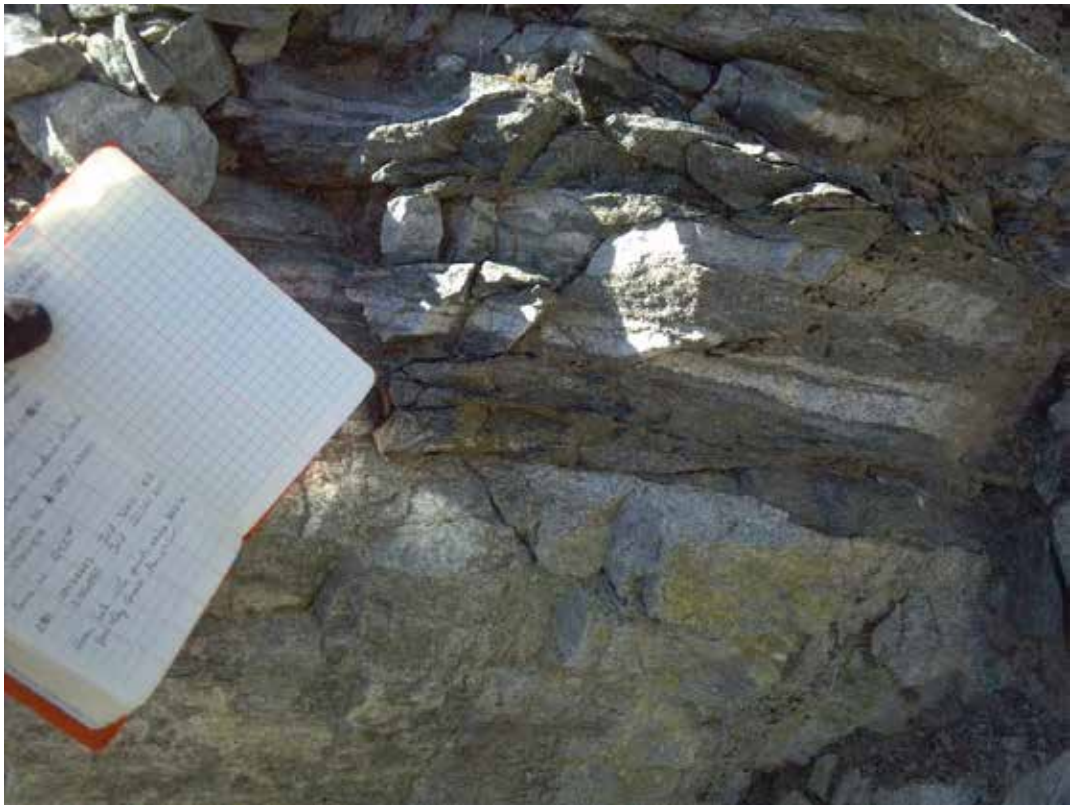

Figure 15. Photo of the Felsic Gneiss/Quartz Diorite transition zone within in-place rock. Contact zone appears to consist of basalt, dacite, and a mafic banded gneiss.

The eighth traverse I walked, also in fall of 2017, was along the southwestern area of the Hog Back Slide scar area (**Figure 16**). The map units included both quartz diorite and felsic gneiss, with a well constrained marker unit contact. This contact shows a transition zone where there is more mafic banding in the felsic gneiss. Some of these bands were made up of dacite and basalt dikes measuring between one inch to three inches thick. There were also some thin pegmatite and quartz veins measuring one-half to two inches. The interface of this contact zone appears to be from magmatic forces that caused some contact metamorphism. (**Figure 15**) Along this traverse, there were areas that had slickenside surfaces. There were also mafic dikes that sharply intruded the host rocks. Along this traverse, the rocks appeared to be much less fractured than the rocks from Sunset Ridge. In all, I collected 10 total waypoints that included 22 measurements.

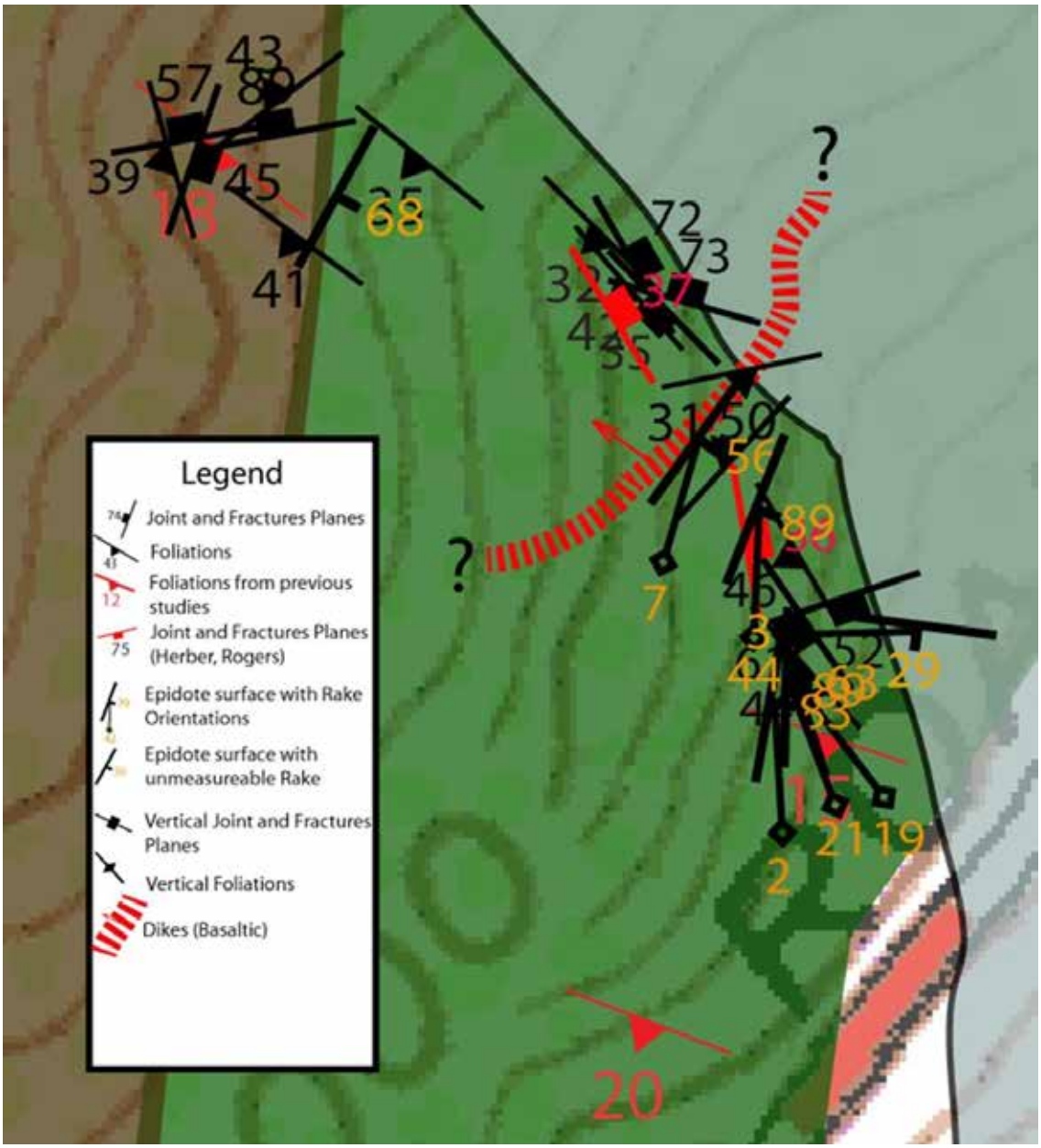

Figure 16. Eighth traverse measurements just southwest of the Hog Back Slide scar, recording strike and dip, epidote surfaces, joints, rock contacts, and mafic dikes. Note tightly constrained contact between the felsic gneiss and quartz diorite units.

The ninth and tenth traverses I walked, also in the fall of 2017 and 2018, were on the northern and the northwestern area of the Hog Back Slide scar area. This traverse was being done to complete the work from the second traverse and to close data gaps (**Figure 9**). The rock was in-place in some areas, loose in other areas. The map units

were quartz diorite and felsic gneiss, with an inferred marker unit contact. I walked in the up-slope direction, past previous measurements to collect foliations and/or joints on the rock faces. I also collected epidote surface measurements along with observed mafic dikes. There were areas that had slickenside surfaces. There were also mafic dikes that appeared to cause moderate weathering to the host rocks. Along this traverse, the rocks appeared to be just as fractured as the rocks on Sunset Ridge (**Figures 17 and 18**). In the ninth traverse, I collected 9 total waypoints that included 29 measurements. In the tenth traverse, I collected 10 total waypoints that included 18 measurements.

Figure 17. Photo of the fractured and weathered felsic gneiss on the Hog Back Slide scar.

Figure 18. Photo of the fractured and weathered quartz diorite on the Hog Back Slide scar

3.2 Structural Data

Described below are stereonet plots of foliation measurements and joint/fracture orientations from intact bedrock of the Hog Back Slide source region and clasts within the landslide deposit. These data allow assessment of the degree of concordance between structures of the two areas. The data sets are organized to provide visual and quantitative comparison of the three--dimensional orientations. These measurements were classified into four types: Quartz Diorite in-place, Felsic Gneiss in-place, Quartz Diorite in- slide, and Felsic Gneiss in-slide. Representative photographs are also provided.

3.2.1 Foliations of In-place Felsic Gneiss

Figure 19 is a photograph showing typical foliation in the Felsic Gneiss unit from the intact (in-place) bedrock area. **Figure 20** gives a stereonet representation of the data set, that emphasizes a strong preferred orientation. The dips range from 22 to 56 degrees to the southwest. There were also a few anomalous measurements with dips directed 30, 32, and 44 degrees to the northwest. However, the majority of 40 foliations demonstrate a remarkably consistent northwest strike and southwest dip consistent northwest strike and southwest dip.

Figure 19. Photo of the Felsic Gneiss in-place, showing typical metamorphic foliation.

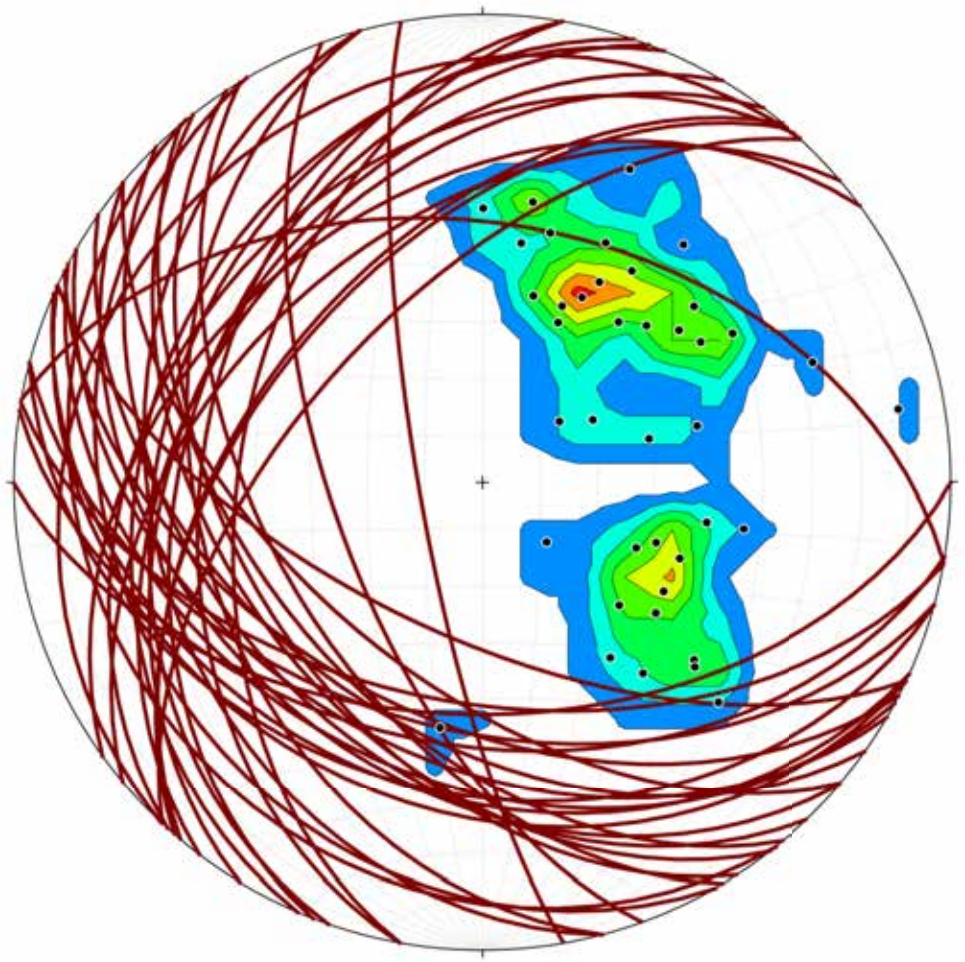

Figure 20. Composite stereonet of the Felsic Gneiss foliations, in-place. There are 40 orientations. The mean strike is 118 degrees and the mean dip is 53 degrees to the southwest. The average strike of the main pole cluster is 118 degrees.

3.2.2 Foliations of In-place Quartz Diorite

Figure 21 is a photograph showing typical foliation in the quartz diorite unit from the intact (in-place) bedrock area. Most of the Quartz Diorite in-place foliations (**Figure 22**) have strikes between 17 to 32, 295 to 329, and 340 to 358 degrees. There was an outlier strike of 089. Most dips ranged from 13 to 78 degrees to the southwest. There were a few dips of 20 to 60 degrees to the northwest. The outlier had a dip of 50 degrees to the southeast. Altogether, this data set demonstrates a strong degree of concordance between quartz diorite and felsic gneiss foliations in the bedrock source are of the Hog Back landslide.

Figure 21. Photo of the foliated Quartz Diorite marker unit.

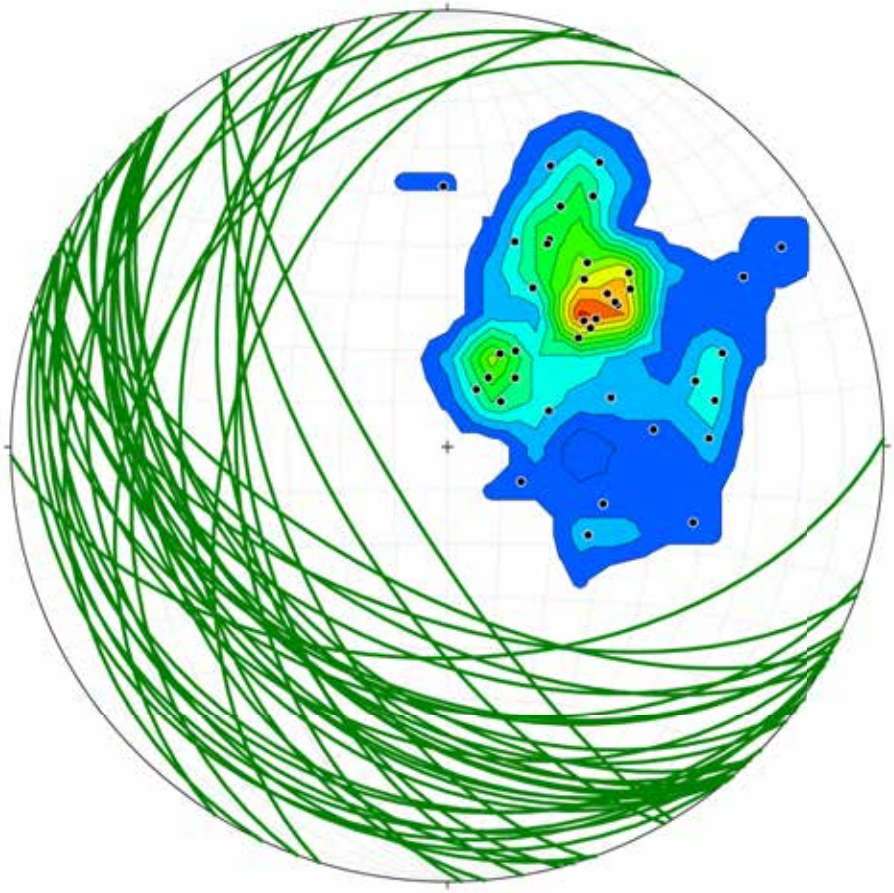

Figure 22. Stereonet of the Quartz Diorite foliations, in-place. There are 41 orientations**.** The mean strike is 135 degrees and the mean dip is 54 degrees to the southwest.

3.2.3 Record of In-place Joints (Felsic Gneiss, Quartz Diorite)

Joint data sets were also collected within the intact bedrock source area of the Hog Back Slide. These measurements were classified into two types: Joints from the Felsic Gneiss in-place (**Figure 23**) and joints from the Quartz Diorite in-place. This structural data set (**Figure 24**) shows much more variability than the foliation data, but a contour plot of poles to joint surfaces brings out several statistical preferred orientations (**Figure 25**). The pole plot for felsic gneiss unit reveals a very significant joint set with northerly strikes and steep dips. This orientation is appropriate for creating tension cracks or breakaway structures (discussed later) that might have facilitated failure of Hog Back landslide. The pole plot of joints in quartz diorite shows several populations. Probably the most significant of these is a moderately southeast-dipping set, represented by the red bulls-eye pole cluster. This orientation is sub-parallel to the southeast dipping slide scar. As mentioned later in the Discussion section, such fractures may exist beneath colluvial cover that was responsible for nucleating the Hog Back Slide plane.

Figure 23. Photo of the felsic gneiss jointing and foliation orientations, in-place.

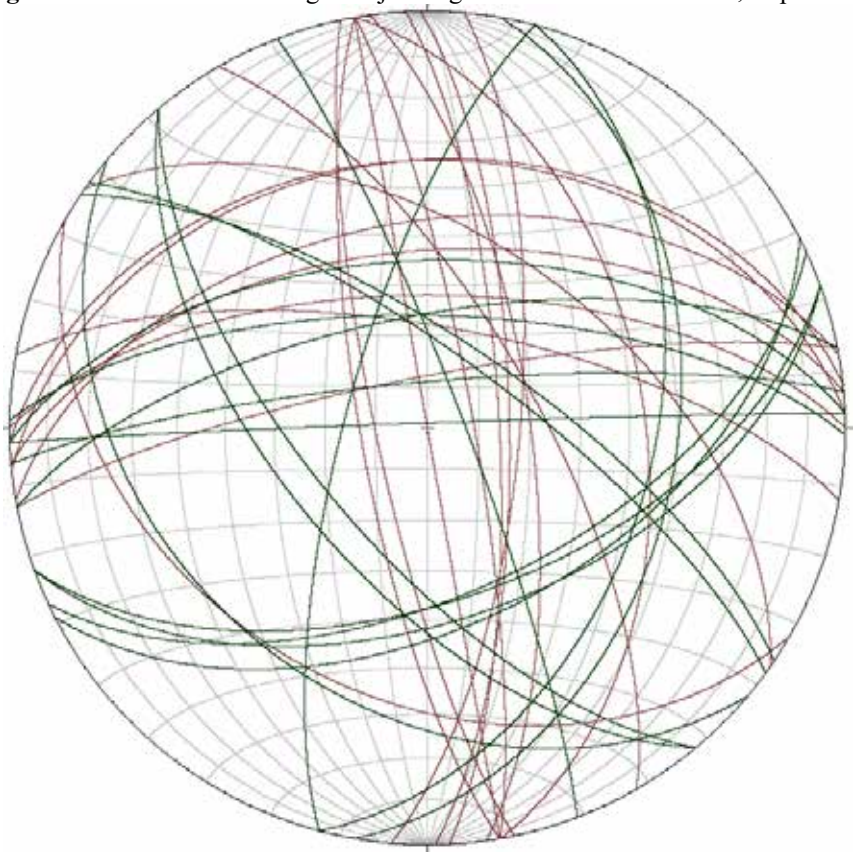

Figure 24: Composite stereonet of the Felsic Gneiss (brown) and Quartz Diorite (green) joint orientations, in-place. There are 37 total orientations: 19 from the Felsic Gneiss, 18 from the Quartz Diorite

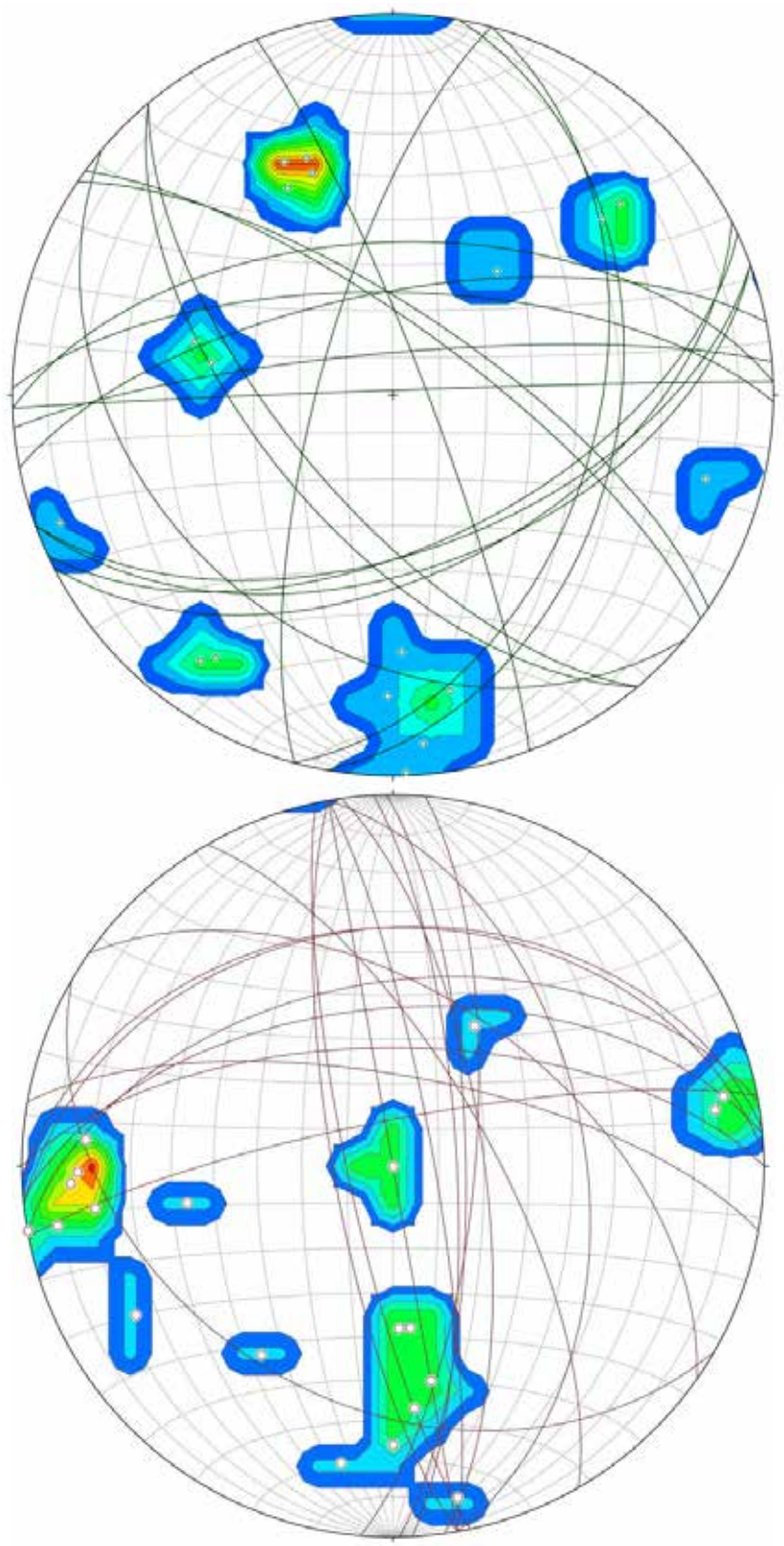

Figure 25A and B: Pole plot stereonet of the Quartz Diorite (Top) and Felsic Gneiss (Bottom) joint orientations, in-place.

3.2.4 Foliations from the Felsic Gneiss Landslide Clasts

The Felsic Gneiss clasts within the slide mass preserve foliations (**Figure 26**) that were very consistent with the in-place measurements, although several anomalous orientations exist. My stereonet (**Figure 27**) divides the data into large and small clasts. The corresponding pole plots (**Figure 28**) shows 4 significant populations.

Figure 26: Photo of foliations within a felsic gneiss landside clast**.**

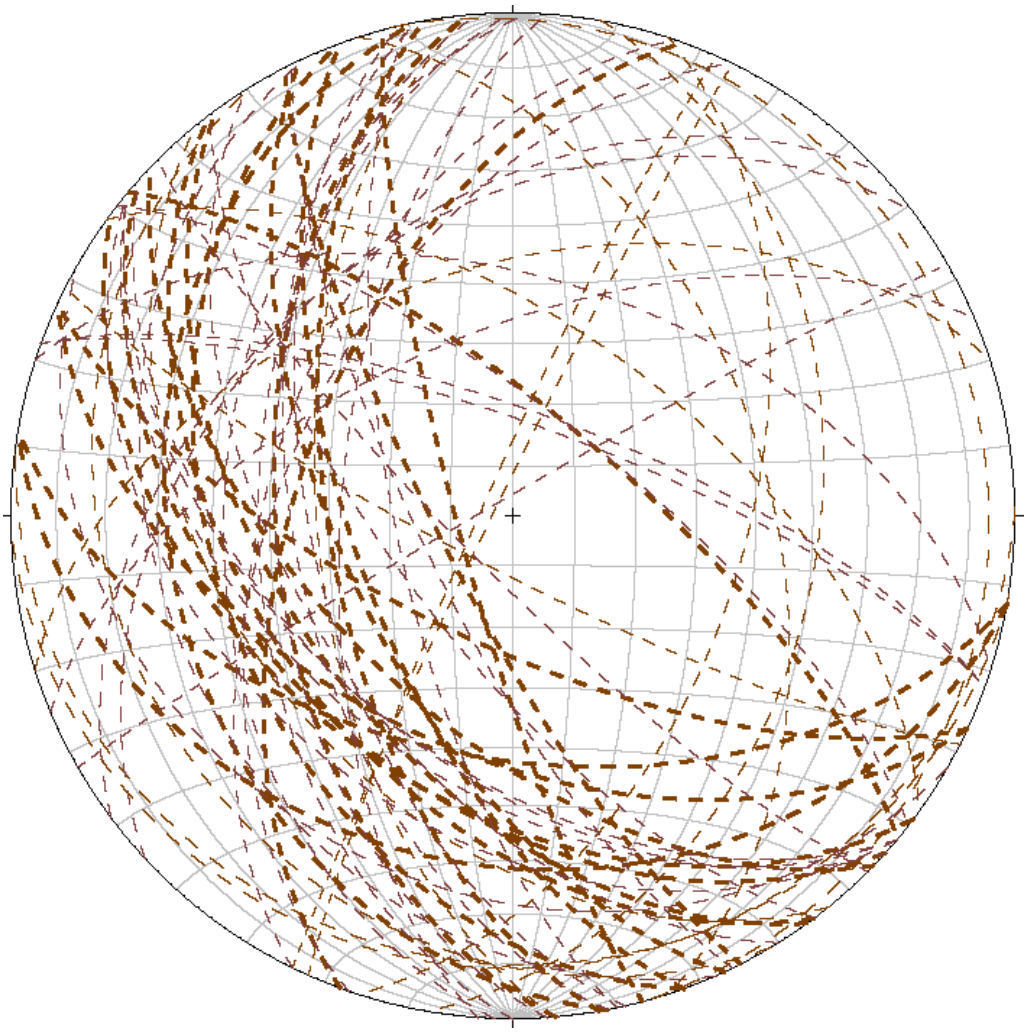

Figure 27: Composite stereonet of the Felsic Gneiss orientations, all sizes in clast. There are 60 total orientations: 36 Large Felsic Gneiss (bold dashed curves), 24 Small Felsic Gneiss (fine dashed curves).

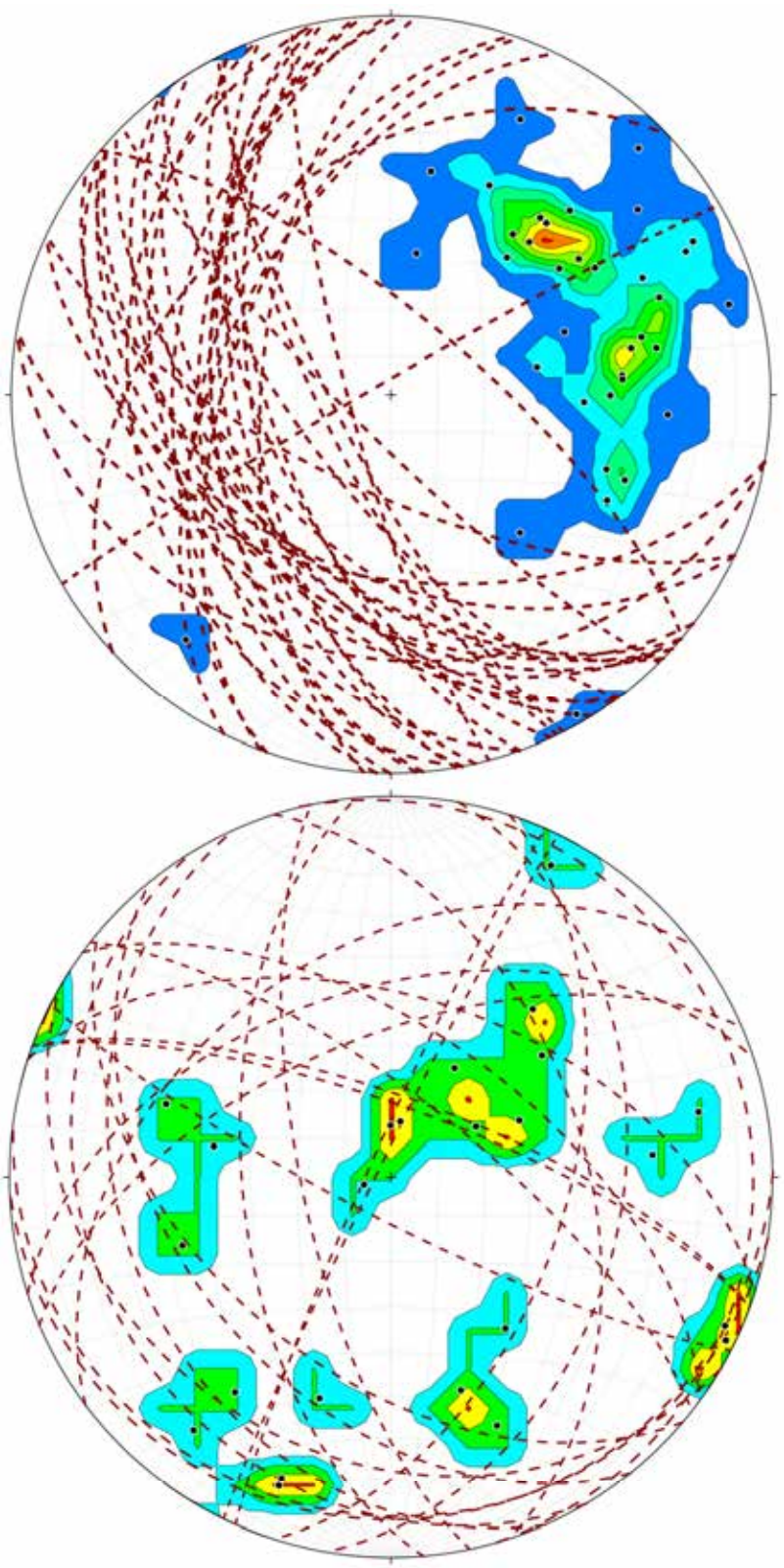

Figure 28A and B: Stereonets of the Felsic Gneiss orientations with the contoured pole plot, for 36 Large Felsic Gneiss (Top) and 24 Small Felsic Gneiss (Bottom).

3.2.5 Foliations from the Quartz Diorite Slide Clasts

Unlike the Felsic Gneiss clasts, the Quartz Diorite clasts within the slide mass (**Figure 29**) display a wide range of foliation orientations. This scattering of data is evident in a stereonet plot of foliation planes (**Figure 30**). A plot of poles to foliation (**Figure 31**) shows that two populations of steeply or moderately southwest-dipping planes persist, but multiple other trends are apparent, including a major population with northeast dips.

Figure 29. Photo of typical foliation within a quartz diorite landslide clast.

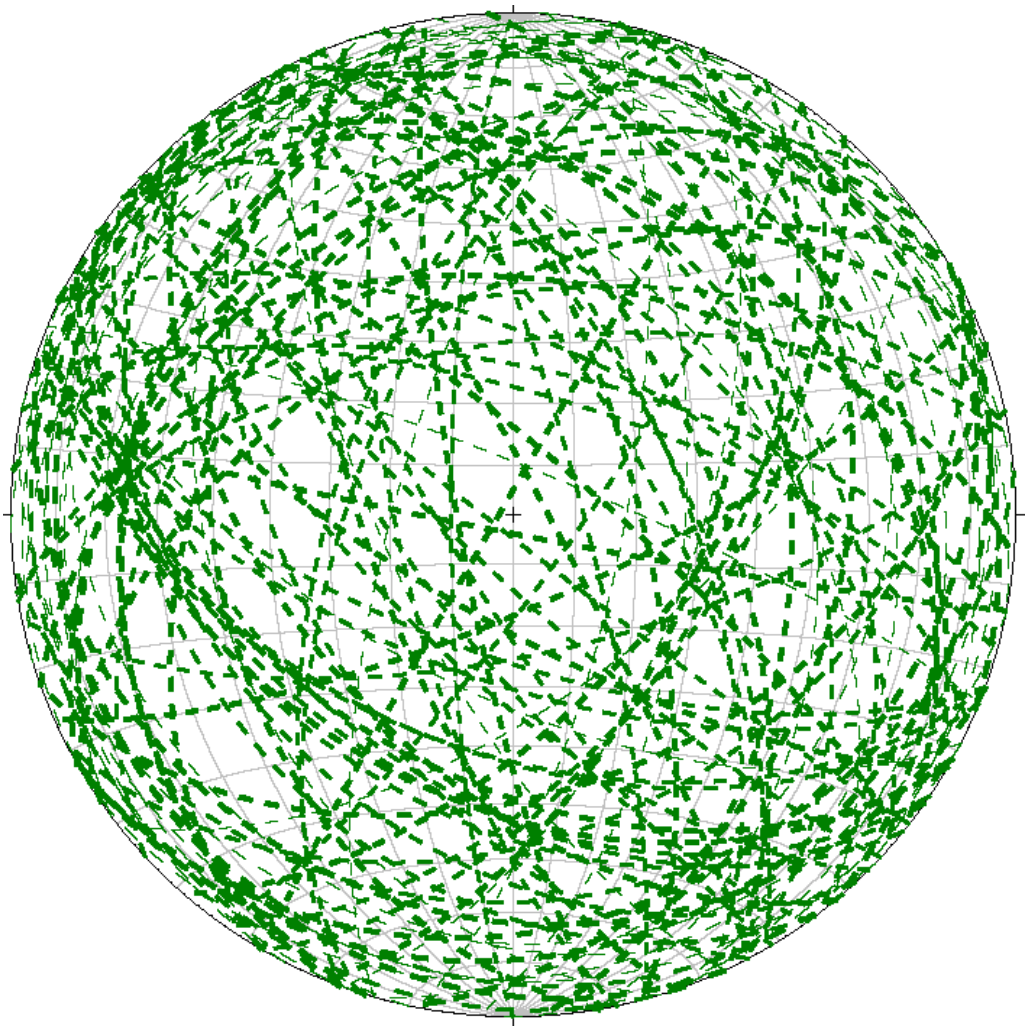

Figure 30: Composite stereonet of the Quartz Diorite foliations, all sizes in clast. There are 100 total orientations: 30 Large Quartz Diorite, 30 Medium Quartz Diorite, 40 Small Quartz Diorite

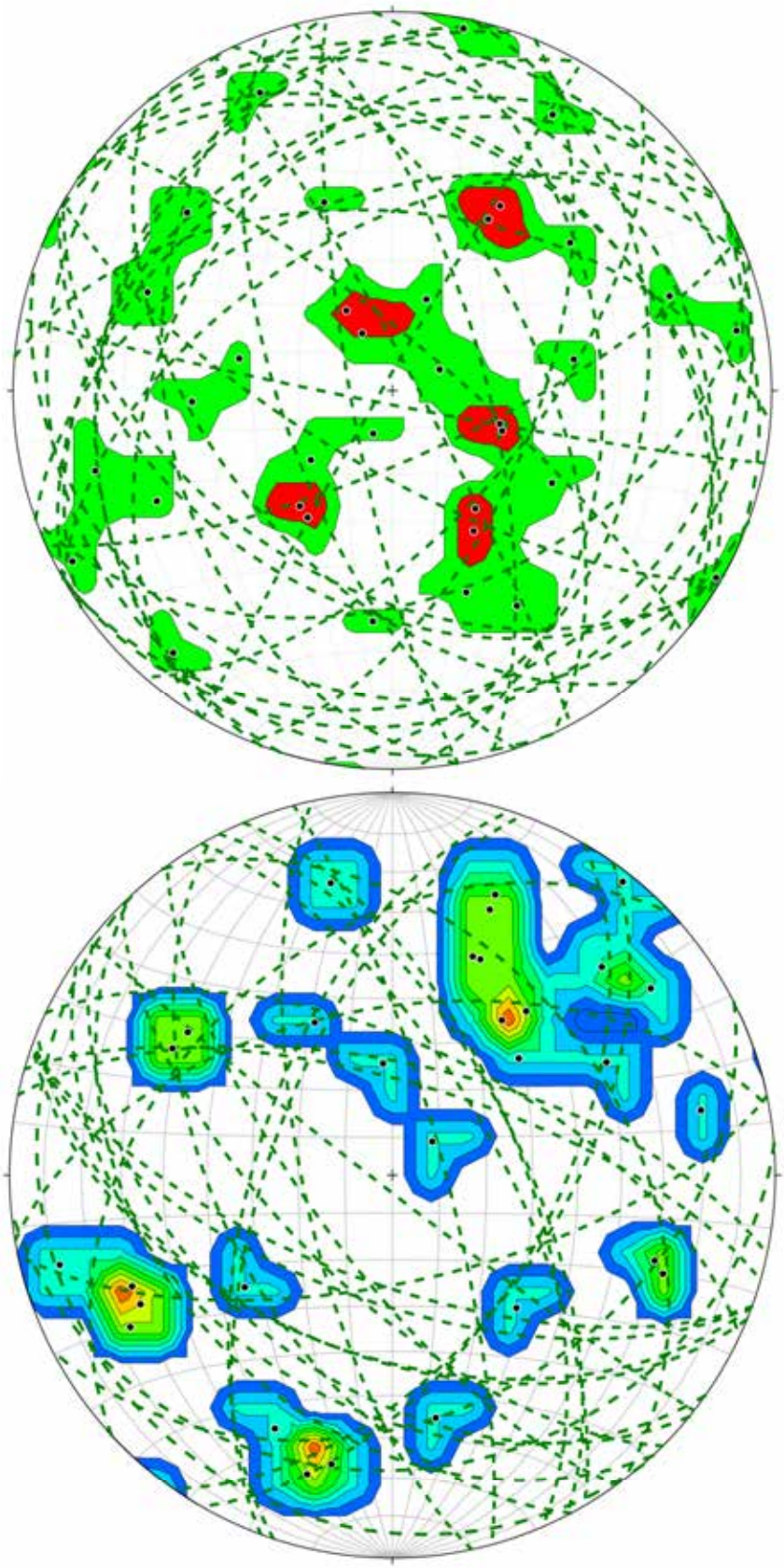

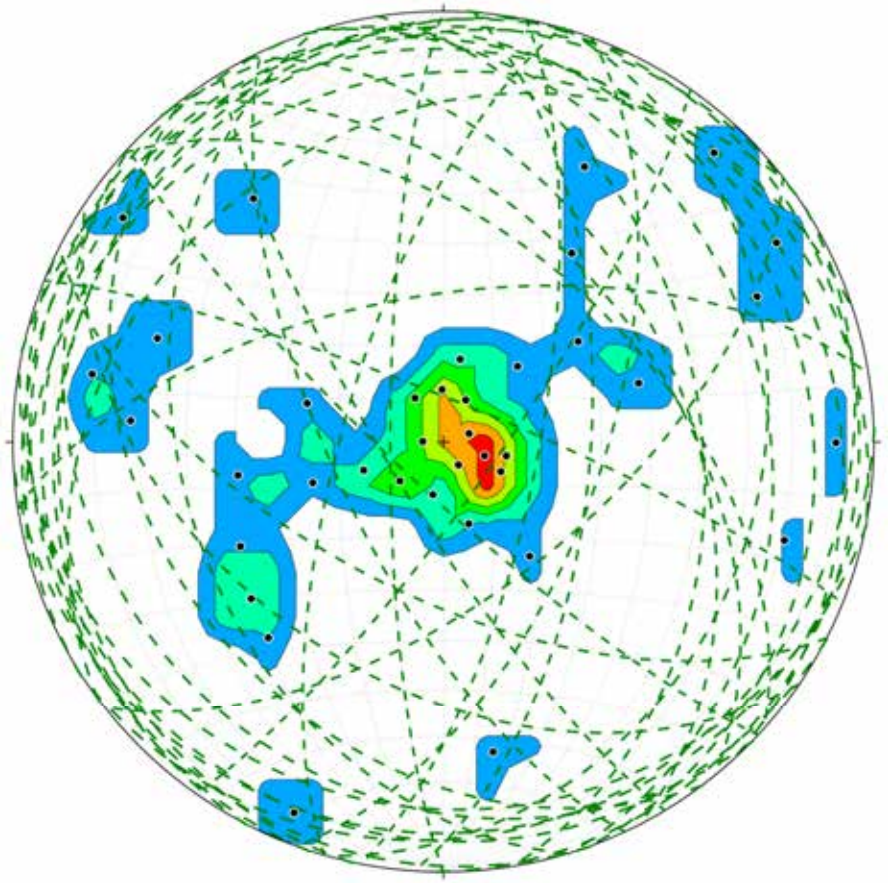

Figure 31A, B, and C: Stereonets of the Quartz Diorite clasts foliations with the contoured pole plots, for 30 Large Quartz Diorite (Top), 30 Medium Quartz Diorite, and 24 Small Quartz Diorite (Bottom).

3.2.6 Records of Epidote Surfaces

Measurements of strike, dip and rake of striated epidote fault surfaces data sets were also collected within the field area (**Figures 32 to 34**). These measurements were classified into 5 sets. My stereonets (**Figures 35-36**) show a wide scattering of this data, perhaps because landslide clasts (possibly rotated) are mixed with intact bedrock. The pole plot (**Figure 36A**) does show a strong population with north-northwest strike and steep dip that likely corresponds to the ancestral San Antonio. The shallow inclinations of rakes plotted on **Figure 36B** also support a strike-slip interpretation for these fault surfaces.

Figure 32. Photo of an epidote surface perpendicular to the foliation.

Figure 33. Photo of an epidote surface, showing the direction of the rake.

Figure 34. Photo of the strike line of this epidote surface

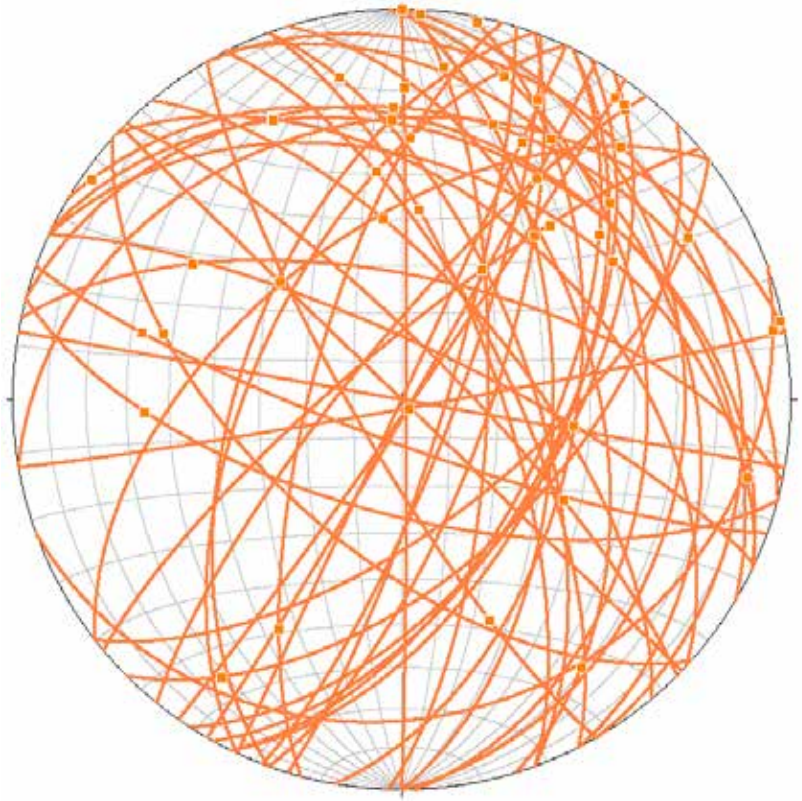

Figure 35: Stereonet showing strike/dip of the epidote slickensided surface orientations. This plot includes both in-place bedrock and clasts. Dots represent slickenlines (striations) measured within the striated surfaces. There are 48 total orientations.

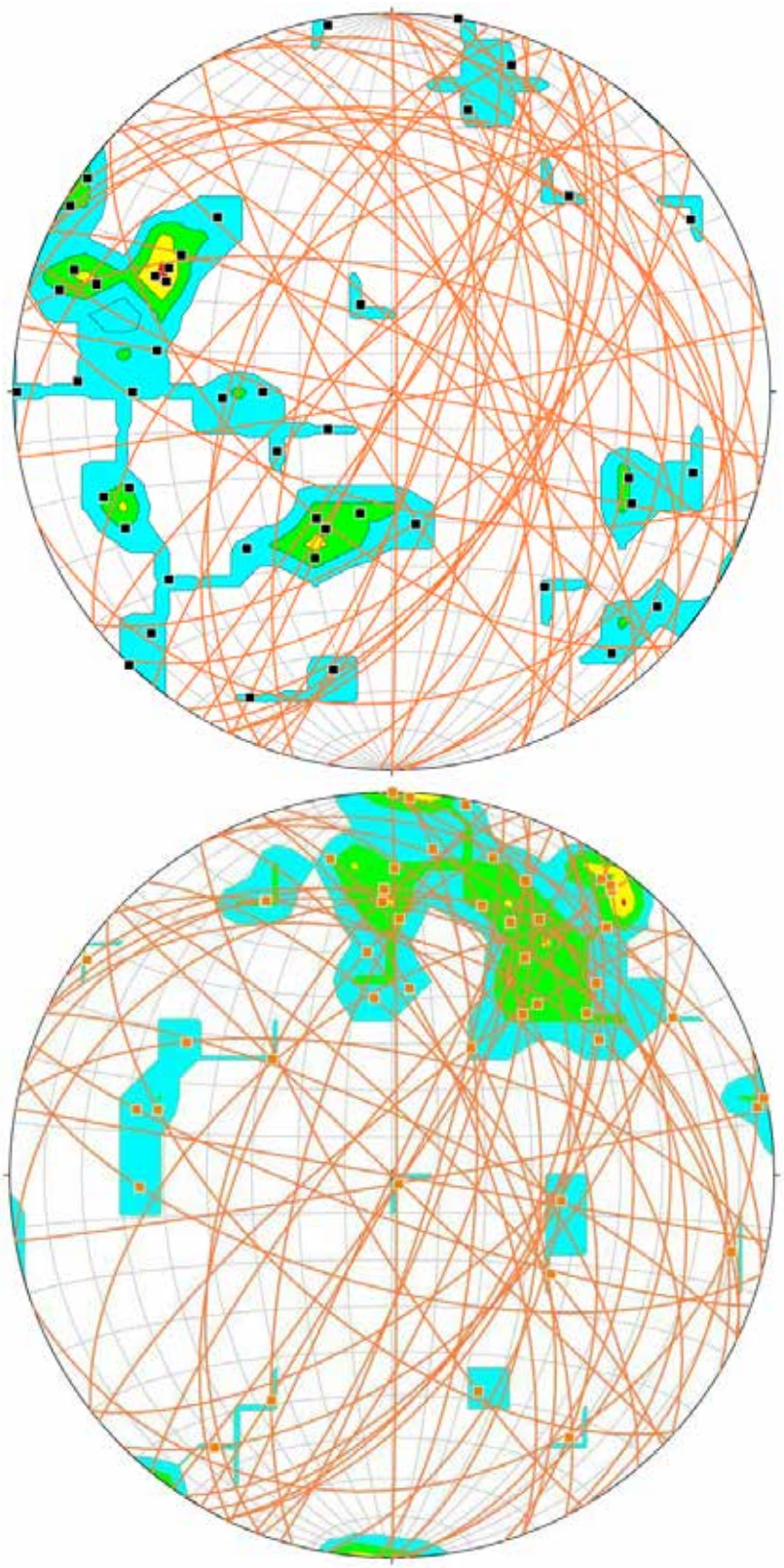

Figure 36 A and B. Stereonet of the slickensurface orientations for in-place bedrock and clasts. Stereonet on the top shows the slickensurfaces with the respective contour plots of the poles. Stereonet on the bottom shows the slickensurfaces with the respective contour plots of the slickenlines.

3.2.7 Records of Mafic Dikes

There were a few dikes encountered in the field area that intruded both the felsic gneiss and the quartz diorite bedrock.. These dikes were mafic in composition (**Figure 37**). In all, seven out of ten of the observed dikes preserve a northeast strike (**Figure 38**) that is similar to the strikes of the epidote surfaces. There are possibly more dikes in the area that are either buried under slide debris or inaccessible to access. According to Marshak (2016), there exist 56 recorded strikes of mafic dikes in the area for Sunset Ridge. Of those 56 measurements, 60 percent of them were striking between 10 to 50 degrees (**Figure 39**).

Figure 37. Photo of mafic dike within felsic gneiss.

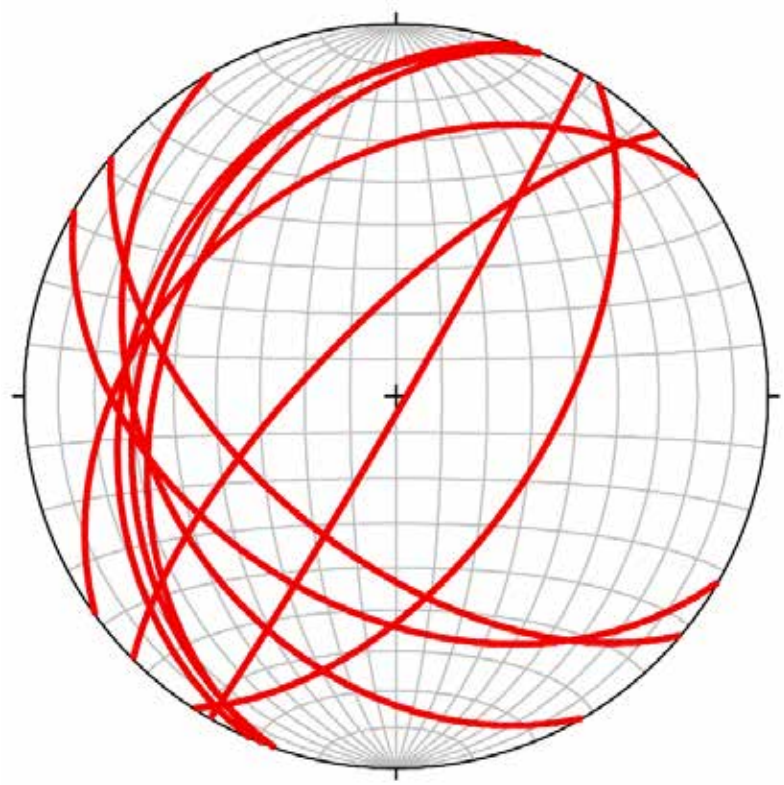

Figure 38: Stereonet of the Mafic Dike measurements collected in the field. There are 10 total orientations**.**

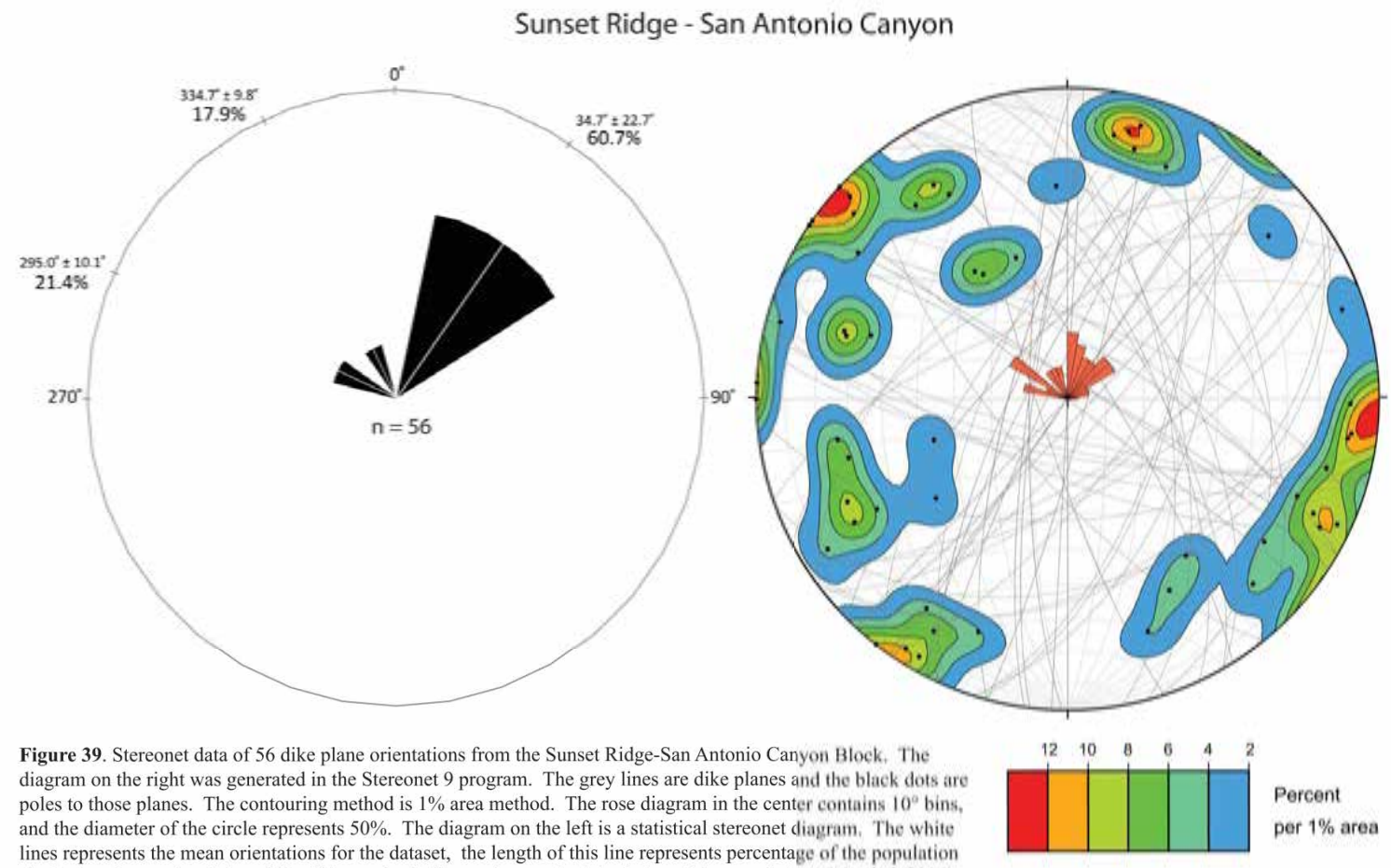

Figure 39. Stereonet data of 56 dike plane orientations from the Sunset Ridge-San Antonio Canyon Block. The diagram on the right was generated in the Stereonet 9 program. The grey lines are dike planes and the black dots are poles to those planes. The contouring method is 1% area method. The rose diagram in the center contains 10° bins, and the diameter of the circle represents 50%. The diagram on the left is a statistical stereonet diagram. The white lines represents the mean orientations for the dataset, the length of this line represents percentage of the population displaying the trend and the width of the wedge indicates the standard deviation of the population. (Marshak 2016)

3.3 Clast Size Distribution

In addition to measuring strike and dip of various structures, I also measured mean clast diameter for each of the clasts documented within Hog Back landslide. Diameters were converted to volumes in cubic feet, using the equation for volume of a sphere. Results are shown in map view in Figure 6 and Figure 40, where clast sizes are plotted as graduated circles corresponding to volume. In this scheme, a 10 ft^3 clast has a diameter of 2 ft, and a 100 ft^3 clast has diameter of 5 ft, etc. I also used stereonets to show the statistical variation of clast size with foliation orientation, as described below. Later, in the discussion section, I plot the data in a series of histograms that reveal the variation of clast size with foliation strike.

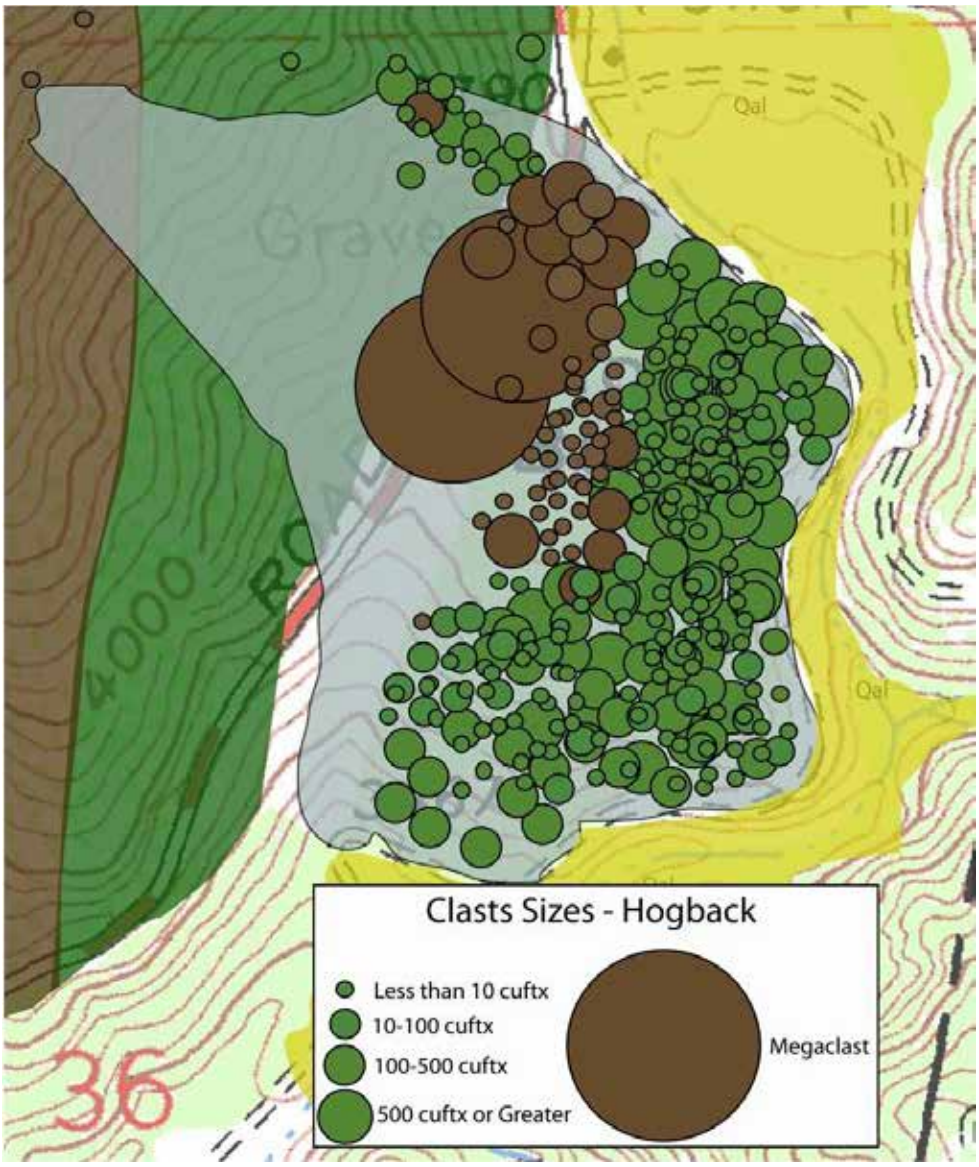

Figure 40. Clasts sizing within the Hog Back slide. Mean diameters were converted to volumes and subdivided into five size categories: less than 10 cuft, 10-100 cuft, 100-500 cuft, greater than 500 cuft, and megaclast.

3.3.1 Foliation Orientation by Clast Size: Felsic Gneiss

After compiling the field data for the felsic gneiss slide clasts, it was observed that the western portion of the slide mass maintained orientations that were nearly identical to the in-place source area. The felsic gneiss exposure along the Mt. Baldy Road (**Figure 41**) is more likely to have come down as a megaclast than as a group of clasts.

This is shown in the stereonet plot where the recorded foliations were nearly identical to one another in the Mt Baldy Road cut (**Figure 42**).

Figure 41. Photo of the Felsic Gneiss Megaclast exposed along the Mount Baldy Road, looking south.

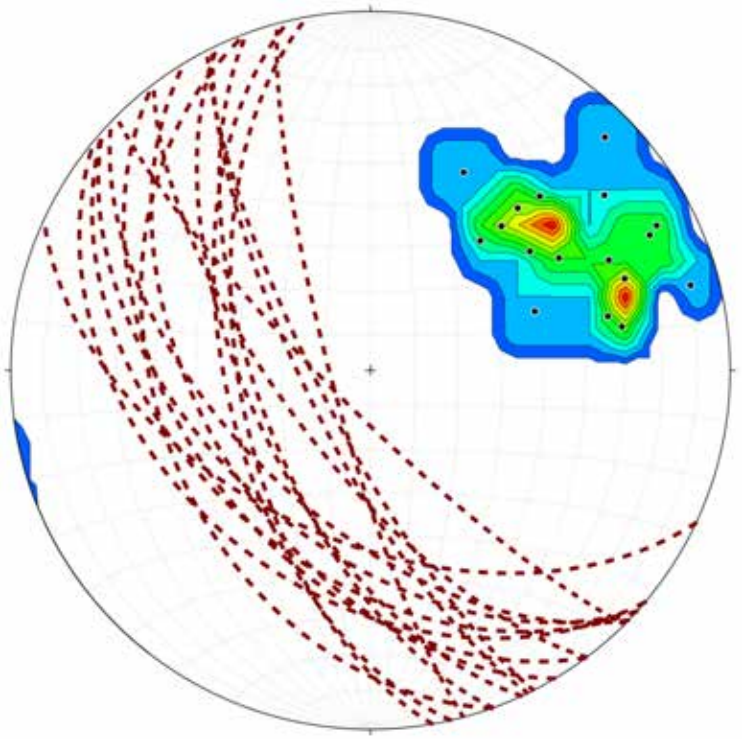

Figure 42: Stereonet of the foliations measured in the Felsic Gneiss Megaclast. There are 16 total orientations. The average strike is 142 degrees.

My general impression from field observations is that the smaller clasts of felsic gneiss to the east of the Mt. Baldy road cut (**Figure 43**) came off of the megaclast during and after transport, whereas larger clasts remained on-strike with the source area. As shown on the stereonet of **Figure 44**, the smaller clasts had more random orientations when the observations went further to the east.

Figure 43. Smaller Felsic Gneiss clasts east of the megaclast.

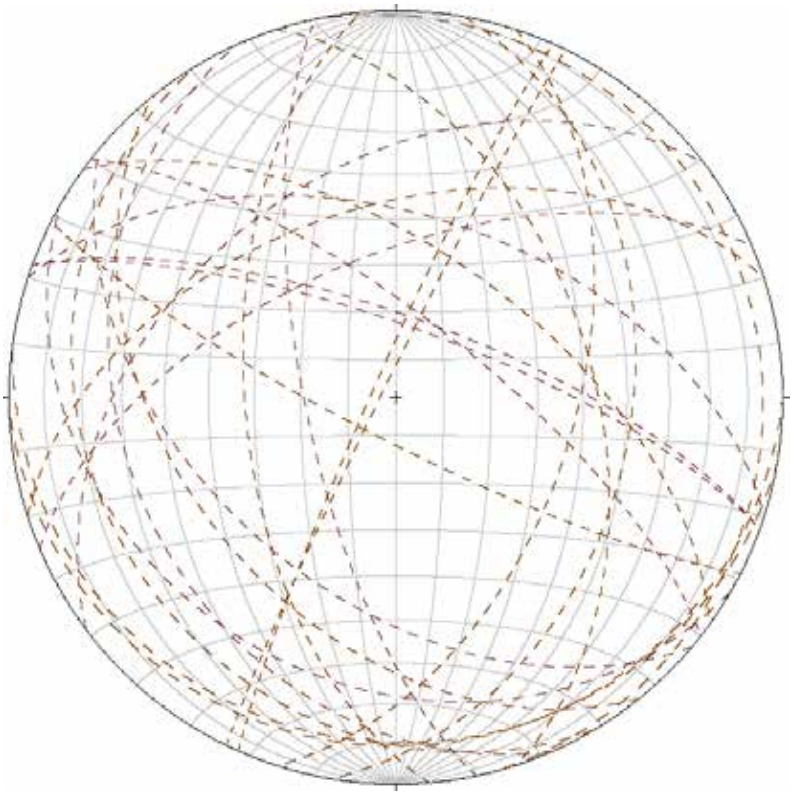

Figure 44. Stereonet of the foliations measured in the smaller Felsic Gneiss clasts measured east of the Mt. Baldy Road.

3.3.2 Foliation Orientation by Clast Size: Quartz Diorite

After compiling the field data for the quartz diorite slide clasts (**Figures 45 and 46**) , it was observed that the eastern slide mass did not maintain orientations that were recorded in the in-place source area. The quartz diorite clasts were more likely to have come down in large to small blocks that broke up into finer clasts as the slide moved eastward. This is shown through stereonet plots of field measurements (**Figures 47, 48, and 49**) in that the recorded foliation orientations are generally random to one another. Small groupings of clasts had similar orientations when compared to one another in their area. Overall, however, there were random orientations in which only a small percentage of the field observations were close to the predominantly southwest-dipping foliations of the source rock. Even the larger clasts (**Figure 47**) did not remain on-strike with the source area. It is more likely that the distance from the source area allowed the clast to shift and tumble away from the in-place orientations. The smaller clasts displayed more random orientations when the observations went further to the east. (**Figures 48 and Figure 49**). It is also believed that the felsic gneiss megaclast had so much mass that it was able to compress and push the quartz diorite clasts out of their original orientation.

Figure 45. Various sizes of Quartz Diorite clasts, looking east on the Hog Back Slide.

Figure 46. Various sizes of Quartz Diorite clasts, looking northeast on the Hog Back Slide**.**

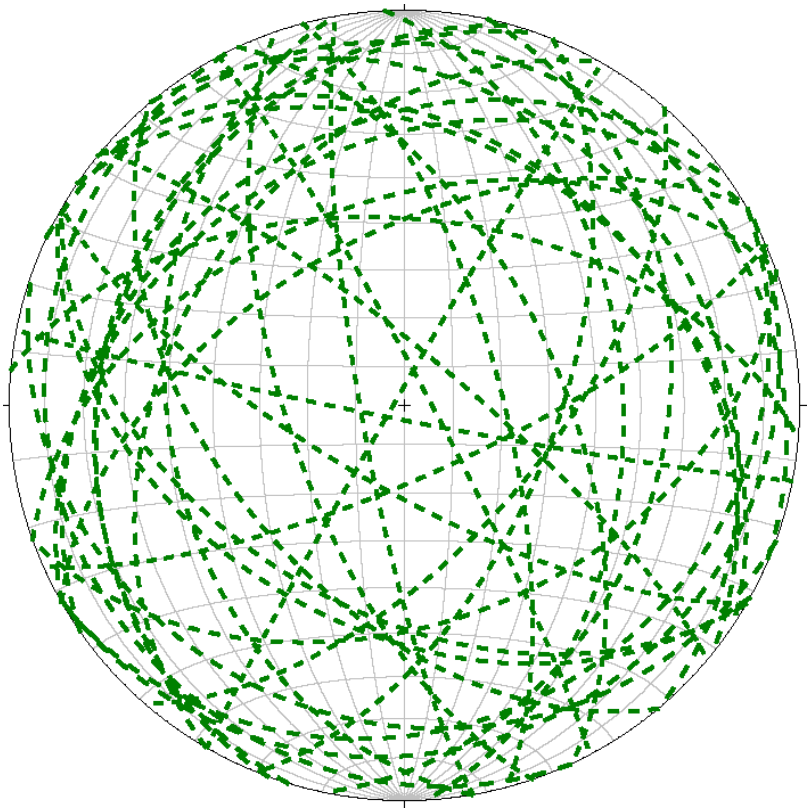

Figure 47: Stereonet of the foliations measured in the Quartz Diorite large clasts.

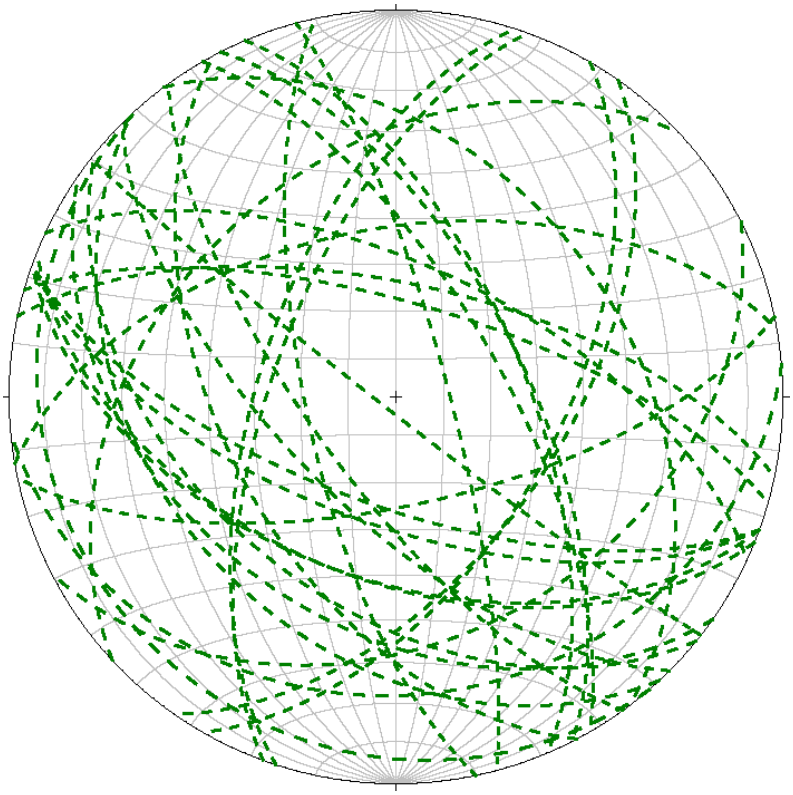

Figure 48: Stereonet of the foliations measured in the Quartz Diorite medium clasts.

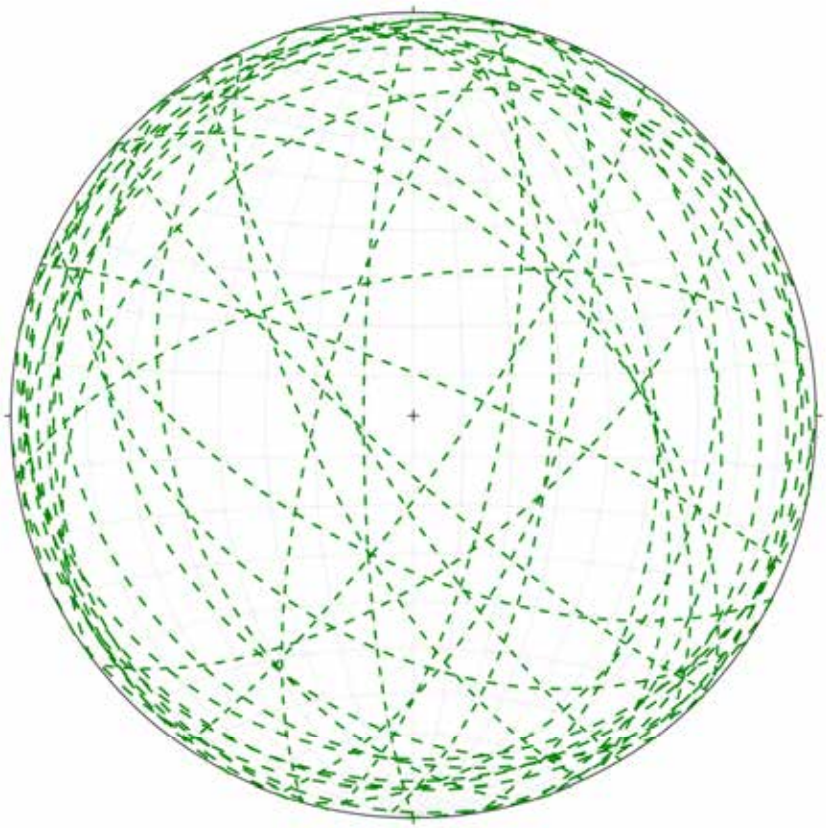

Figure 49: Stereonet of the foliations measured in the Quartz Diorite Small Clasts

CHAPTER 4: INTERPRETATION AND DISCUSSION OF DATA

In this section I discuss the relationship of my data set to the two hypotheses proposed earlier: (1) Hog Back landslide failed as a semi-coherent mass, preserving –pre-slide stratigraphy and structural orientations, and (2) Its translatory mode of failure aided in the preservation of the contacts between rock units, and consistently oriented structures, both of which can be observed in the field. To accomplish this I will address in detail seven related Research Questions.

4.1 Discussion of Research Questions

1. What are the geologic and structural characteristics of the slide scar region?

The geological characteristics of the intact bedrock in the slide scar region are mapped on **Figure 6**. The area is underlain by two main foliated rock units: Precambrian felsic gneiss and Cretaceous quartz diorite. The Gneiss overlies the quartz diorite along a moderately southwest-dipping contact that is crosscut by Hog Back landslide scar. In addition to these two rock units, there are numerous Mid-Miocene dikes of basalt, dacite, and andesite composition. Quartz veins and pegmatite dikes are also present, however, the age of these features are unknown. Lastly, there are unconsolidated colluvial deposits of angular pebble, cobble, and boulder sized material that form rubble at the base of slopes.

The structural characteristics of the slide scar region include foliation and systematic faulting and fracturing of the in-place rock units. In general, foliations in the region of the slide scar strike northwest and dip to the southwest. Specifically, the mean strike is 118 degrees and the mean dip is 53 degrees to the southwest for the felsic gneiss (**Figure 20)** and 135 degrees and the mean dip is 54 degrees to the southwest for the

quartz diorite **(Figure 22**). This orientation does not create an adversely dipping slide condition. However, there is also an indication of a basement antiform possibly buried by colluvium in the middle part of the slide scar. As discussed later, a dip reversal to the southeast in this area would provide a good place to localize sliding. Also observed in the rock units were stretching lineations (defined by elongate minerals), and slickenlines or slickensides that record pre-slide displacements on fault planes.

My stereonets of **Figures 24 and 25** illustrate several populations of fractures and joints that are important for assessing the stability of the slide area. Perhaps most important are joints that have a northeast strike and steeply dip to the southeast. These create a preferred geometry for hypothetical tension fractures (rear release fractures) that are discussed later. The slide mass was translated in a southeast direction orthogonal to these fractures. Also important are steeply dipping fractures and joints with northwest strikes. This orientation is conducive to creating low-cohesion side-release planes that may have facilitated breakaway of the slide block. Finally, there is a statistically significant population of moderately southeast-dipping joints mapped in the quartz diorite unit (**Figure 25A**).

2. *How much translation of marker units and contacts occurred during slide emplacement*? *How much rotation?*

As shown in **Figures 50 and 51**, there was an approximate translation of 1,300 foot of the marker units from the in-place slope to the resting slide area in the southeast as measured by the displaced gneiss-quartz diorite contact mapped on **Figure 6**. This marker unit contact is clearly demarcated in the clast distribution of the slide mass. The rockslide was translational and coherent enough during down-slope transport to maintain

a unit contact. The contact of these two marker units was made by the clasts that did not intermix during the slide process. The observation was first noted in 1987 by Herber. According to Herber, any small rotations and translations were most likely caused by slight internal disruptions that lead to a near jumbled surface. Previous fractures, jointing, and epidote surfaces are more likely to aid in the jumbled appearance.

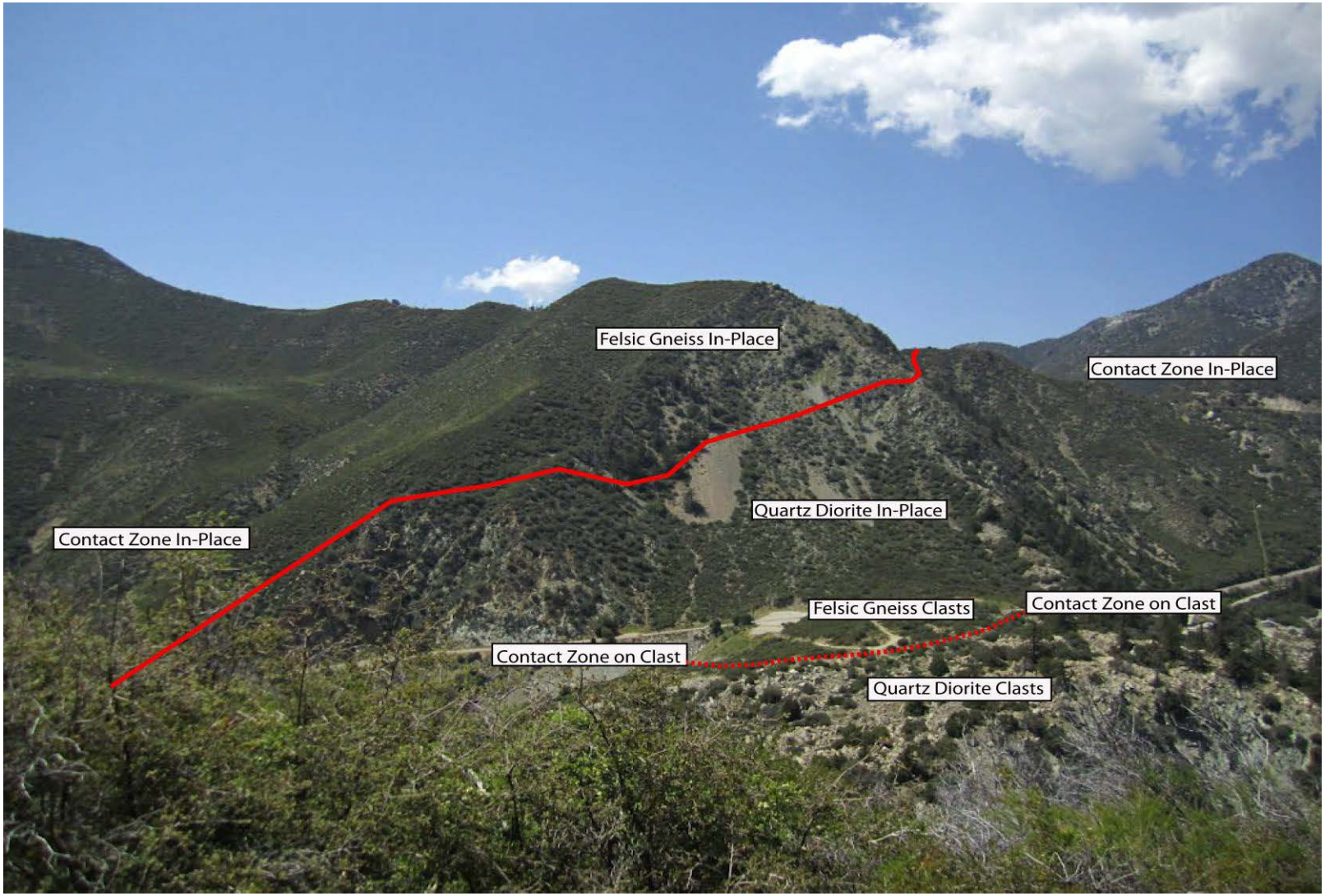

Figure 50. Photo of the present Hog Back Slide and scar, looking west toward Sunset Ridge. Solid red line shows location of the intact gneiss-quartz diorite on Sunset Ridge. Dashed red line shows the displaced contact within Hogback Landslide

Figure 51. Vertically oriented Google Earth image of Hog Back Landslide and it's breakaway scar. Solid and dashed red lines indicate locations of the intact and displaced gneiss-quartz diorite contact, respectively. Felsic gneiss is on western side; quartz diorite on the eastern side.

In general, the slide blocks derived from the Felsic Gneiss marker unit display little rotation as compared to the in-place rock. The traces of most foliation planes plotted on **Figure 52** overlap nicely. However, part of the felsic gneiss appears to have broken off as a megaclast in which a measurable clockwise rotation is documented. As discussed earlier, the megaclast block of felsic gneiss along the Mount Baldy road cut preserves a common southwest-dipping foliation. In detail, its foliation strikes have rotated off strike by a mean of 24 degrees clockwise relative to the in-place bedrock (**compare Figure 20 with Figure 42**). Furthermore, several large blocks of felsic gneiss that were found further to the east had rotated of 40 to 50 degrees off strike of the in-place rock. There were only four measurements taken here due to the extent of soil and vegetation cover.

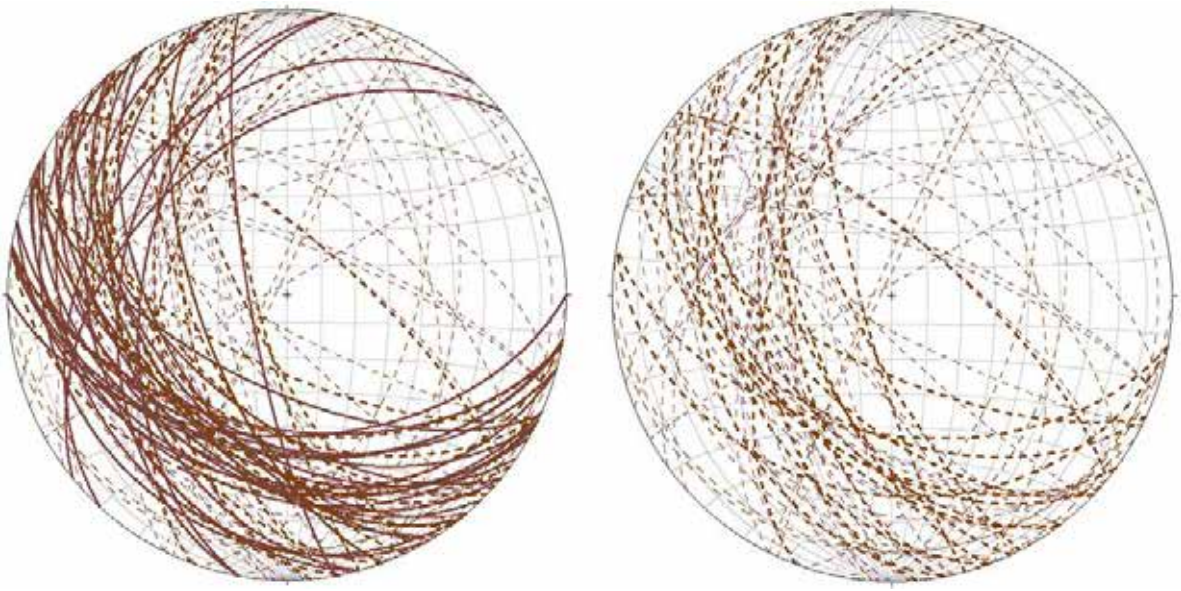

Figure 52: Left: Composite stereonet showing foliations of in-place felsic gneiss (bold solid lines) relative to large clast and medium clasts of felsic gneiss (dashed lines). Right: The various felsic gneiss clast sizes (small, medium, large). Line weights are related to clast sizes**.**

The quartz diorite marker unit exhibited a large degree of rotation during slide emplacement (**Figure 53**). There were very few matching trends in the quartz diorite marker unit to track a level of rotation. The abundance of fractures and joints within the quartz diorite marker unit more than likely caused the slide mass unit to be chaotic.

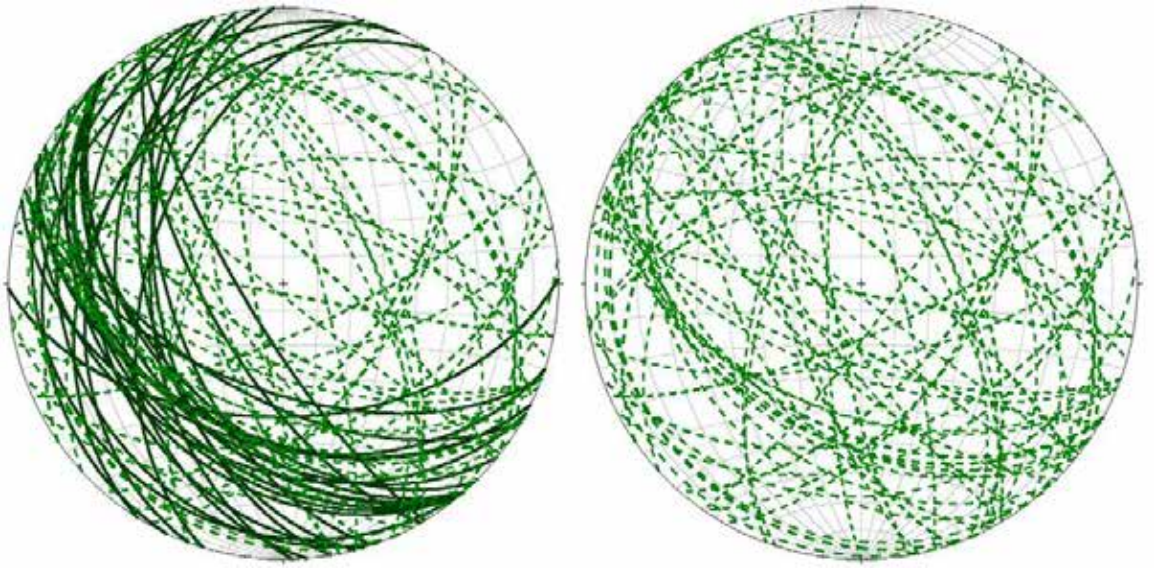

Figure 53: Left: Composite stereonet showing foliations of in-place quartz diorite (bold solid lines) relative to large clast and medium clast of quartz diorite (dashed lines). Right: The various quartz diorite clast sizes (small, medium, large). Line weights are related to clast sizes.

3 Are there chaotic vs. ordered clast orientations?

In general, the larger clasts in the felsic gneiss unit are more likely to have maintained northwesterly foliation strikes and southwest dips similar to those of the in-place rock in the slide scar (**Figure 27**), but the larger quartz diorite clasts display almost random orientation of foliation (**Figure 47**) . It was also observed that the Felsic gneiss clasts that were small and medium were less abundant than the Quartz Diorite clasts that were small and medium (compare **Figure 44 with Figures 48 and 49**). **Figure 54** (below) provides another way of viewing this same relationship. There was a megaclast of the felsic gneiss marker unit in the slide mass, but no comparable quartz diorite megaclasts were observed in the area. As best shown in **Figure 40**, there were far more quartz diorite clasts than there were felsic gneiss clasts. This could be caused by there being more pre-existing fractures within the quartz diorite than within the felsic gneiss.

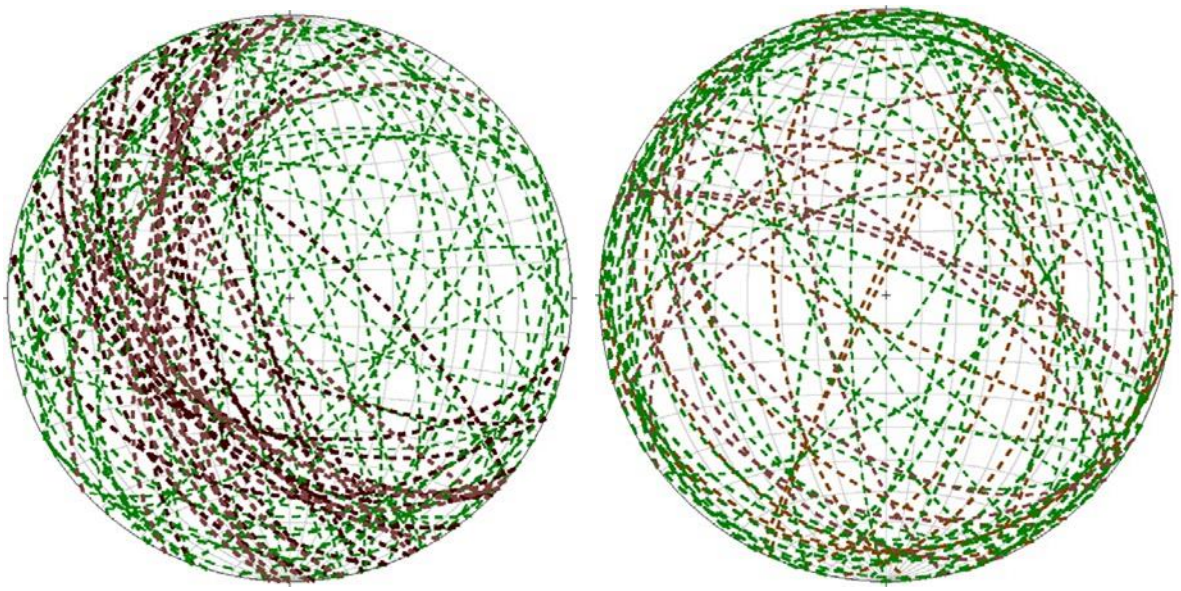

Figure 54: Left: Composite stereonet plot showing foliations of large clasts of felsic gneiss (brown) and quartz diorite (green). Right: Composite plot showing foliations of small and medium clasts of felsic gneiss and quartz diorite. The colors are: felsic gneiss (brown) and quartz diorite (green).

4. Are there statistical differences in orientation between small vs. large clasts?

As discussed in Question #3, the quartz diorite clasts had far more variance in the observed foliation than the felsic gneiss clasts, and there is a sense that smaller clasts tend to be more chaotically oriented. Another way to analyze this relationship is to use a series of histograms (**Figures 55-57**) to plot the number of measurements for specific ranges of foliation strikes.

A baseline data set is provided by **Figure 55** which shows the existing variation in foliation strike for in-place outcrops of felsic gneiss and quartz diorite. This chart confirms the preponderance of strikes in the northwest quadrant (between azimuth of 271 and 360), associated with southwest-dipping foliation. One minor anomaly in this data set is the grouping of felsic gneiss strikes between 31 and 60 degree azimuth. These data reflect 9 measurements with generally northwest dips, most of which that were mapped near the crest of Sunset Ridge away from the landslide scar (**Figure 6**).

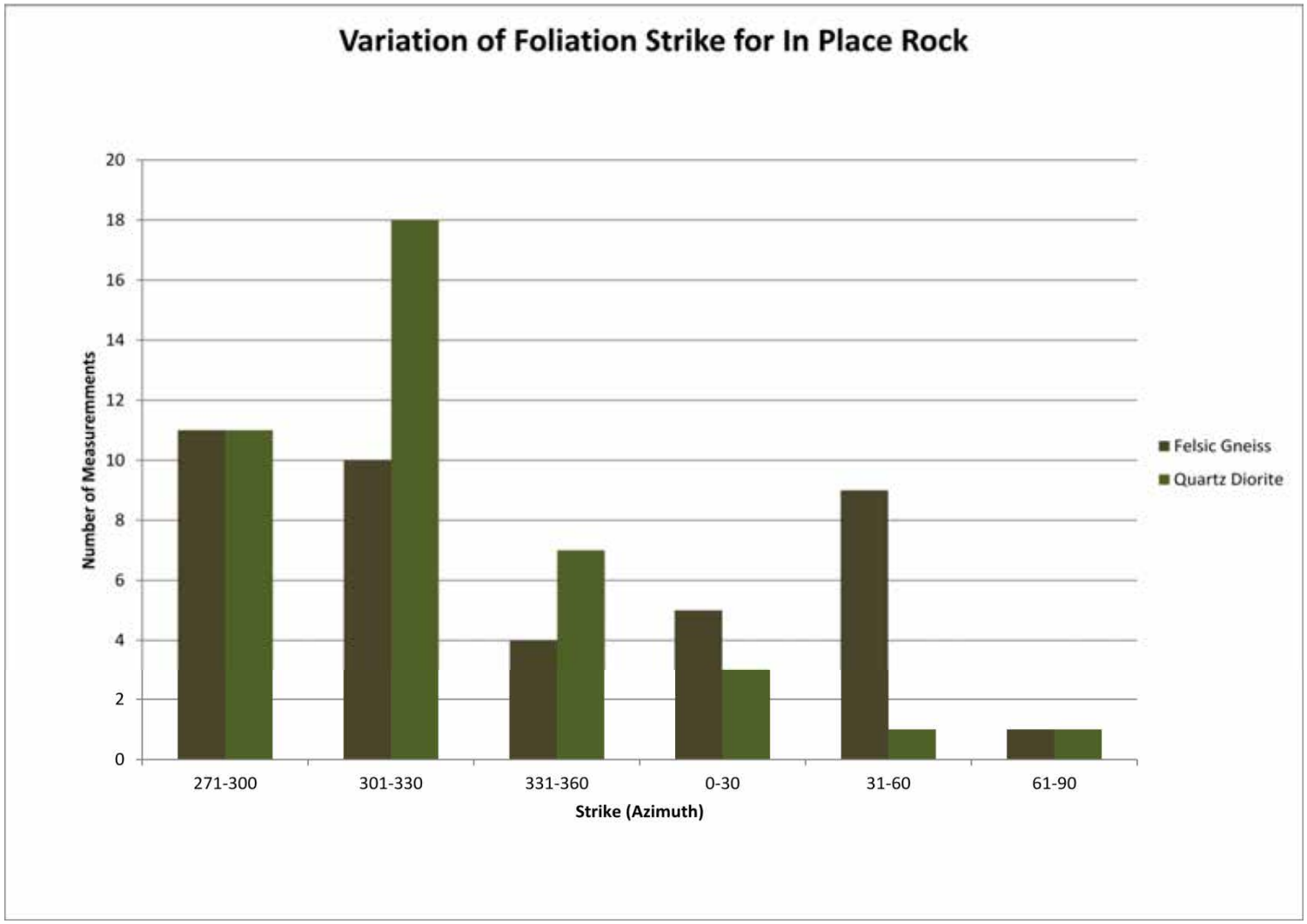

Figure 55. Comparative histogram for in-place bedrock measurements. This plot shows total number of felsic gneiss vs quartz diorite bedrock outcrops measured, plotted against foliation strike. Strikes originally recorded in southern quadrants are converted to equivalent northern azimuths.

Figures 56 and 57 show variation of foliation strike measured from both clast types. The most striking feature of **Figure 56** (which does not distinguish clast size) is that almost all of the felsic gneiss clasts record northwest striking foliations (azimuths between 271 and 360 degrees), whereas more than 1/3 of the foliations in the quartz diorite clasts strike northeast (azimuths between 0 and 90 degrees). Although the majority of quartz diorite clasts still record northwest striking foliation, the contrast with the felsic gneiss clasts stands out, as it did in a comparison of stereonet plots of **Figures 27 and 30**.

Figure 57 displays the data from both clast types according to clast size and foliation azimuth. This plot is a bit more complex, but it shows that small and medium sized clasts tend record a wide range of foliation strikes, whereas the large clasts tend to fall within the azimuth range of 271 to 360. This is especially evident for the large felsic gneiss clasts. The small clasts of the quartz diorite are especially scattered, with orientations that cover all of the strike azimuths. These relationships support the previous discussion under Question #3.

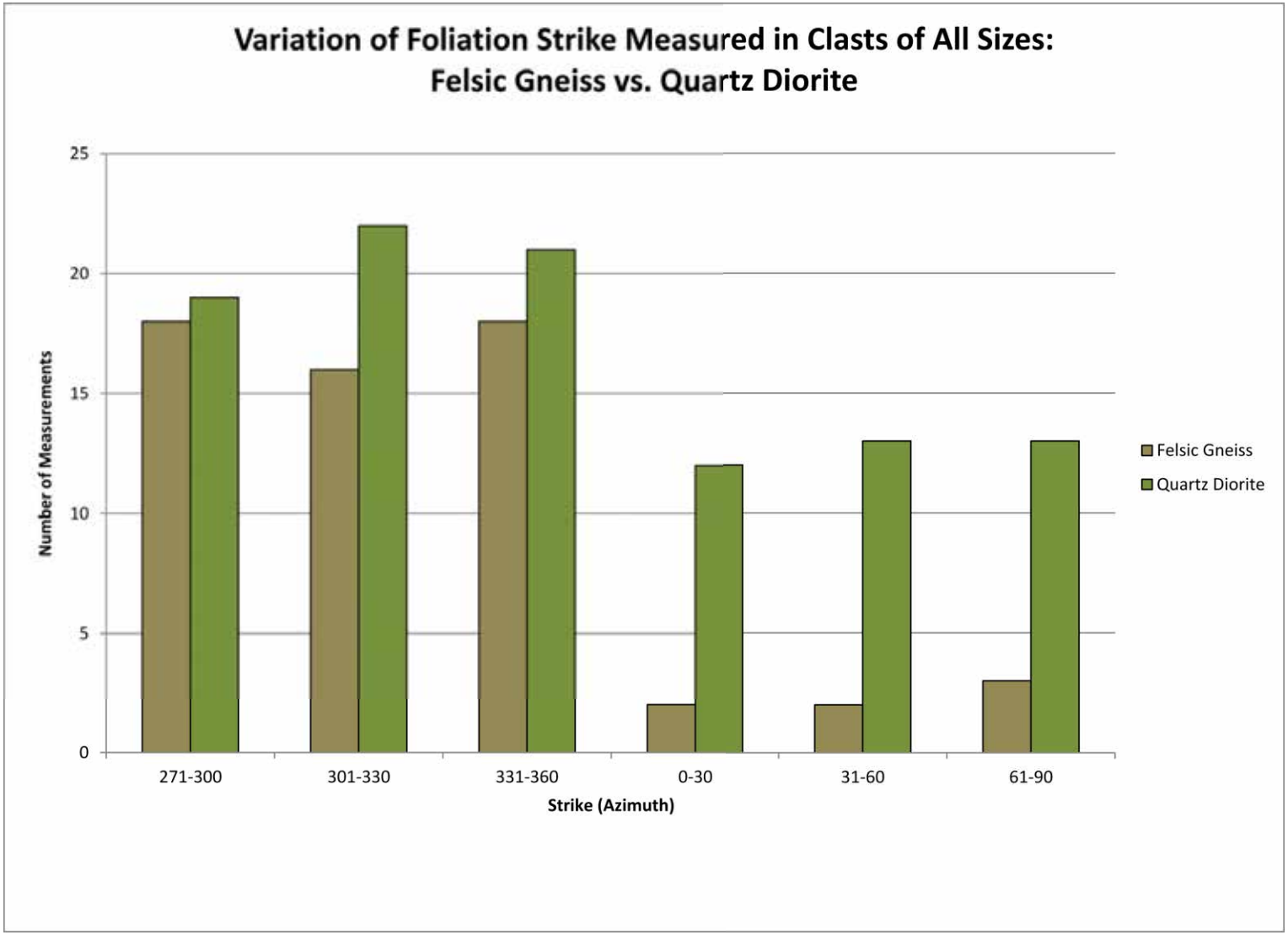

Figure 56. Histogram showing total number of felsic gneiss vs quartz diorite clasts measured, plotted against foliation strike. Strikes originally recorded in southern quadrants are converted to equivalent northern azimuths.

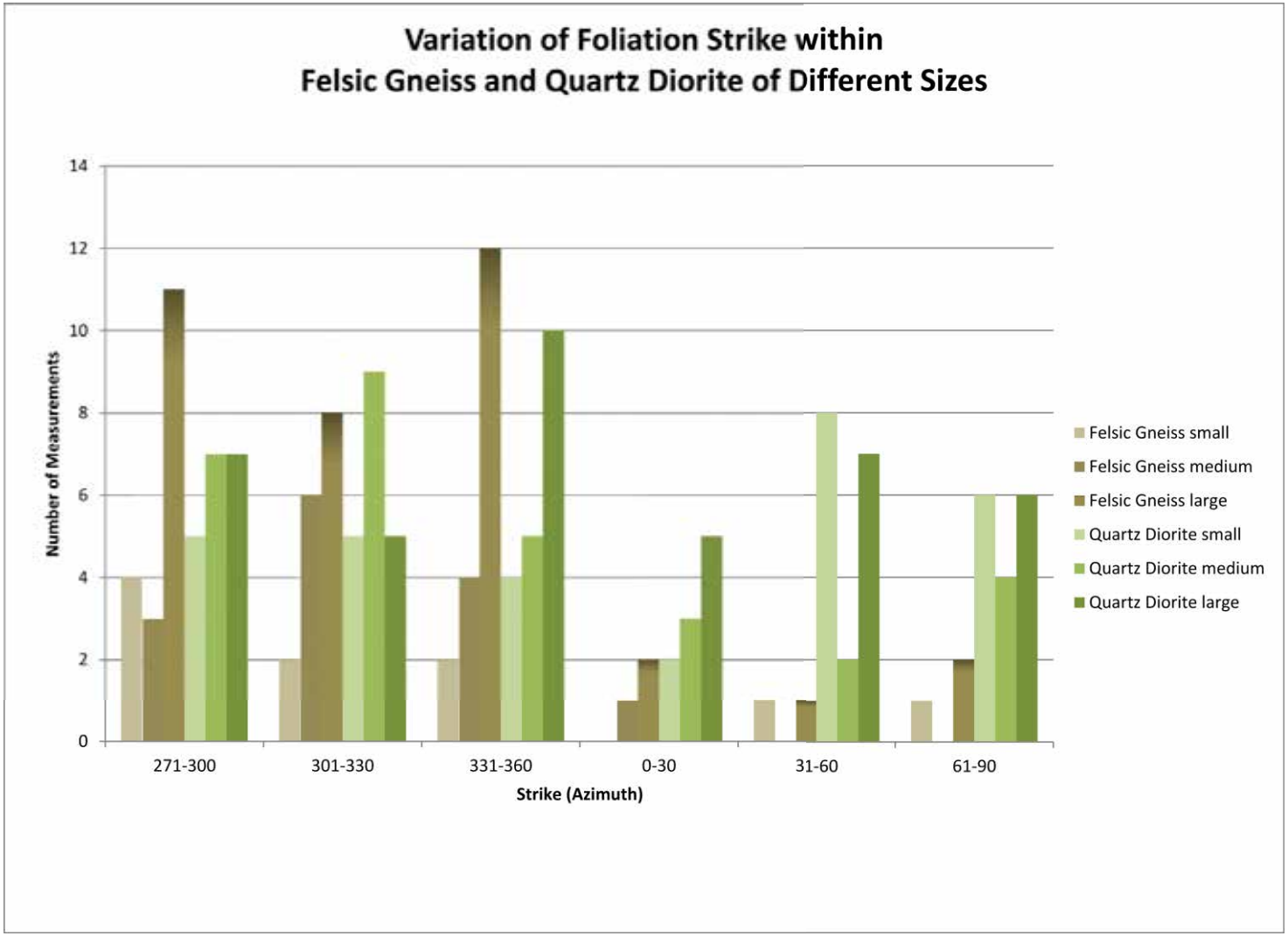

Figure 57. Composite histogram showing variation of clast sizes with foliation strike for all felsic gneiss and quartz diorite clasts measured within Hog Back Landslide. Strikes originally recorded in southern quadrants are converted to equivalent northern azimuths .

5. How does the intact bedrock structure compare with that of the clasts?

There is no question that the Hogback landslide originated from a specific area on the east face of Sunset Ridge. In addition to containing two very distinct rock units, multiple structural elements (metamorphic foliation, joints, fractures, slickensided fault surfaces) are common to both the source area and the slide mass. The main question is: How do the orientations of these structural features compare between in-place and displaced rock?

After compiling the field data for in-place bedrock and the landslide clasts it was observed that foliations of clasts within the slide mass generally maintained a similar northwest strike and a southwest dip. This orientation is strikingly similar to the gross foliation of the bedrock source area. However, there is a section within Sunset Ridge had a different pattern of foliations, where there were strikes to the northeast and dips to the northwest. These measurements occurred in an area that was in the middle of the slope (**Figure 6**). Also, they occurred at nearly the same elevation on the eastern slope. It is possible that this feature represents the remnants of a fold structure within the landslide scar (see later discussion).

Comparison of the fracture and joint populations between the two areas is difficult to assess. There is the wide range of joint orientations present within the intact bedrock source area (**Figures 25A and 25B**). Unfortunately, the only such structures measured in the landslide clasts were epidote-slickensided faults. These are not distinguished from similar joints from the bedrock source area on **Figures 35 and 36**, so correlation is not possible without separating the two data sets.

As discussed previously under Question 2, felsic gneiss slide clasts in the western slide mass display foliation orientations that appear to be rotated 30+ degrees clockwise

from foliations in the bedrock source area. This is shown through field measurements in that the recorded foliations were nearly identical to one another in the Mt Baldy Road cut but different from those in outcrops of the source gneiss farther west. Regarding the field data for the quartz diorite slide clasts, however, the eastern slide mass did not maintain orientations that were found in the in-place source area.

6. How did the slide fail? What were the most likely mechanisms?

Preliminary assessment of this question is based on some general inferences from inspection of structural patterns, and constraints provided by the displaced contact. My brief speculations presented here are later supported by safety factor calculations that build in the actual geometry and structure of the site.

The slide most likely failed due to the fracture network within the pre-slide slope surface. Along with minor faults within the in-place rock, fractures and joints may have allowed the mafic dikes to penetrate into the host rock during the Miocene (Marshak, 2016). After this event, water from storm events was able to flow into apertures within the rock to erode some to the mafic dikes that were extruded there. The fracture and joint systems that were present could have interconnected where the water would flow to the bottom of the slope. This action may have produced seasonal springs in the slope face, as illustrated in **Figure 58**. Over a period of time, the waters that percolated within the fractures of rock began to freeze and thaw. This action may have begun to reduce the cohesion of the rock, causing the slide. Alternatively, cohesion could have been reduced during an earthquake (large earthquakes are certainly known in this area)

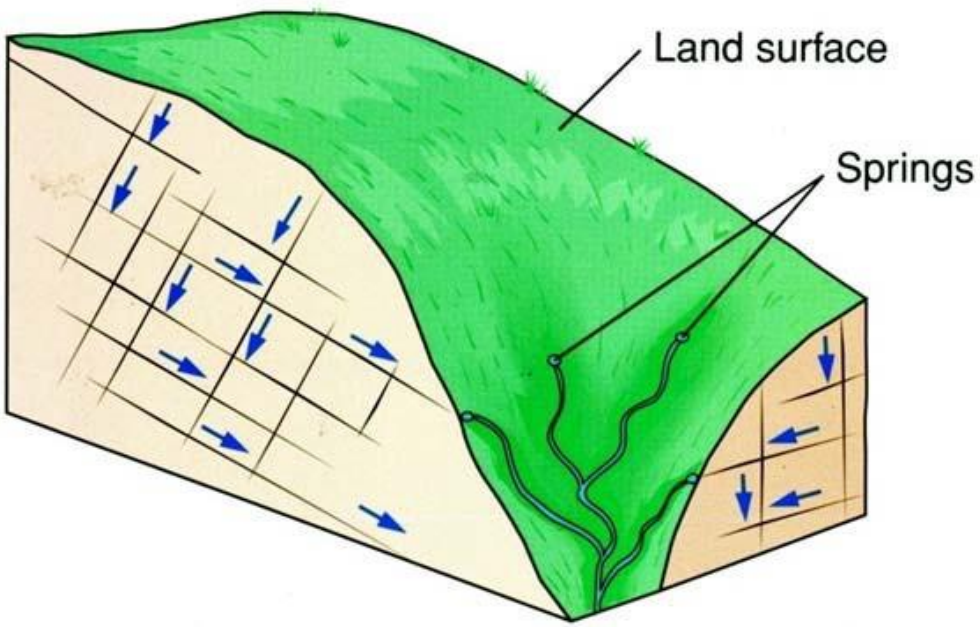

Figure 58. Possible fracture and spring system in pre-failure Hog Back slope.

7. Can various safety factor parameters be resolved or constrained?

To better understand how Hog Back landslide initially failed, one needs to hypothetically recreate the geometry, shear strength, and water conditions at the time of failure. Safety factor analysis is a commonly used engineering practice that allows quantitative assessment of two key shear strength parameters: **cohesion** (C) and **angle of internal friction** (Φ). Below I present two different safety factor approaches, with the goal of deducing various possible combinations of cohesion and friction angle that led to landslide failure.

4.2 Safety Factor Approach #1: Application Of Site Geometry Parameters Presented In Herber (1987)

The GSA centennial article by Larry Herber (1987) presents nicely scaled drawings of Hog Back Landslide from which important dimensions and angles may be extracted for use in safety factor calculation. As shown on Figures 59 and 60, the combination of geologic map and cross section implicitly provides all of the fixed quantities needed for input to the safety factor equation.

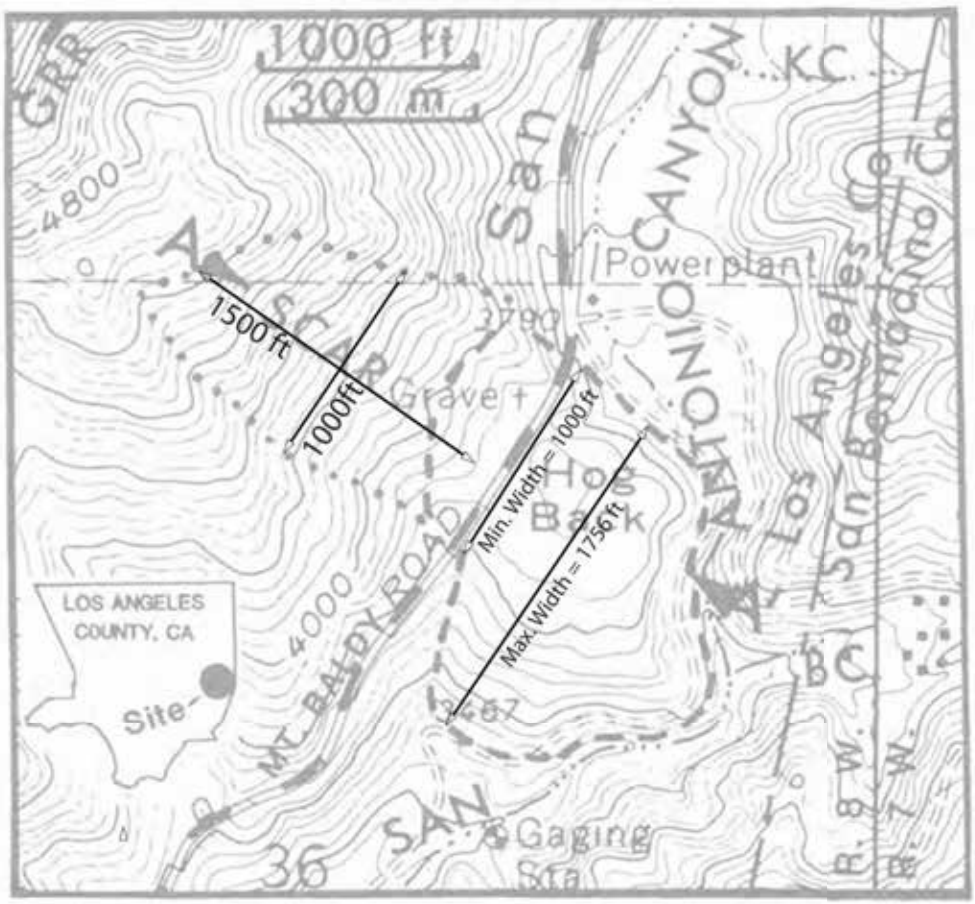

Estimated Slide Plane Area in Plan View:

(1500 ft)(1000 ft) = 1,500,000 sqft

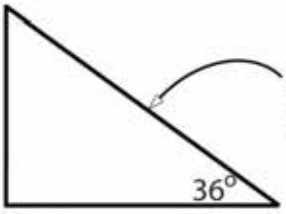

Slide Plane Area along 36° slope:

Area of basal slide plane

Area = (1,500,000 sqft)/(cos 36°) = 1,854,101 sqft

Mean Distance Perpendicular to line of Section:

$$\frac{(1000\text{ ft} + 1756\text{ ft})}{2} = 1378\text{ ft}$$

Figure 59. Geologic map of Hog Back landslide from Herber (1987), showing important dimensions used to constrain the size of the landslide and dimensions of the slide plane. Calculations are given to show values used in the safety factor analysis.

Slide Volume Adjusted for Porosity of 40%:

$$\text{porosity} = \frac{V_{voids}}{V_{bulk}} = \frac{V_{voids}}{V_{rock} + V_{voids}}$$

V_{voids} = (0.40)(405,793,440 cuft) = 162,317,376 cuft

V_{rock} = 405,793,440 cuft - 162,317,376 cuft = 243,476,064 cuft

Slide Weight = $(V_{rock})(\rho_{rock})$
= (243,476,064 cuft)(160 lbs/cuft)
= 3.896×10^{10} lbs

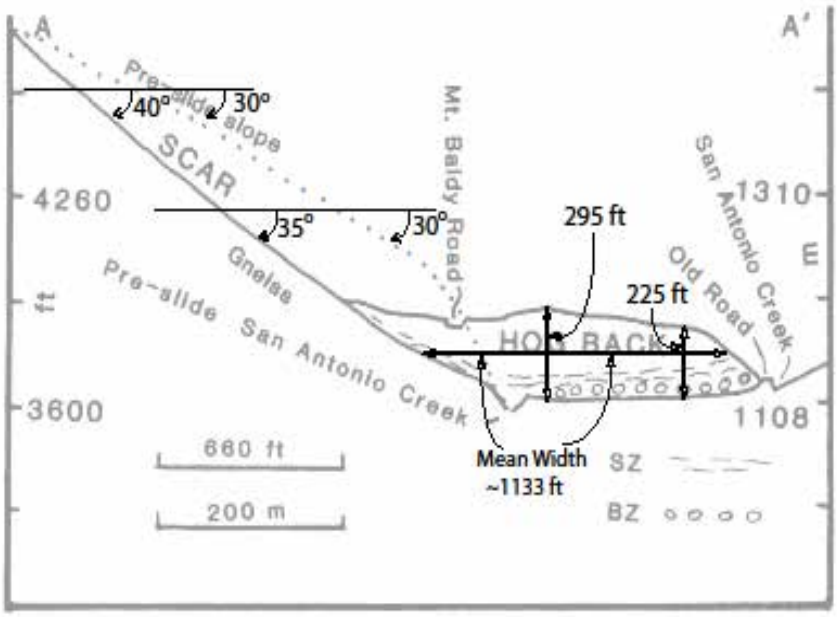

Area estimate along cross section A-A' = (Mean Height)(Mean Width)

$$\frac{(295 \text{ ft} + 225 \text{ ft})}{2}(1133 \text{ ft}) = 294{,}480 \text{ sqft}$$

Slide Volume estimate =
Area along profile A-A' multiplied by the mean width perpendicular to section
= (294,480 sqft)(1,378 ft) =405,793,440 cuft

Figure 60. Geologic cross section through Hogback landslide from Herber (1987), showing important angles and dimensions used to constrain the size of the landslide and dip of the slide plane. Calculations are given to show values used in the safety factor analysis.

Using the map scale with a ruler and protractor and some basic geometry and algebra, I was able estimate the following parameters (all units are in English system, following engineering convention):

Θ= Dip of slide plane = 36^0

A = Area of slide plane = area in plan view projected onto 36 degree slope = 1,854,101 ft^2

V = Slde volume (converted to volume of non-porous crystalline rock) = 243,476,064 ft^3

W = Weight of slide block (assuming unit weight of 160 lb/ft^3) = 3.896 x 10^{10} lbs

h = height of breakaway point above bottom of slide plane = 920 ft

These quantities are illustrated below on the schematic cross section of Hog Back Landslide (**Figure 61**). The weight of the slide block is broken into perpendicular and parallel components with respect to the dipping slide plane. The stability of the slope is governed by a safety factor equation that varies depending on whether or not water is present.

Herber Hog Back Dimensions; SF equation with no water.

$$SF = \frac{\text{Resisting Stress}}{\text{Driving Stress}} = \frac{C+\tan\Phi\,[(\text{Weight})\cos\text{Ø}/(\text{Area})]}{(\text{Weight})\sin\text{Ø}/(\text{Area})}$$

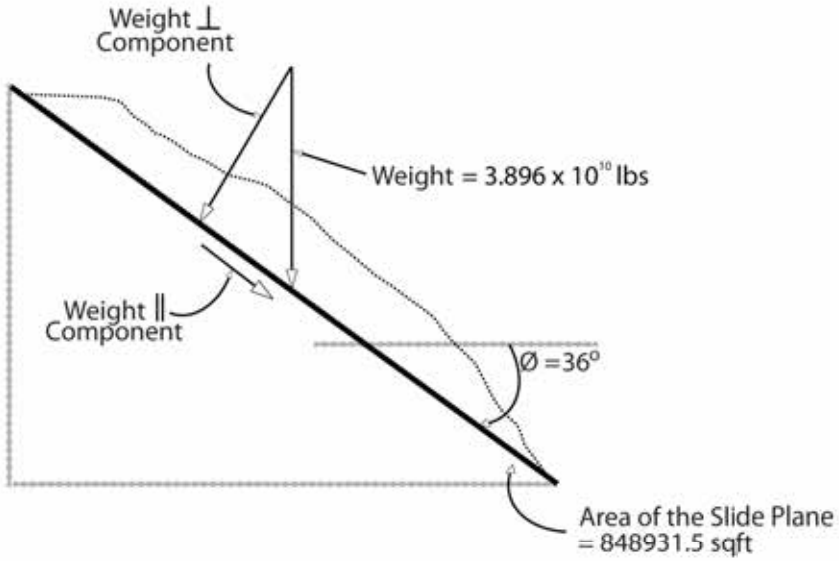

$$SF = \frac{C+\tan\Phi\,[(3.896 \times 10^{10}\ \text{lbs})\cos\text{Ø}/(848931.5\ \text{sqft})]}{(3.896 \times 10^{10}\ \text{lbs})\sin\text{Ø}/(848931.5\ \text{sqft})}$$

$$SF = \frac{[C+\tan\Phi\,(37128)]\text{lbs/sqft}}{(26975\ \text{lbs/sqft})}$$

C	Φ	SF
0	40	1.15
0	36	1.00
0	30	0.79
0	20	0.50
0	10	0.24

$$SF = 1.00 = \frac{[C+\tan\Phi\,(37128)]\text{lbs/sqft}}{(26975\ \text{lbs/sqft})}$$

$$(26975\ \text{lbs/sqft}) = C+\tan\Phi\,(37128)]\text{lbs/sqft}$$

C	Φ	SF
0	36	1.00
500	35.49	1.00
1000	34.9	1.00
2000	33.9	1.00
5000	30.6	1.00
10000	24.6	1.00
20000	10.6	1.00
25000	3.04	1.00

Figure 61. Schematic cross section showing pre-slide geometry of Hog Back landslide recreated from Herber (1987) drawings. Key forces and angles applicable to safety factor analysis are also indicated.

4.2.1 Safety Factor Under Dry Conditions

This is the simplest case in which the dry shear strength of the slide plane resists downward translation induced by weight component parallel to the slide plane. The appropriate safety factor equation is relatively simple, with shear strength given by Coulomb's Law of Friction :

$$\mathbf{SF_{dry} = Resisting\ Stress\ /\ Driving\ Stress} = \frac{\mathbf{C+\tan\Phi\ [W\cos\Theta/A]}}{\mathbf{W\sin\Theta/A}}$$

where, SF is the safety factor, Θ is the dip of the slide plane (36 degrees for this case), C is the cohesion, Φ is the angle of internal friction, W is the weight of the slide block, and A is the area of the basal slide surface.

4.2.2 Safety Factor Under Wet Conditions

This case assumes that water has permeated a through-going fracture along the base of the slide block. The resulting water pressure has a triangular distribution as shown in **Figure 61**, and acts as a buoyant force against the perpendicular component of the slide block weight, thereby lowering the effective normal stress and shear resistance acting along the slide plane. Calculation of the average water pressure took some thought. From **Figure 61**, it can be seen that the water pressure varies from zero at the top of the slide block to 57,508 lbs/ft^2 at the toe. If one simply applies an average of these two values (28,704 lbs/ft^2) the resulting water pressure exceeds the normal stress component of the slide block weight (17,000 lbs/ft^2). This excessive buoyancy would cause the block to float, which is unreasonable. Also unlikely is a condition where water permeates the entire area of the

basal slide plane. It seems that a reduced upward water pressure is more appropriate.

To estimate water pressure acting upward along the base of the slide block, I applied a value comparable to that used in safety factor calculations for water saturated porous slide masses. In such cases the buoyancy effect of water pressure is taken to be 1/3 of the normal stress exerted by the slide mass (this works because the density of water is ~ 1/3 that of rock). So, for Hogback landslide, the average upward water pressure is assumed to be 1/3 of the 17,000 lbs/ft^2 normal stress component of the slide block weight, i.e., P_{H20} up = 5667 lbs/ft^2 .

The appropriate safety factor equation for the wet case is given by:

$$\mathbf{SF_{wet} = Resisting\ Stress\ /\ Driving\ Stress} = \frac{\mathbf{C+\tan\Phi\ [(W\cos\Theta/A)-average\ P_{H2O}Up]}}{\mathbf{W\sin\Theta/A}}$$

Safety factor equations permit the engineer to either (1) plug in known or assumed values of cohesion and friction angle to assess stability, or (2) perform a forensic "back calculation" for a specific safety factor of 1.0 to determine different combinations of cohesion and friction angle at the time of failure (failure would occur when SF =1.0). **Table 1** shows results of applying the dry and wet safety factor equations above to the geometric parameters derived from drawings in Herber (1987).

Hog Back Safety Factor Results (Approach #1): Larry Herber (1987) Slide Parameters					
Dry Case			Wet Case (Water pressure acting up along base)		
Friction Angle (Ø)	Cohesion (lbs/ft^2)	Safety Factor	Friction Angle (Ø)	Cohesion (lbs/ft^2)	Safety Factor
45	0	1.38	45	1018	1
40	0	1.15	40	2841	1
36	0	1	36	4117	1
30	2536	1	30	5808	1
25	4423	1	25	7066	1
20	6164	1	20	8226	1
15	7796	1	15	9314	1
10	9353	1	10	10353	1
7	10264	1	7	10959	1

Table 1. Results of calculations for Safety Factor Approach #1, using Herber (1987) site parameters. The family of Cohesion (C) and friction angle (Φ) values shown for SF = 1.0 are the result of "back calculation" intended to determine the range of possible shear strength constants applicable at the time of failure.

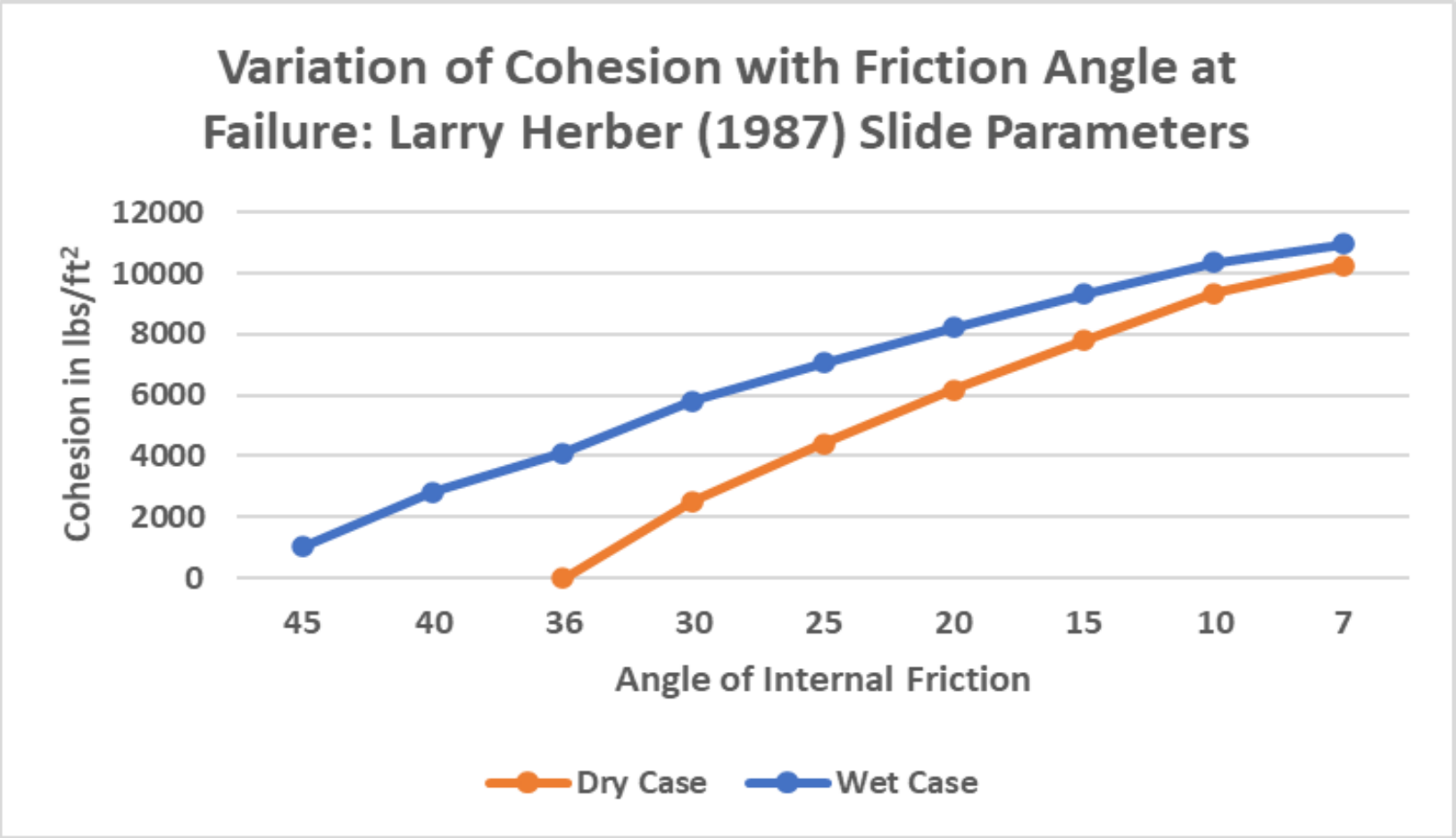

Figure 62. Graph showing different combinations of Cohesion and Friction Angle at failure for the dry and wet cases.

4.3 Safety Factor Approach #2: Slide Volume Determined From Method Of Slices; Slide Block Released At Rear By Vertical Fracture

For a comparative analysis, I chose to calculate the slide volume differently than in the Herber (1987) scenario, and also decided to consider a different release mechanism. **Figure 63** illustrates the essential geometric elements and forces applicable to safety factor calculation under dry and wet conditions. In this approach, the upper boundary of the slide volume is constrained by projecting a surface between the two sloped ridge lines that form the northeast and southwest edges of the slide scar. The lower boundary of the slide volume corresponds to a plane with a uniform southeast dip of 36 degrees. I used the method of slices to calculate the slide volume (see below). This resulted in a thinner slide block and smaller volume than that calculated using the Herber (1987) scenario. Another important difference of Approach #2 is the assumption that a vertically oriented tension fracture developed at the top of the slide block and facilitated its release. If filled with water, additional forces would have acted perpendicular to the back of the slide block, adding to the driving stress, and reducing the resisting stress.

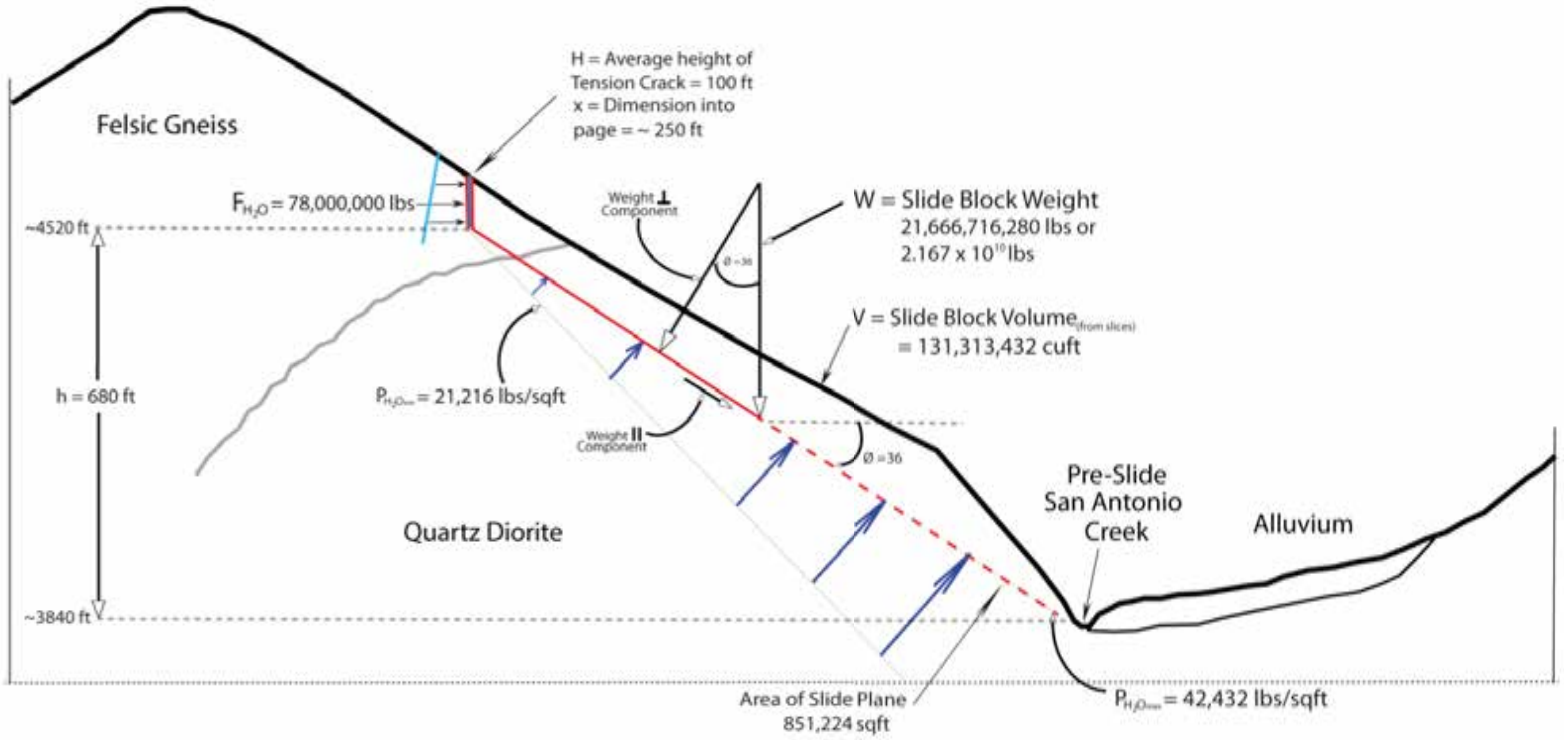

$$F_{H_2O} = (P_{H_2O\ \text{centroid of submerged area}})(\text{Area Submerged})$$
$$= (\rho_{H_2O})(50\text{ ft})(100\text{ ft})(250\text{ ft})$$
$$= (62.4\text{ lbs/cuft})(50\text{ ft})(100\text{ ft})(250\text{ ft})$$
$$= 78{,}000{,}000\text{ lbs}$$

A = Area of Slide Plane
= (Area of Scar in Plan View)/(cos 36)

$$= \frac{(1/2)(1{,}318\text{ ft})(1{,}045\text{ ft})}{\cos 36} = 851{,}224\text{ sqft}$$

W = Slide Block Weight
$= (\rho_{rock})(V)$
$= (165\text{ lbs/cuft})(131{,}313{,}432\text{ cuft})$
$= 21{,}666{,}716{,}280\text{ lbs or } 2.167 \times 10^{10}\text{ lbs}$

$$P_{H_2O_{ave}} = (1/2)(P_{H_2O_{max}})$$
$$= (1/2)(42{,}432\text{ lbs/sqft})$$
$$= 21{,}216\text{ lbs/sqft}$$

$$P_{H_2O_{max}} = \rho_{H_2O}h$$
$$= (62.4\text{ lbs/cuft})(680\text{ ft})$$
$$= 42{,}432\text{ lbs/sqft}$$

Figure 63. Cross section illustrating pre-slide geometric parameters and forces applicable to Safety Factor Approach #2

Some additional notes are worth commenting upon here before I present the related calculations:

(1) In the lower 2/3 of the slide scar, the slide plane is buried under an unknown amount of talus that was deposited in the aftermath of the slide. Without seeing the slide surface, it is assumed that the slide plane (primary failure plane) had a dip angle between 30 to 40 degrees dipping to the southeast. I used an angle of 36 degrees that is consistent with the present-day slope angle in the upper reaches of the slide scar. Herber (1987) and Roger et al. (1992) illustrate a similar angle in their figures.

(2) Given the fact that southeast-dipping fractures do not pervade mapped area of intact bedrock, one might wonder why the slide surface developed where it did. From my mapping, I noticed there is a section within Sunset Ridge had a different pattern of foliations, with a strike to the northeast and a dip to the northwest. These measurements occurred in an area that was in the middle of the slope, between 4200 and 4800 feet. Also, similar anomalous foliations occurred at nearly the same elevation in the southern canyon and along the northeastern end of Sunset Ridge (**Figure 64**). It is possible that this area represents one limb of a fold structure within the slope. Hypothetically, a complementary southeast-dipping limb may be buried beneath colluvium farther down in the slide scar, providing a point of failure for the Hog Back Slide. More measurements and focus regarding this feature are needed to determine if such an antiform exists (**Figure 65**).

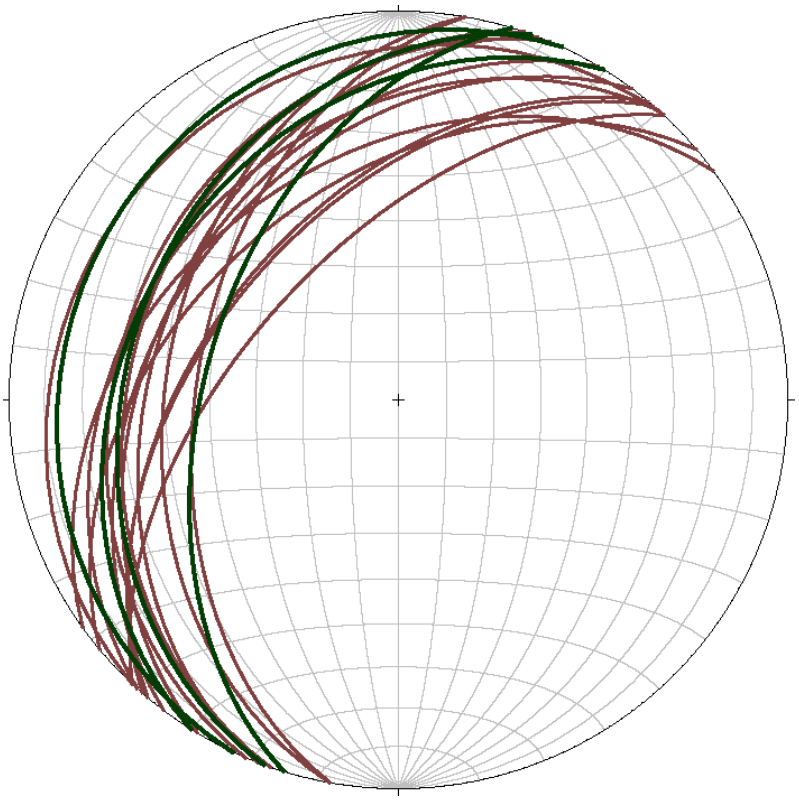

Figure 64: Combined anomalous outlier foliations from felsic gneiss (brown) and quartz diorite (green) which could be one limb of a fold.

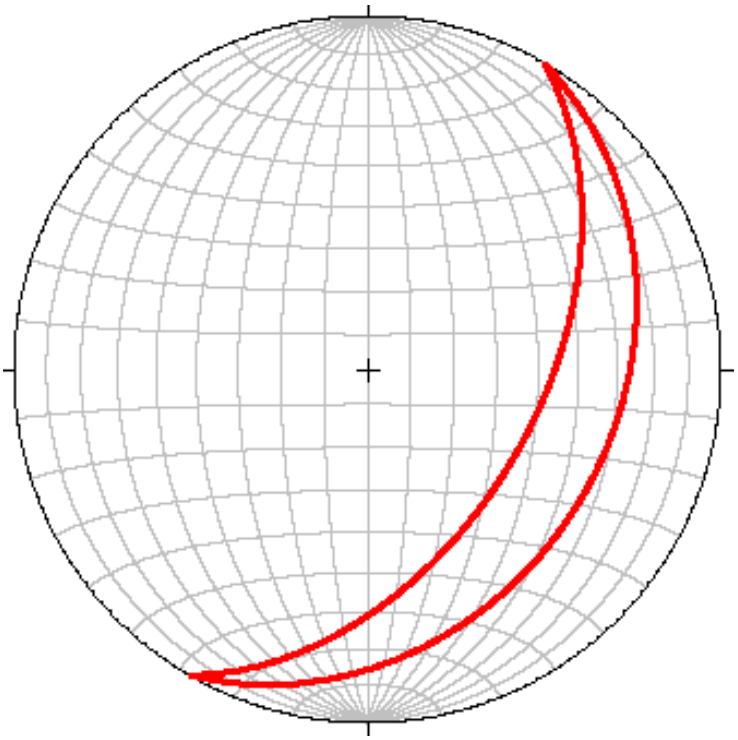

Figure 65. Likely orientations of the inferred slide surface within the covered area of the landslide scar. If these planes correspond to foliation in rock, a northeast-trending antiform may exist. Alternatively, the slide could have nucleated along one of the southeast-dipping fracture planes shown on Figures 24 or 35.

(3) I used a different (smaller) Area for the slide surface in my calculations. My mapping constrained by GPS locator (**Figure 6**) yielded a smaller area of slide scar than shown on the geologic map (**Figure 59**) of Herber (1987). I estimated the slide surface area by measuring the dimensions of a triangle in plan view, then projecting the calculated area onto a 36-degree sloping surface.

(4) In Safety Factor Approach #2, I employed a vertical tension crack at the top of the slide block, with a northeast strike perpendicular the direction of slide translation. Such a structure is justified by mapping of intact bedrock in the area. For example, several mafic dikes with northeast strikes transect Sunset Ridge directly north of the upper part of the slide scar (**Figures 7 and 9)**. In general, these dikes fill a steeply dipping northeast-striking fracture network (Marshak, 2016). Furthermore, a population of steep, epidote-filled, striated fault surfaces with north-northeast strikes corresponding to the ancestral San Antonio Fault have been documented in the Hog Back area (Nourse, 2003; see **Figure 66**). A few of these epidote surfaces were also measured by me during my study (**Figures 24 and 25**).

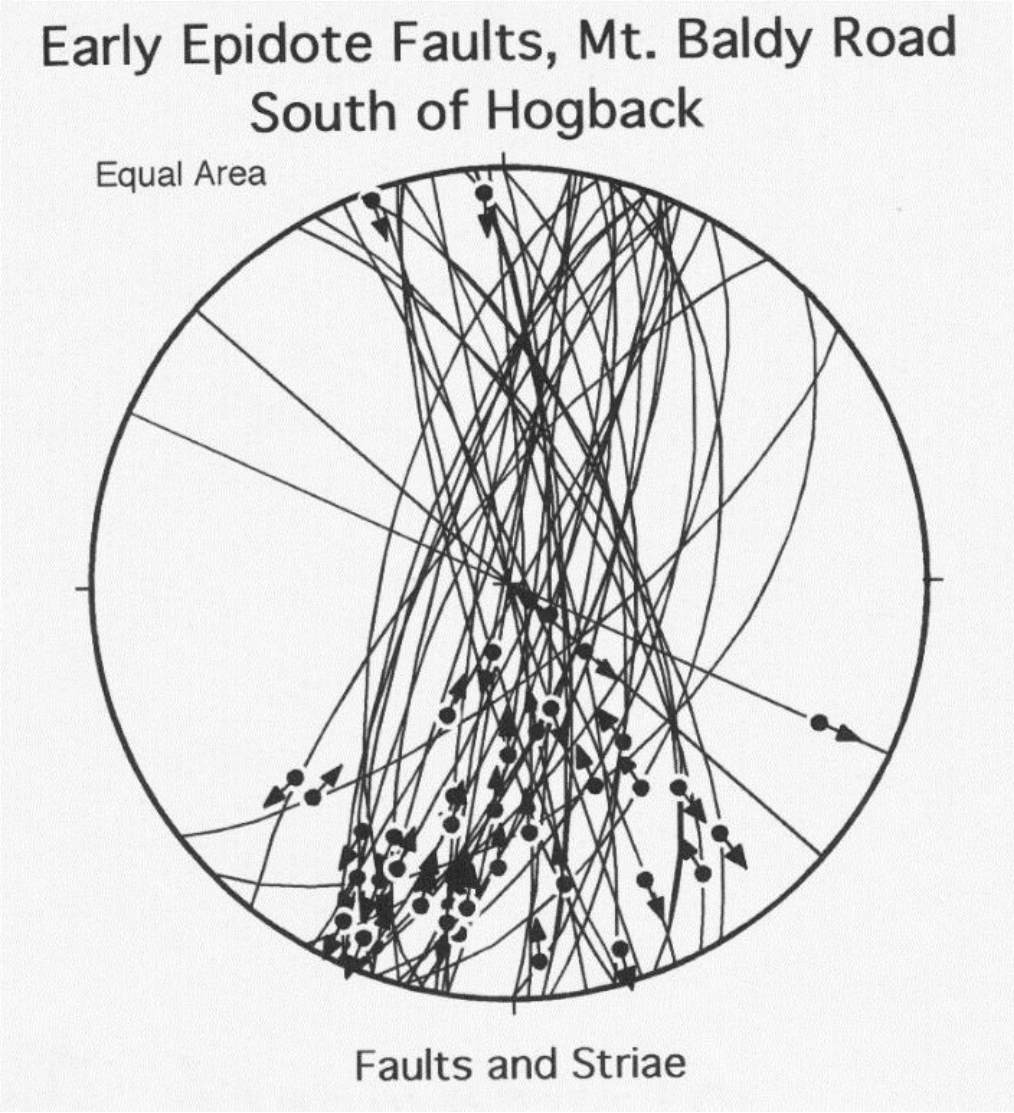

Figure 66. Stereonet of epidote-filled, striated fault surfaces measured in quartz diorite outcrop along the Mt. Baldy Road just south of Hog Back. Reproduced from Figure 12 of Nourse (2003).

Volume Calculations:

Described below is the method of vertical slices I used to constrain the volume of the Hog Back slide block.

The computer program Adobe Illustrator was used to create cross sections of the landslide for total volume calculations. The landslide map area was split into 5 sections, through which the profiles were drawn (**Figure 67**). For each profile the existing (current)

topography was drawn by creating a cross sectional grid from the USGS topographic base map. The pre-landslide upper surface was then reconstructed by extrapolating the elevations from the USGS topographic base map and projecting to the edges of landslide (dotted lines in profiles, **Figure 68,** higher resolution is in Appendix C). I used both the slopes from the southwest and the northeast of the slide scar to project a theoretical pre-slide surface. The landslide area for each section is therefore represented by the area between the previous land surface and the current topographic surface. This area was calculated by counting the squares of the representative area on the cross section (in Adobe Illustrator, one square is equal to approximately 55 square feet).

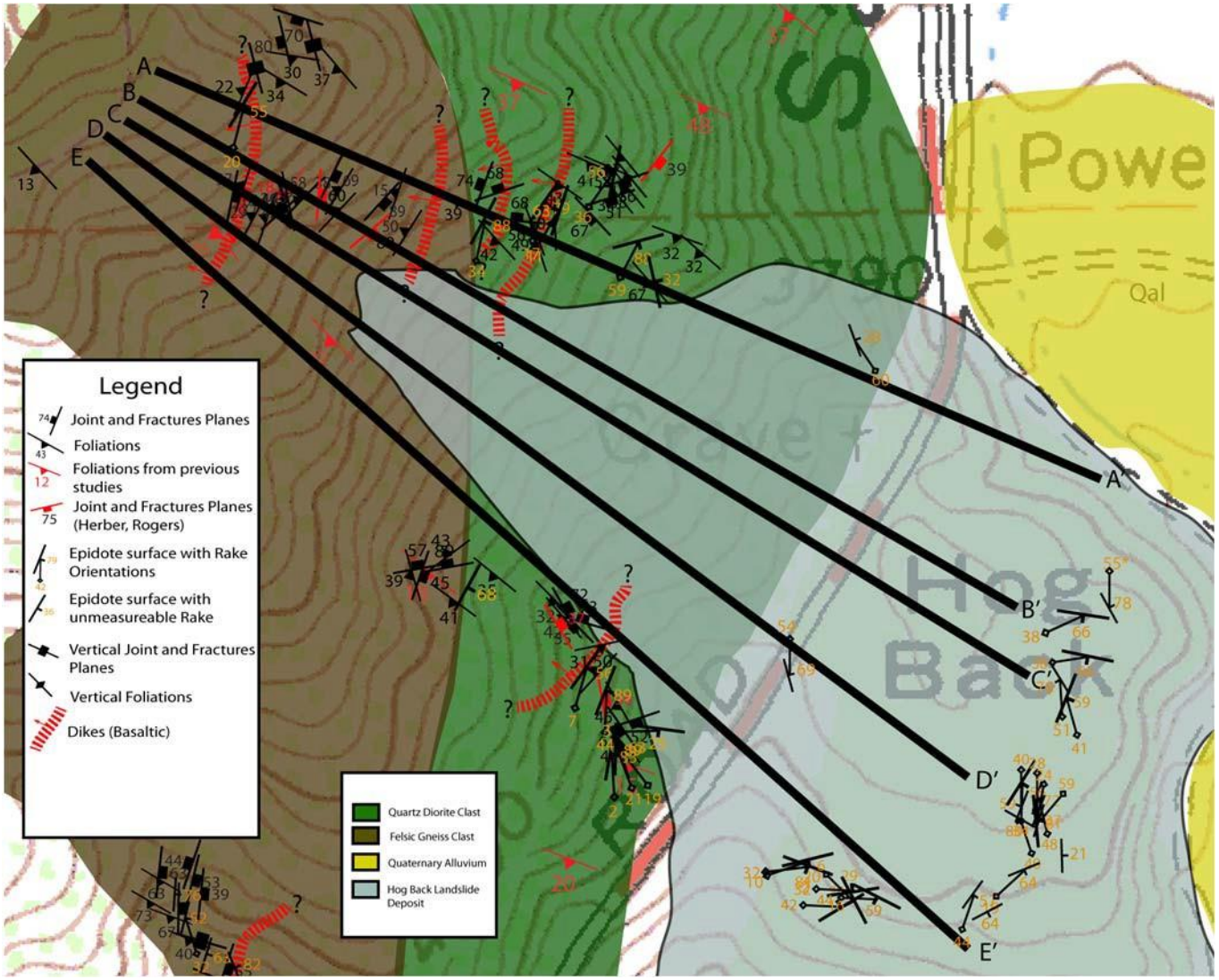

Figure 67. Cross Section lines used for volume calculation of the Hog Back Slide.

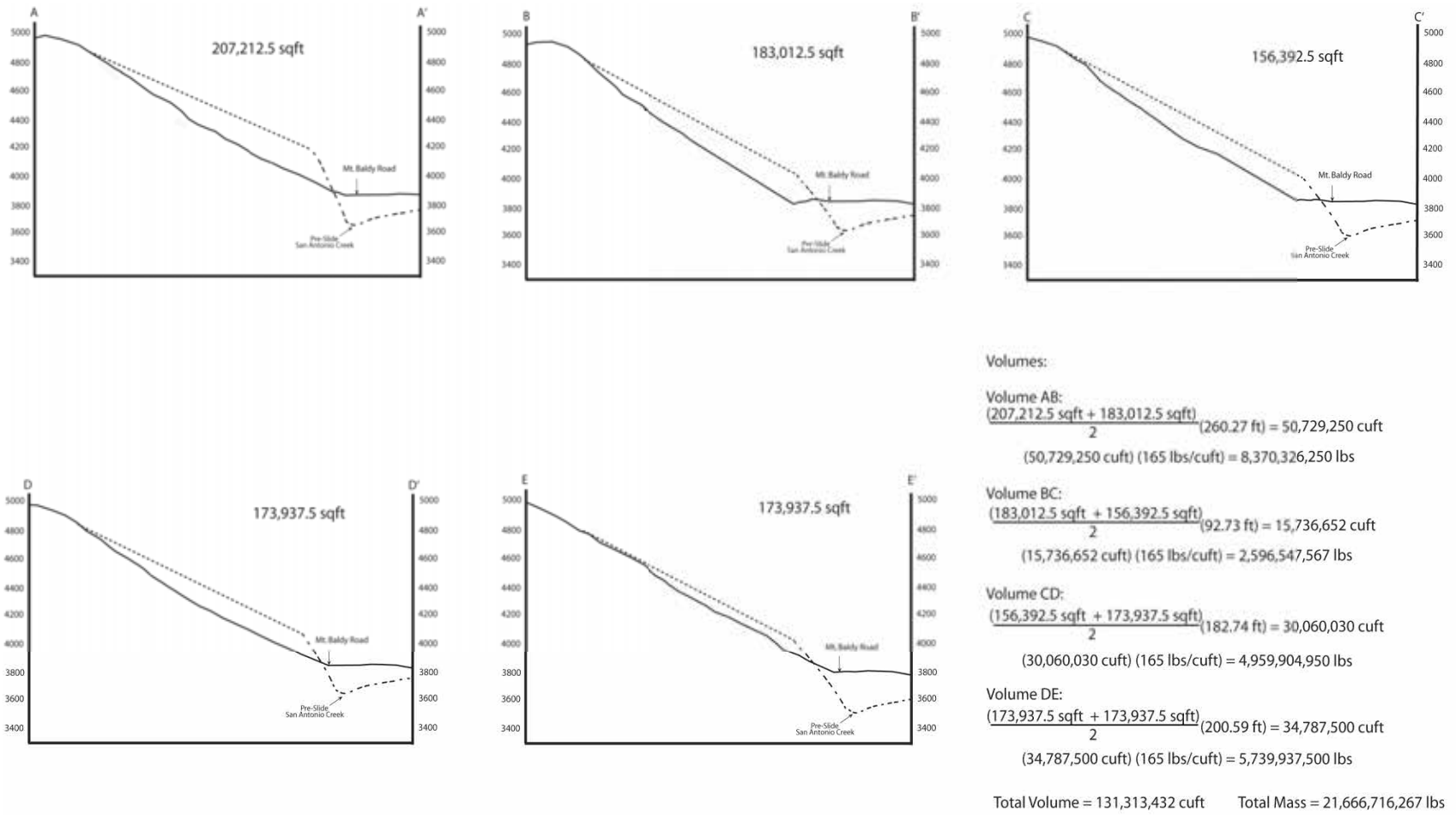

Figure 68. Cross sections through restored Hog Back Landslide used for "Method of Slices" volume calculation. See Figure 67 for location of section lines. Larger version available as Appendix C.

To calculate volume, the areas of adjacent cross section lines were averaged and then multiplied by the distance between them. This results in a volume for that "vertical slice" of the landslide. For example, the landslide area from A-A' is 207,212 square feet. The area from B-B' is 183,012 square feet. By taking the average of these two values results in an average area of 195,112 square feet. This average area is then multiplied by the distance between the two cross sectional lines (260 feet), resulting in a section volume of 50,729,250 cubic feet. The total landslide volume was then calculated by adding the four slices together as well as the volume estimated on the edges of the landslide. This total volume was found to be about 131,313,432 cubic feet. Multiplying this volume by a unit weight of 160 pounds per cubic foot (which is a representative weight for crystalline rock such as granite) yields an estimated value of the landslide material dry weight of 21,666,716,267 pounds (**Figure 68**).

Safety Factor Calculation:

The slide mass was modeled as an irregular shaped block on an inclined slide plane with a dip of 36 degrees, bounded on the upper end by a vertical tension fracture (**Figure 63**). This dip angle represents an estimate of what the angle of failure would be, because that surface is covered by an unknown amount of colluvium. The block was released at the rear along a vertical tension crack with zero cohesion. Safety factor equations for various combinations of friction angle and cohesion were solved for assuming the safety factor is equal to one. Both dry conditions and wet conditions (with the tension crack filled with water) were considered. Most of the geometric parameters used in this calculation differ significantly from those in Safety Factor Approach #1:

Θ= Dip of slide plane = 36^0

A = Area of slide plane = area in plan view projected onto 36 degree slope = 851,224 ft^2

V = Slide volume (converted to volume of non-porous crystalline rock) = 131,313,432 ft^3

W = Weight of slide block (assuming unit weight of 165 lb/ft^3) = 2.17 x 10^{10} lbs

h = height of breakaway point above bottom of slide plane = 680 ft

F_{H2O} = horizontal water force acting against submerged vertical tension crack at near the top of the slide block = 78,000,000 lbs (this quantity is derived from hydrostatics and assumes the tension crack is 100 ft high and 250 ft wide)

Dry Safety Factor Case:

The stability equation representing dry conditions is the same as that used for the Herber (1987) scenario, and given by the following equation:

$$\mathbf{SF = \frac{C+\tan\Phi\,[W\cos\Theta/A]}{W\sin\Theta/A}}$$

Where SF is the safety factor, Θ is the dip of the slide plane, C is the cohesion, Φ is the angle of internal friction, W is the weight of the slide block, and A is the area of the basal slide surface.

Setting the SF equal to 1.0 (failure condition), various combinations of C and Φ were solved for. The results are presented in **Table 2**, and graphed in **Figure 69**.

Wet Safety Factor Case:

A more complicated stability equation is needed to calculate Φ for varying values of C under water saturated conditions. This equation includes a component of water pressure

acting upward against the slide surface, and a horizontal water force acting against the tension crack bounding the rear of the slide block. The appropriate safety factor equation is given by:

$$SF = \frac{C + \tan\Phi \{[W\cos\Theta - F_{H2O}\sin(36)]/A - \text{average } P_{H20} \text{ up}\}}{[W\sin\Theta + F_{H2O}\cos(36)]/A}$$

Where, F_{H2O} (Force of Water) is the resolved force of the water on the back of the tension crack. The 36° angle is used to calculate components of F_{H2O} acting perpendicular and parallel to the slide plane (this angle would be different if the tension crack were oriented with less than a 90 degree dip). The force of the water is equal to the average water pressure on the back of the block multiplied by the submerged area. This value works out to be 78,000,000 lbs. For this approach, I applied two different estimates for the average upward water pressure, following the logic presented above for Safety Factor Approach #2. For a moderately saturated case, I used water pressure of 6875lbs/ft^2, equal to 1/3 the normal stress component exerted by the slide block. For an extreme case, I used a water pressure of 13,749 lbs/ft^2, equivalent to 2/3 the normal stress component of the weight. Again, multiple values for C were chosen and Φ was then solved for from the equation when SF is set at 1.0.

Results of safety factor calculations under dry and wet conditions are shown in **Table 2** and graphed in **Figure 69**.

Hog Back Safety Factor Results (Approach #2):								
Dry Case			Wet Case (Moderate Water Pressure Up w/Tension Crack			Wet Case (Extreme Water Pressure Up w/Tension Crack)		
Friction Angle (Ø)	Cohesion (lbs/ft^2)	Safety Factor	Friction Angle (Ø)	Cohesion (lbs/ft^2)	Safety Factor	Friction Angle (Ø)	Cohesion (lbs/ft^2)	Safety Factor
45	0	1.38	45	1363	1	45	8237	1
40	0	1.15	40	3567	1	40	9335	1
36	0	1	36	5108	1	36	10102	1
30	3076	1	30	7151	1	30	11120	1
25	5367	1	25	8672	1	25	11877	1
20	7477	1	20	10073	1	20	12575	1
15	9458	1	15	11388	1	15	13230	1
10	11347	1	10	12643	1	10	13855	1
7	12451	1	7	13376	1	7	14220	1

Table 2. Results of safety factor calculations using Safety Factor Approach #1. The family of Cohesion (C) and friction angle (Φ) values shown for SF = 1.0 are the result of "back calculation" intended to determine the range of possible shear strength constants applicable at the time of failure

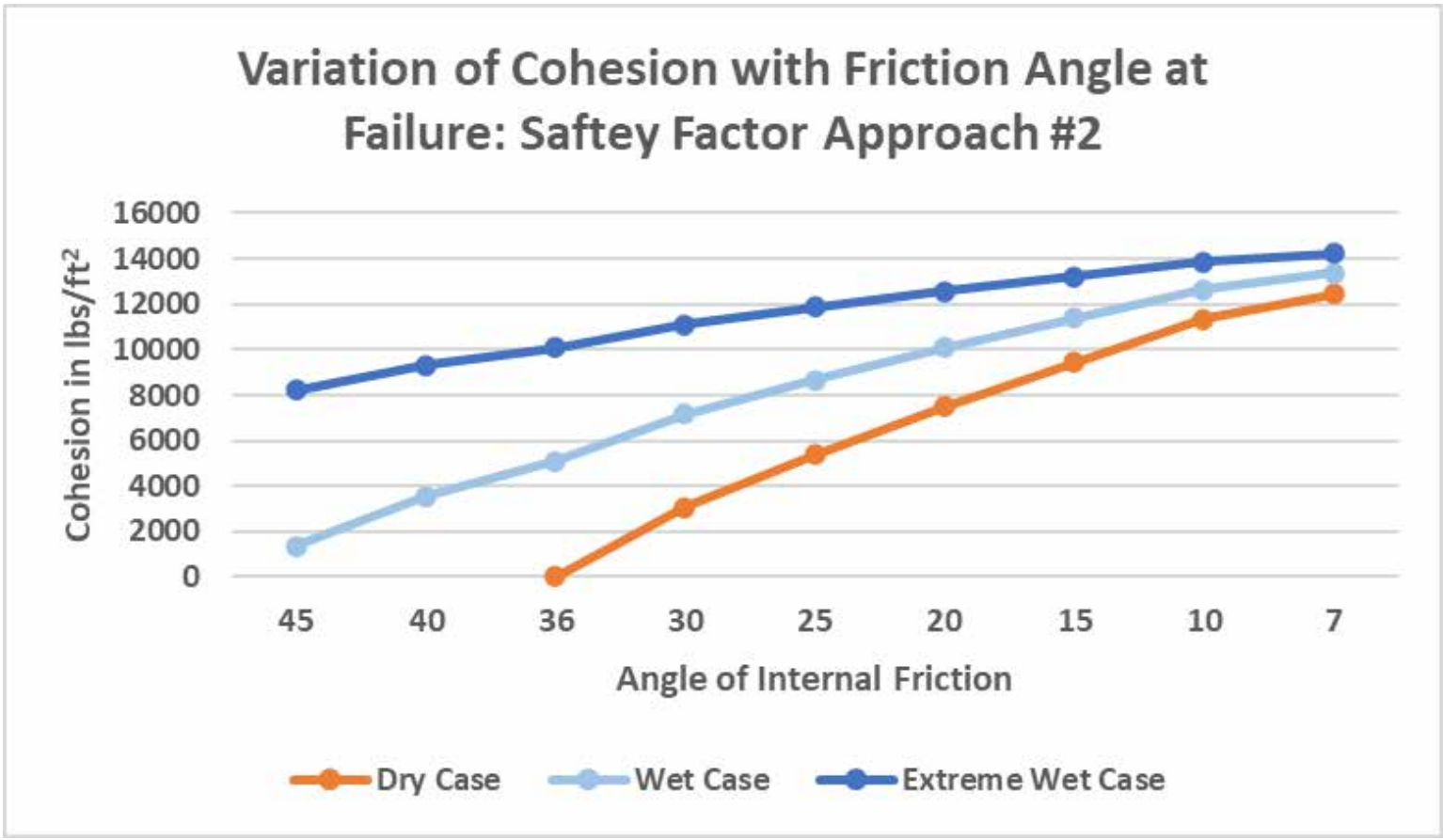

Figure 69. Graph illustrating various combinations of friction angle and cohesion, calculated at a failure condition of SF =1.0. There are noteworthy differences between wet and dry cases for safety Factor Approach #2

4.4 Discussion Of Potential Environmental Factors Influencing Cohesion And Friction Angle

The geology system that was present in the pre-slide Sunset Ridge area may have formed a favorable condition to promote mechanical weathering. Precipitation from storm events could have become trapped in the fractured rock. As more water became trapped in the rock, the water may have been able to freeze in the fractures, creating a frost wedge. This wedge could widen small fractures into larger fractures, increasing aperture spacing. There was likely more precipitation in a climate such as the Late Pleistocene than there is today. Also, the temperatures would have been colder in order to facilitate frost wedging. One result of this would be the reduction of cohesion, C. Frost wedging is likely in the San Gabriel Mountains due to the appearance of conifer trees (**Figure 70**) that have grown into the widened fractures in the future slide scar foot print and the surrounding area. Also quite likely is the possibility for large earthquakes that, through ground vibration, could significantly reduce cohesion along fractures, potentially to a value of zero. Given the nearby active San Andreas and Cucamonga fault systems, the study area has certainly experienced many magnitude 7+ and 8+ earthquakes during Quaternary time.

Figure 70: Conifer trees seen to the north of the Hog Back Slide scar, looking south.

Likewise, the angle of internal friction (friction angle) for fractured rock is known decrease with clay content. The process of long-term chemical weathering will convert feldspathic bedrock to clay. This chemical weathering effect would be accelerated along fractures with fault gouge (which are common in the study area).

A modern comparative example pertaining to the failure mechanisms occurs in the Alpine region of Northern Italy at the Mont de La Saxe rockslide (Agliardi et al, 2013). This area is an active slide zone where a deep-seated deformation, undergoing a major phase of acceleration in the last decade and exposing the valley bottom to a high risk, is discussed. To reach a more complete understanding of the process, an intense investigation program has been developed. Boreholes have been drilled, logged, and

instrumented (open-pipe piezometers, borehole wire extensometers, inclinometric casings) to assess the landslide volume, the rate of displacement at depth, and the water pressure.

4.5 Conceptual Model For Failure Of Hog Back Landslide

Let's now return to Research Question 6: How did the slide fail? Given that we cannot return to the specific time of landslide movement, the answer is somewhat speculative but supported by the science described above. In my opinion, a special combination of geologic, structural, and climactic conditions created a perfect set of conditions for failure. **Figures 71-76** utilize a block diagram extrapolated from cross sections in Rogers et al. 1992 as a starting point to illustrate my conceptual model for evolution of Hogback Landslide:

A pre-existing, densely fractured rock slope was generally affected by rainfall percolation, groundwater flow, and chemical weathering over a long period of time (**Figure 70**). As the fractures became larger, it may have been possible to form a short-lived fractured aquifer. The water that was flowing through the rock's joint system may have had no room for movement during freeze-thaw cycles. Over time, these fractures and joints could have begun to cross-connect, promoting increased fracture flow (**Figure 71**). This flow may have been able to reach the toe of the slope where seeps and/or springs could have formed. The fracture flow through the rock, combined with the Late Pleistocene location of San Antonio Creek, could have weakened the rock near the toe, or along the entire length of the future slide plane. When adding the weight of the water in the fractures to the previous two factors, instability may have created a tension crack at the top (**Figure 72**). An additional trigger may have been a heavy Pleistocene rainstorm,

perhaps followed by a freezing event. The safety factor decreased to a point where the area failed catastrophically and translated down slope, becoming the Hog Back Slide (**Figures 73-76**).

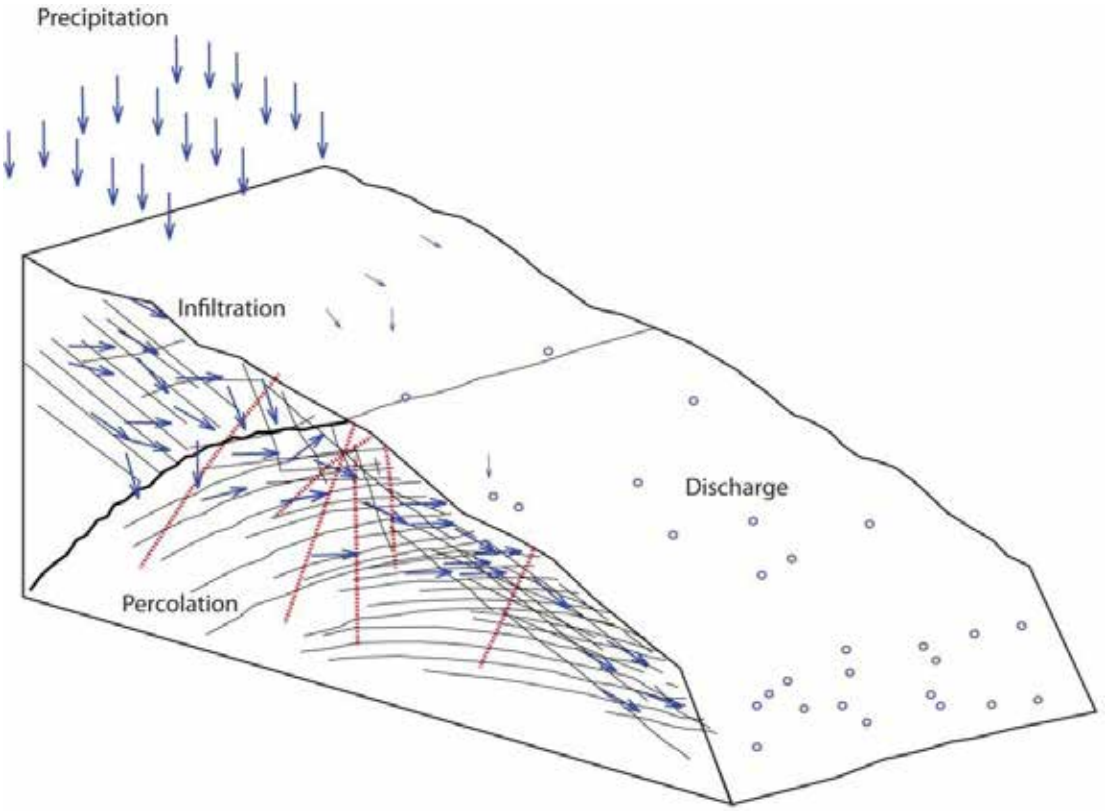

Figure 71. Three dimension block diagram of the Hog Back Slide. Showing the water cycle interacting with the slope. Precipitation, along with infiltration, percolation, and discharge. Modified from geometric constraints illustrated in cross section by Rogers et al. (1992), Figure 16.

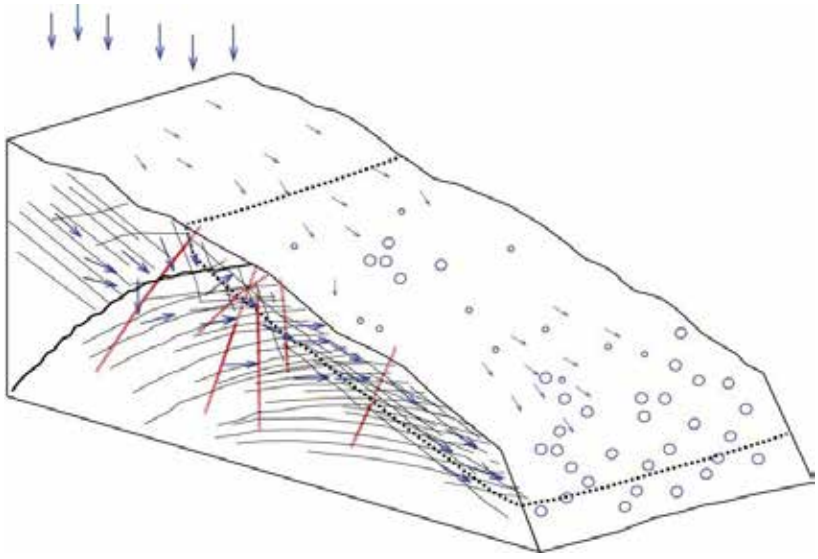

Figure 72. Increased discharge is causing the chemical and mechanical weathering of the surrounding rock.

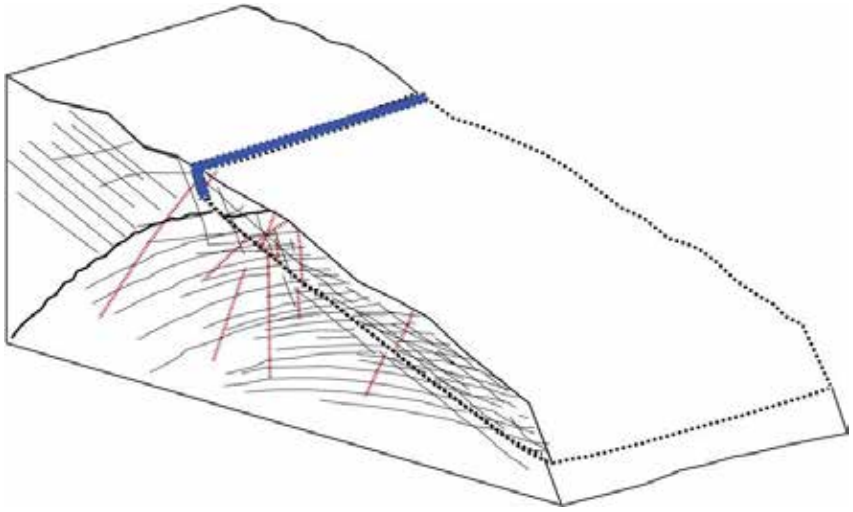

Figure 73. Decrease of cohesion and increase of pore pressure as tension crack at rear of slide block fills up with water. Modified from cross section in Rogers et al., 1992, Figure 18.

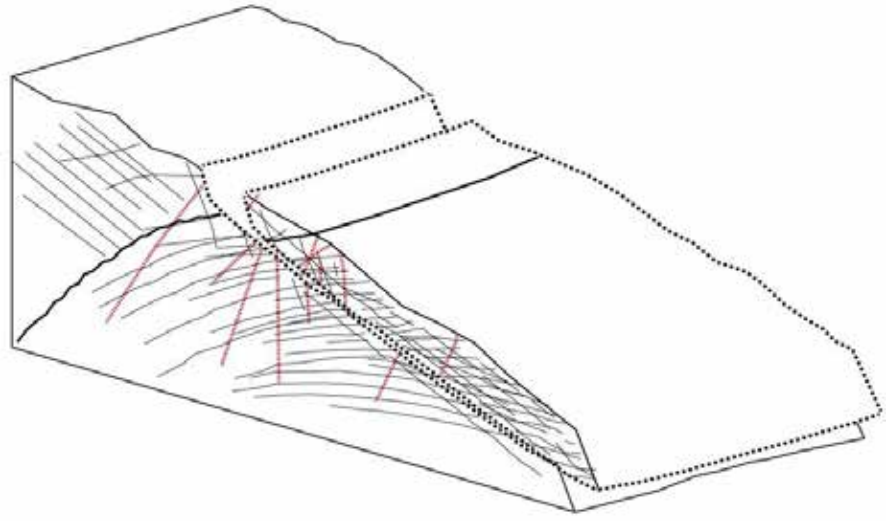

Figure 74. Release of the slope along NE strike, SE dipping planes.

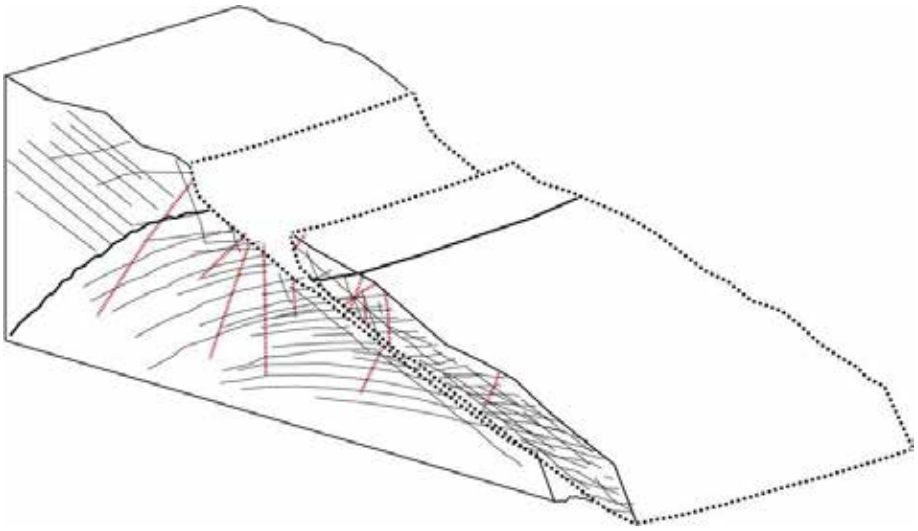

Figure 75. Complete failure of the slope. The slide is translatory in nature.

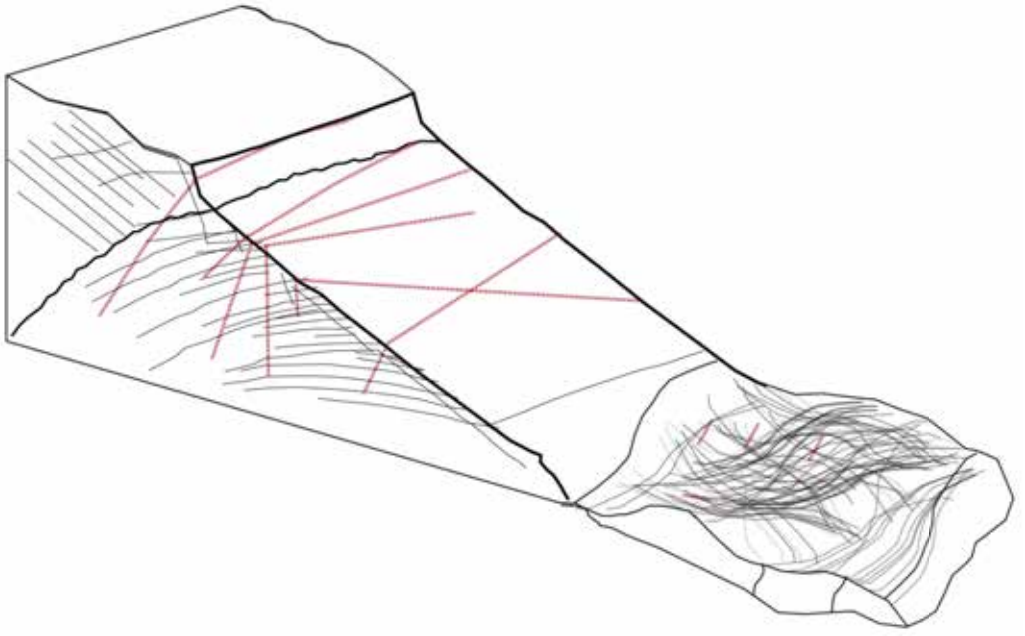

Figure 76. Complete failure of the slope. Slide mass returns to a position of stability in San Antonio Canyon. Modified from cross section in Rogers et al., 1992, Figure 19.

CONCLUSIONS

As a result of mapping, compiling, analyzing preferred orientations, referencing and modeling various geologic data (contacts, foliations, dikes, joints, epidote surfaces, clast sizes), the data reveals the following significant conclusions about the evolution of Hog Back slide:

- The slide area is underlain by two main foliated rock units: Precambrian felsic gneiss and Cretaceous quartz diorite. The Gneiss overlies the quartz diorite along a moderately southwest-dipping contact that is crosscut by Hog Back landslide scar. The foliations in the region of the slide scar strike northwest and dip to the southwest. Specifically, the mean strike is 118 degrees and the mean dip is 53 degrees to the southwest for the felsic gneiss and 135 degrees and the mean dip is 54 degrees to the southwest for the quartz diorite. A very distinctive geologic contact in source area shows up in distribution of displaced landslide debris. This contact shows a transition zone where there is more mafic banding in the felsic gneiss.
- There was an approximate translation of 1,300 foot of the marker units from the in-place slope to the resting slide area in the southeast as measured by the displaced gneiss-quartz diorite contact. The rockslide was translational and coherent enough during down-slope transport to maintain a unit contact.
- Statistical analysis using stereonet plots and histograms shows that foliations and other planar structures match between source and landslide clasts. There is no question that the Hogback landslide originated from a specific area on the east face of Sunset Ridge. In addition to containing two very distinct rock units, multiple

structural elements (metamorphic foliation, joints, fractures, slickensided fault surfaces) are common to both the source area and the slide mass.

- Part of the felsic gneiss appears to have broken off as a megaclast in which a measurable clockwise rotation is documented. As discussed earlier, the megaclast block of felsic gneiss along the Mount Baldy road cut preserves a common southwest-dipping foliation. In detail, its foliation strikes have rotated off strike by a mean of 24 degrees clockwise relative to the in-place bedrock.
- Clast size analysis shows that larger landslide fragments retained original orientation but small clasts tended to be jumbled, especially in the eastern side of the slide deposits. Few large quartz diorite clasts exist; smaller clasts are abundant due to denser nature of fracture network in quartz diorite source area.
- Geologic reconstruction shows two different approaches yielded slide volumes of 243,476,064 cuft and 131,313,432 cuft, with slide areas of 1,854,101 sqft and 851,224 sqft, respectively. Specific fracture geometries mapped from in-place outcrops area provided optimal orientations to nucleate and release the Hogback landslide from its bedrock source.
- Safety factor calculations under a variety of conditions yielded reasonable shear strength constants (C and Φ) for SDF =1.0. The ranges of cohesion (C) and friction angles (Φ) are zero to 12,451 lbs/sqft and 36 to 7 degrees for the dry cases, respectively. For the wet cases, the ranges of cohesion (C) and friction angles (Φ) are 1,363 to 13,376 lbs/sqft and 45 to 7 degrees, respectively. For the extreme wet cases, the ranges of cohesion (C) and friction angles (Φ) are 8,237 to 14,220 lbs/sqft and 45 to 7 degrees, respectively.

- The existence of mafic dikes allowed for the aperture spacing to be expanded and later eroded facilitating fluid flow. A pre-existing, densely fractured rock slope was generally affected by rainfall percolation, groundwater flow, and chemical weathering over a long period of time. As the fractures became larger, it may have been possible to form a short-lived fractured aquifer. The water that was flowing through the rock's joint system may not have had room for movement. The failure model that perhaps best fits the conditions of failure would be a scenario in which the tension crack is filled with water. The effects of this fluid not only added extra pressure on the back surface of the slide mass (at the tension crack) but also the likely reduced friction angle on the basal slide surface. Water within the slide mass itself would make it heavier and cause a subsequent driving force downhill.

RECOMMENDATIONS

A further study of the adverse strikes and dips that occur in the middle of the eastern sunset ridge slope should occur. I was not able to draw any conclusions to whether this was a synform or an antiform. Also, it would interesting to find out how far this structure extends to determine its size.

If it were possible to monitor the area before the slope failure (not possible), a few methods of monitoring could have been used. One method would have been to show the pre- slide area and the rate of displacement that was dependent on season and annual changes such as rainfall, snowmelt, and temperature flux. This method is being used for the Alpine region of Northern Italy at the Mont de La Saxe rockslide. The monitoring would be able to provide a description of the evolution of movement, followed by an estimate the expected displacement and eventual collapse time. The monitoring network should have a surface system to monitor any real-time displacement and a subsurface system to show the level of groundwater that is deep in the mountainside. (Piezometers would be in placed within the rock to monitor fluid flow and the rock cores to measure and record in-place foliations, faults, fracture locations.)

Another study for the Hog Back Slide would be to look for present-day, subsurface fractures in the slide scar. One possible method to explore this would be to use Very Low Frequency delineation. This method is used to find subsurface fractures for hydrogeologic exploration. . The analyzed data from each scan are presented graphically showing a cross section of the various geologic structures and differing lithologic units. Using the VLF on the Hogback Slide scar can determine if there are fractures and if there is any water in those fractures.

REFERENCES

Agliardi, F., Castellanza, R., Crosta, G.B., Frattini, P., Frigerio, G, and di Prisco, C., 2013, Chasing a complete understanding of the triggering mechanisms of a large rapidly evolving rockslide, Mont de La Saxe rockslide, Northern Italy, Univ. degli Studi di Milano Bicocca

Agunwah, Reginald I., 2008, Structural Analysis of Oriented Blocks in the Hog Back Landslide Deposit, Eastern San Gabriel Mountains, California: senior thesis, Cal Poly Pomona

Barth, Nicolas C., 2020, Recent advancements in geochronology, geologic mapping, and landslide characterization in basement rocks of the San Gabriel Mountains block, Part 3: Legacy and Hazard of Large Landslides in San Antonio Canyon, San Gabriel Mountains, California, Geological Society of America Field Guide 59, P. 76-89.

Dibblee, Thomas W., Jr., 2002, Geologic Map of the Mt. Baldy Quadrangle California: Thomas W. Dibblee Foundation, Santa Barbara, California.

Herber, Lawrence J., 1987, Hog Back: A grossly stable prehistoric rock block slide, San Antonio Canyons, Southern California, Geological Society of America Centennial Field Guide, P. 201-202.

Krause, Anselm, 2017, Analysis of the Hogback Landslide, San Antonio Canyon, San Gabriel Mountains, Southern California, senior thesis, University of California at Riverside.

Morton, D.M., Sadler, P.M., Minnich, R.A, 1987, Large rock-avalanche deposits: examples from the central and eastern San Gabriel Mountains of southern California. Inland Geological Society, Volume 2, Part III, p. 20-31.

Morton, D.M., and Miller, F.K. 2003, Preliminary geologic map of the San Bernardino 30’ x 60’ quadrangle, California: U.S. Geological Survey Open-File Report 03-293.

Marshak, Jonathan, 2016, What Dike Orientations In The Eastern San Gabriel Mountains Reveal About Middle Miocene Stresses and Block Rotations, Master’s Thesis, Cal Poly Pomona.

Nourse, Jonathan A., Morton, D.M., and Matti, J.C., 1998, Geologic map of the Mt. Baldy quadrangle, San Gabriel Mountains, California; United States Geological Survey Open File Report 98-BDY.

Nourse, J.A., 2002, Middle Miocene Reconstruction of the Central and Eastern San Gabriel Mountains, Southern California, with implications for evolution of the San Gabriel Fault and Los Angeles Basin, in Barth, A., ed., Contributions to crustal evolution of the southwestern United States: Geological Society of America Special Paper 365, p. 161-185.

Nourse, Jonathan A., 2003, *Late Cenozoic Magmatism, Faulting, Uplift, Flooding, Erosion in the Eastern San Gabriel Mountains and Pomona Valley,* in Weigand, P. W. (ed.), A Day in the Field With Tom Dibblee, Field Trip Guidebook published by the Thomas W. Dibblee, Jr. Foundation, May 24.

Rogers, David J., Herber, Lawrence J., and Hibner, Thomas H., 1992, Paleolandslides in San Antonio Canyon, Eastern San Gabriel Mountains, California. p. 579-594.

APPENDIX

Appendix A: Hog Back Slide Field Data

Appendix B: Hog Back Slide Composite Map

Appendix C: Cross Section Restored "Method of Slices" Volume Calculations

Appendix A: Hog Back Slide Field Data

Northing	Easting	Strike	Dip	Surface Info	Rock Type	Foliation/Surface/Joint/Fault	In-Place/Slide	Size
438059	3786201	N21W	61NE		Felsic Gneiss	Foliation	In-Place	N/A
438059	3786215	N59W	49SW		Felsic Gneiss	Foliation	In-Place	N/A
438061	3786230	N70E	89SE		Felsic Gneiss	Foliation	In-Place	N/A
				S70E/28	Felsic Gneiss	Epidote Surface	In-Place	N/A
438056	3786246	N89E	49S		Felsic Gneiss	Foliation	In-Place	N/A
		N80W	44SW		Felsic Gneiss	Foliation	In-Place	N/A
		N10W	81NE		Felsic Gneiss	Joint	In-Place	N/A
		N55W	52NE		Felsic Gneiss	Joint	In-Place	N/A
438053	3786249	N30W	69NE		Felsic Gneiss	Joint	In-Place	N/A
438048	3786264	N60W	36SW		Felsic Gneiss	Joint	In-Place	N/A
438053	3786275	N10W	79SW		Felsic Gneiss	Foliation/Fault	In-Place	N/A
438046	3786286	N10W	47NE		Felsic Gneiss	Joint/Epidote Surface	In-Place	N/A
438047	3786289	N25W	65NE		Felsic Gneiss	Fault	In-Place	N/A
438050	3786296	N45E	73NW		Dike (Mafic)	Mafic Intrusion	In-Place	N/A
438047	3786299	N75W	34SW		Felsic Gneiss	Foliation	In-Place	N/A
		N80E	49NW		Felsic Gneiss	Joint	In-Place	N/A
		N10W	77SW		Felsic Gneiss	Joint	In-Place	N/A
438471	3786598	N50W	51SW		Felsic Gneiss	Foliation	Slide	MEGA
438491	3786618	N24W	75SW		Felsic Gneiss	Foliation	Slide	MEGA
438508	3786648	S42E	51SW		Felsic Gneiss	Foliation	Slide	MEGA
438518	3786656	S50E	39SW		Felsic Gneiss	Foliation	Slide	MEGA
438488	3786646	N4W	51SW		Felsic Gneiss	Foliation	Slide	MEGA
438495	3786641	N26E	53NW		Felsic Gneiss	Foliation	Slide	MEGA
438508	3786659	NORTH	48W		Felsic Gneiss	Foliation	Slide	MEGA
438522	3786662	N47E	41NW		Felsic Gneiss	Foliation	Slide	MEGA
438499	3786470	S21E	54SW		Felsic Gneiss	Foliation	Slide	MEGA
438573	3786458	N6W	74SW		Quartz Diorite	Foliation	Slide	medium
438557	3786437	N32W	53SW		Contact	Foliation	Slide	

438533	3786426	N27W	69SW		Quartz Diorite	Foliation	Slide	
438325	3786420	N70E	78NW		Quartz Diorite	Foliation	Slide	
438532	3786387	S82W	51SE		Quartz Diorite	Foliation	Slide	
438544	3786468	S45E	81SW		Felsic Gneiss	Foliation	Slide	
438561	3786510	N43E	40NW		Quartz Diorite	Foliation	Slide	
438560	3786509	S24E	55SW		Contact	Foliation	Slide	
438577	3786537	S37E	70SW		Felsic Gneiss	Foliation	Slide	
438582	3786467	N13W	53SW		Quartz Diorite	Foliation	Slide	
438337	3887447	S42E	46SW		Quartz Diorite	Foliation	In-Place	N/A
438042	3786297	N42W	39SW		Felsic Gneiss	Joint	In-Place	N/A
		N22E	66SE		Felsic Gneiss	Joint	In-Place	N/A
		N32W	28SW		Felsic Gneiss	Joint	In-Place	N/A
438044	3786314	N456	40SW		Felsic Gneiss	Foliation	In-Place	N/A
		N42W	33SW		Felsic Gneiss	Foliation	In-Place	N/A
		N50W	28SW		Felsic Gneiss	Foliation	In-Place	N/A
		N80W	87NE		Felsic Gneiss	Joint	In-Place	N/A
		N48W	86SW		Felsic Gneiss	Joint	In-Place	N/A
		N70E	83NW		Felsic Gneiss	Joint	In-Place	N/A
		N81W	74NE		Felsic Gneiss	Joint	In-Place	N/A
438053	3786334	N50W	38SW		Felsic Gneiss	Foliation	In-Place	N/A
		N35E	60SE		Felsic Gneiss	Epidote Surface	In-Place	N/A
		N50E	36SE		Felsic Gneiss	Epidote Surface	In-Place	N/A
438089	3786336	N6W	72NE		Felsic Gneiss	Fault	In-Place	N/A
		N8W	84NE		Felsic Gneiss	Fault	In-Place	N/A
		N43W	83NE		Felsic Gneiss	Joint	In-Place	N/A
		N41W	33SW		Felsic Gneiss	Foliation	In-Place	N/A
		N47W	40SW		Felsic Gneiss	Foliation	In-Place	N/A
		N44W	38SW		Felsic Gneiss	Fault	In-Place	N/A
438043	3786334	N34W	48SW		Felsic Gneiss	Foliation	In-Place	N/A
		N21E	55SE		Felsic Gneiss	Joint	In-Place	N/A
		N71W	87SW		Felsic Gneiss	Joint	In-Place	N/A
		N24W	82NE		Felsic Gneiss	Fault	In-Place	N/A
438033	3786355	N41W	40SW		Felsic Gneiss	Foliation	In-Place	N/A
		N75W	90		Felsic Gneiss	Joint	In-Place	N/A
		N22E	63SE		Felsic Gneiss	Fault	In-Place	N/A
438011	3786388	N20E	53SE		Felsic Gneiss	Joint	In-Place	N/A

		N39W	73SW		Felsic Gneiss	Foliation	In-Place	N/A
		N15E	39SE		Felsic Gneiss	Joint	In-Place	N/A
		N75W	67SW		Felsic Gneiss	Foliation	In-Place	N/A
		N32E	44NW		Felsic Gneiss	Joint	In-Place	N/A
438020	3786390	N	58E	N20E/32	Felsic Gneiss	Joint/Epidote Surface	In-Place	N/A
438010	3786400	N7E	76E		Felsic Gneiss	Fault	In-Place	N/A
438003	3786408	N51W	63SW		Felsic Gneiss	Foliation	In-Place	N/A
		N4E	63E		Felsic Gneiss	Joint	In-Place	N/A
437944	3786482	N25W	26SW		Felsic Gneiss	Foliation	In-Place	N/A
437920	3786482	N29E	24NW		Felsic Gneiss	Foliation	In-Place	N/A
438533	3786859	N68W	86SW		Quartz Diorite	Foliation	In-Place	N/A
438557	3786737	N52E	55NW		Quartz Diorite	Foliation	Slide	
438541	3786725	N8E	6SE		Quartz Diorite	Foliation	Slide	
		N4W	80NE		Quartz Diorite	Joint	Slide	
		N30E	17SE		Quartz Diorite	Foliation	Slide	
		N22E	9SE		Quartz Diorite	Foliation	Slide	
438528	3786740	N80W	72NE		Quartz Diorite	Foliation	Slide	
438527	3786748	N84E	32NW		Quartz Diorite	Foliation	Slide	
438523	3786949	N46W	16SW		Quartz Diorite	Foliation	Slide	
		N51W	12NE		Quartz Diorite	Foliation	Slide	
438505	3786769	N76W	68SW		Quartz Diorite	Foliation	Slide	
438505	3786767	N12W	90		Quartz Diorite	Foliation	Slide	
438497	3786726	N21E	60SE		Quartz Diorite	Foliation	Slide	
		N27W	28NE	N3E/60	Quartz Diorite	Epidote Surface	Slide	
438478	3786782	N88E	35SE		Quartz Diorite	Foliation	Slide	
438441	3786816	N25W	30SW		Quartz Diorite	Foliation	Slide	
438421	3786833	EAST	40S		Quartz Diorite	Foliation	Slide	
438389	3786841	N34W	32SW		Quartz Diorite	Foliation	Slide	
438377	3786852	N73W	32SW		Quartz Diorite	Foliation	Slide	
438512	3786669	N60E	87NW		Felsic Gneiss	Foliation	Slide	
438511	3786654	N19E	50NW		Felsic Gneiss	Foliation	Slide	
438501	3786655	N2E	42NW		Felsic Gneiss	Foliation	Slide	
438493	3786644	N4E	62NW		Felsic Gneiss	Foliation	Slide	
438487	3786634	N13W	57SW		Felsic Gneiss	Foliation	Slide	
438508	3786471	N20W	74SW		Felsic Gneiss	Foliation	Slide	
438589	3786452	N20E	54NW		Quartz Diorite	Foliation	Slide	
438506	3786439			N25E/59NW/40	Quartz Diorite	Epidote Surface	Slide	
438607	3786438	N65E	81NW		Quartz Diorite	Foliation	Slide	
				N25E/90/28	Quartz Diorite	Epidote Surface	Slide	
438609	3786436			N30W/80SW/40	Quartz Diorite	Epidote Surface	Slide	

				N17E/81SE/59	Quartz Diorite	Epidote Surface	Slide	
438629	3786408	N65E	24NW		Quartz Diorite	Foliation	Slide	
438627	3786398	N32E	21NW		Quartz Diorite	Foliation	Slide	
		N42W	64NE		Quartz Diorite	Foliation	Slide	
				N1W/21NE	Quartz Diorite	Epidote Surface	Slide	
438607	3786399	N36E	27NW		Quartz Diorite	Foliation	Slide	
				N52E/64SE/19	Quartz Diorite	Epidote Surface	Slide	
438581	3786368	N40W	71SW		Quartz Diorite	Foliation	Slide	
438586	3786383	N46W	81NE		Quartz Diorite	Foliation	Slide	
				N29E/57SE/44	Quartz Diorite	Epidote Surface	Slide	
438566	3786400	N15W	52SW		Quartz Diorite	Foliation	Slide	
				N55E/64SE	Quartz Diorite	Epidote Surface	Slide	
438565	3786407	N39E	24NW		Quartz Diorite	Foliation	Slide	
				N39E/79NW/7	Quartz Diorite	Epidote Surface	Slide	
				N17W/49NE/25	Quartz Diorite	Epidote Surface	Slide	
438553	3786394	N30W	31NE		Quartz Diorite	Foliation	Slide	
438551	3786393	N10W	78SW		Quartz Diorite	Foliation	Slide	
				N59W/32NE/5	Quartz Diorite	Epidote Surface	Slide	
438555	3786415	N24E	30SE		Quartz Diorite	Foliation	Slide	
				N2E/72SE/16	Quartz Diorite	Epidote Surface	Slide	
438618	3786434	N41E	61NW		Quartz Diorite	Foliation	Slide	
				N20E/72SE/48	Quartz Diorite	Epidote Surface	Slide	
438635	3786428	N70W	70NE		Quartz Diorite	Foliation	Slide	
438653	3786417	N49W	46NE		Quartz Diorite	Foliation	Slide	
438653	3786427	N79W	21NE		Quartz Diorite	Foliation	Slide	
438652	3786445	WEST	70S		Quartz Diorite	Foliation	Slide	
438657	3786451	N34E	88NW		Quartz Diorite	Foliation	Slide	
438661	3786461	N5W	23NE		Quartz Diorite	Foliation	Slide	
438651	3786477	N38E	26NW		Quartz Diorite	Foliation	Slide	
438646	3786473	N80E	68NW		Quartz Diorite	Foliation	Slide	
438645	3786472	N69W	52SW		Quartz Diorite	Foliation	Slide	
438627	3786496	N60W	61SW		Quartz Diorite	Foliation	Slide	
		N20E	52SW		Quartz Diorite	Foliation	Slide	
438626	3786449	N5E	67NW		Quartz Diorite	Foliation	Slide	
				NORTH/28EAST/3	Quartz Diorite	Foliation	Slide	
438633	3786439			N35E/88SE/6	Quartz Diorite	Foliation	Slide	
438627	3786431			N25W/40NE/16	Quartz Diorite	Foliation	Slide	
438450	3786567			N20W/70NE/54	Quartz Diorite	Foliation	Slide	
				N2768NE/45	Quartz Diorite	Foliation	Slide	
438760	3786605	N17W	89SW		Quartz Diorite	Foliation	Slide	

438718	3786649	N75W	21NE		Quartz Diorite	Foliation	Slide	
438597	3786691	N20E	64NW		Quartz Diorite	Foliation	Slide	medium
438591	3786690	N70W	51SW		Quartz Diorite	Foliation	Slide	medium
438594	3786699	N65W	62NE		Quartz Diorite	Foliation	Slide	medium
438583	3786674	N24E	30NW		Felsic Gneiss	Foliation	Slide	small
438576	3786694	N15W	79NE		Quartz Diorite	Foliation	Slide	medium
438511	3786593	N12W	71SW		Felsic Gneiss	Foliation	Slide	small
438565	3786598	N53E	41NW		Felsic Gneiss	Foliation	Slide	small
438573	3786595	N52W	73NE		Felsic Gneiss	Foliation	Slide	medium
438583	3786601	N72W	66NE		Felsic Gneiss	Foliation	Slide	small
438585	3786613	N60W	27SW		Felsic Gneiss	Foliation	Slide	medium
438589	3786610	N74W	70NE		Felsic Gneiss	Foliation	Slide	medium
438599	3786619	N60W	90		Quartz Diorite	Joint	Slide	large
		N20W	67SW		Quartz Diorite	Foliation	Slide	medium
438601	3786622	N70E	72NW		Quartz Diorite	Foliation	Slide	medium
		SOUTH	75E		Quartz Diorite	Foliation	Slide	
		N65W	81NE		Quartz Diorite	Foliation	Slide	medium
438597	3786639	N50W	48SW		Felsic Gneiss	Foliation	Slide	small
		N72W	21NE		Felsic Gneiss	Foliation	Slide	small
		N70W	75NE		Felsic Gneiss	Foliation	Slide	small
438594	3786650	N67E	60NW		Felsic Gneiss	Foliation	Slide	small
438608	3786630	N45W	66SW		Quartz Diorite	Foliation	Slide	large
438613	3786633	N78E	67SE		Quartz Diorite	Foliation	Slide	medium
438618	3786638	N85E	24SE		Quartz Diorite	Foliation	Slide	medium
438622	3786653	N60W	73SW		Quartz Diorite	Foliation	Slide	large
438622	3786652	N50W	79NE		Quartz Diorite	Foliation	Slide	large
438635	3786647	N65W	11SW		Quartz Diorite	Foliation	Slide	large
438641	3786641	N35E	80SE		Quartz Diorite	Foliation	Slide	medium
438665	3786624	NORTH	80W		Quartz Diorite	Foliation	Slide	medium
		N16W	81SW		Quartz Diorite	Foliation	Slide	small
438671	3786612	N20W	5SW		Quartz Diorite	Foliation	Slide	medium
438676	3786615	N26W	44SW		Quartz Diorite	Foliation	Slide	medium
		N35E	89NW		Dike (Mafic)	Foliation	Slide	
		N20W	59NE		Quartz Diorite	Foliation	Slide	medium
438652	3786599	N56W	33NE		Quartz Diorite	Foliation	Slide	large
		N61E	80NW		Dike (Mafic)	Foliation	Slide	
438658	3786587	N70E	44SE		Quartz Diorite	Foliation	Slide	large
438672	3786588	N11W	87SW		Quartz Diorite	Foliation	Slide	large
438672	3786584	N40W	23NE		Quartz Diorite	Foliation	Slide	large
				N25W/78NE/55	Quartz Diorite	Epidote Surface	Slide	

438439	3786531	N60W	32NE		Quartz Diorite	Foliation	Slide	MEGA
				N45W/79SW/51	Quartz Diorite	Epidote Surface	Slide	
438505	3786633	N62W	59SW		Felsic Gneiss	Foliation	Slide	MEGA
				N64W/33NE/44	Felsic Gneiss	Epidote Surface	Slide	
438496	3786639			N43W/43NE/31	Felsic Gneiss	Epidote Surface	Slide	
438443	3786411	N70W	73NE		Felsic Gneiss	Foliation	Slide	medium
438453	3786931	N35E	55SE		Quartz Diorite	Foliation	Slide	medium
		N30E	56SE		Quartz Diorite	Foliation	Slide	medium
		N47E	20SE		Quartz Diorite	Foliation	Slide	medium
				N70E/20SE/10	Quartz Diorite	Epidote Surface	Slide	
				N70W/81SW/32	Quartz Diorite	Epidote Surface	Slide	
438463	3786373	N27W	44NE		Quartz Diorite	Foliation	Slide	large
438474	3786382	N27W	63NE		Quartz Diorite	Foliation	Slide	large
		N66E	75SE		Quartz Diorite	Foliation	Slide	
		N55E	31NW		Quartz Diorite	Foliation	Slide	
				N50E/79NW/42	Quartz Diorite	Epidote Surface	Slide	
438479	3786383	N41E	61SE		Quartz Diorite	Foliation	Slide	large
				N30W/16SW	Quartz Diorite	Epidote Surface	Slide	
				N80E/29NW/2	Quartz Diorite	Epidote Surface	Slide	
438495	3786385	N30W	68NE		Quartz Diorite	Foliation	Slide	medium
		N25W	58NE		Quartz Diorite	Foliation	Slide	large
		N37W	40NE		Quartz Diorite	Foliation	Slide	medium
		N23W	63NE		Quartz Diorite	Foliation	Slide	medium
				N48W/59SW/44	Quartz Diorite	Epidote Surface	Slide	
438510	3786391	N52W	87SW		Quartz Diorite	Foliation	Slide	medium
		N63E	37SE		Quartz Diorite	Foliation	Slide	medium
		N80E	54NW		Quartz Diorite	Foliation	Slide	medium
		N36W	72SW		Quartz Diorite	Foliation	Slide	medium
438612	3786452	N19W	66SW		Quartz Diorite	Foliation	Slide	large
		N28W	53SW		Quartz Diorite	Foliation	Slide	medium
		N18E	61NW		Quartz Diorite	Foliation	Slide	medium
				N26E/56SE/34	Quartz Diorite	Epidote Surface	Slide	
				N2W/37NE/24	Quartz Diorite	Epidote Surface	Slide	
438639	3786514	N60W	47SW		Quartz Diorite	Foliation	Slide	large
		N43W	37SW		Quartz Diorite	Foliation	Slide	medium
		N37W	32SW		Quartz Diorite	Foliation	Slide	small
		N68W	51SW		Quartz Diorite	Foliation	Slide	medium
		N70SW	63SW		Quartz Diorite	Foliation	Slide	medium
		N51W	46SW		Quartz Diorite	Foliation	Slide	medium
				N26E/59SE/41	Quartz Diorite	Epidote Surface	Slide	

438643	3786532	N41W	79SW		Quartz Diorite	Foliation	Slide	small
		N59W	81SW		Quartz Diorite	Foliation	Slide	small
		N55W	41SW		Quartz Diorite	Foliation	Slide	medium
		N58W	51NE		Quartz Diorite	Foliation	Slide	small
		N61W	43SW		Quartz Diorite	Foliation	Slide	large
		N41W	11SW		Quartz Diorite	Foliation	Slide	medium
		N81E	62NW		Quartz Diorite	Foliation	Slide	small
				N75W/66SW/38	Quartz Diorite	Epidote Surface	Slide	
438245	3787346	N16E	49NW		Quartz Diorite	Joint	In-Place	N/A
		N10E	40SE		Quartz Diorite	Joint	In-Place	N/A
		N56W	78NE		Quartz Diorite	Joint	In-Place	N/A
438224	3787331	N85E	81NW		Quartz Diorite	Joint	In-Place	N/A
		N5W	39SW		Quartz Diorite	Foliation	In-Place	N/A
		N20W	20SW		Quartz Diorite	Foliation	In-Place	N/A
		N17W	52SW		Quartz Diorite	Foliation	In-Place	N/A
		N19W	83NE		Quartz Diorite	Joint	In-Place	N/A
		N31W	78SW		Quartz Diorite	Foliation	In-Place	N/A
438221	3787329	N20E	31NW		Quartz Diorite	Foliation	In-Place	N/A
		N5E	90		Felsic Gneiss/QuartzDio	Contact	In-Place	N/A
438068	3787134	N50E	44NW		Felsic Gneiss	Foliation	In-Place	N/A
		N70E	54SE		Felsic Gneiss	Joint	In-Place	N/A
		N68E	57SE		Felsic Gneiss	Foliation	In-Place	N/A
		N42E	32NW		Felsic Gneiss	Joint	In-Place	N/A
		N67E	NA		Felsic Gneiss	Fault	In-Place	N/A
438029	3787098	N50W	56SW		Felsic Gneiss	Foliation	In-Place	N/A
					Dike (Mafic)		In-Place	N/A
437929	3786909	N41W	13SW		Quartz Diorite	Foliation	In-Place	N/A
438352	3786505			N80W/29SW/3	Quartz Diorite	Epidote Surface		N/A
438328	3786492	N64W	44SW		Quartz Diorite	Foliation	In-Place	N/A
		N40W	61SW		Quartz Diorite	Joint	In-Place	N/A
				N20W/63NE/19	Quartz Diorite	Epidote Surface	In-Place	N/A
				N10E/83SE/2	Quartz Diorite	Epidote Surface	In-Place	N/A
				NORTH/89E/21	Quartz Diorite	Epidote Surface	In-Place	N/A
		N70E	52SE		Quartz Diorite	Joint	In-Place	N/A
438326	3786819	N41W	46SW		Quartz Diorite	Foliation	In-Place	N/A
438316	3786545	N32E	31NW		Quartz Diorite	Foliation	In-Place	N/A
				N33E/31NW/7	Quartz Diorite	Epidote Surface	In-Place	N/A
438310	3786558	N89E	58SE		Quartz Diorite	Foliation	In-Place	N/A
				N15E/89NW/44	Quartz Diorite	Epidote Surface	In-Place	N/A

				N60W	Dike (Mafic)	Foliation	In-Place	N/A
438298	3786580	N40W	42SW		Quartz Diorite	Foliation	In-Place	N/A
		N80W	73NE		Quartz Diorite	Joint	In-Place	N/A
		N50W	35SW		Quartz Diorite	Joint	In-Place	N/A
438290	3786586	N40W	32SW		Felsic Gneiss/Quartz Diorite	Contact	In-Place	N/A
		N56W	72NE		Felsic Gneiss/Quartz Diorite	Contact	In-Place	N/A
438237	3786619	N40W	35SW		Quartz Diorite	Foliation	In-Place	N/A
438208	3786625	N40E	43NW		Felsic Gneiss	Foliation	In-Place	N/A
		N88E	89NW		Felsic Gneiss	Joint	In-Place	N/A
438194	3786622	N21W	39SW		Felsic Gneiss	Foliation	In-Place	N/A
		N88E	57NW		Felsic Gneiss	Joint	In-Place	N/A
		N15E	45SE		Felsic Gneiss	Joint	In-Place	N/A
438353	3786817	N30W	67SW		Quartz Diorite	Foliation	In-Place	N/A
		N5W	32NE		Quartz Diorite	Foliation	In-Place	N/A
438349	3786845			N80E/88SE/89	Quartz Diorite	Epidote Surface	Slide	N/A
438337	3786584	N51W	37SW		Quartz Diorite	Foliation	In-Place	N/A
		N58W	34SW		Quartz Diorite	Foliation	In-Place	N/A
		N49W	41SW		Quartz Diorite	Foliation	In-Place	N/A
		N44W	48SW		Quartz Diorite	Foliation	In-Place	N/A
		N70E	56SE		Quartz Diorite	Joint	In-Place	N/A
		N65E	57SE		Quartz Diorite	Joint	In-Place	N/A
		N63E	51SE		Quartz Diorite	Joint	In-Place	N/A
438322	3786883	N70W	58SW		Quartz Diorite	Foliation	In-Place	N/A
		N68W	41SW		Quartz Diorite	Foliation	In-Place	N/A
		N40W	67SW		Quartz Diorite	Joint	In-Place	N/A
				N20E/56NW/36	Quartz Diorite	Epidote Surface	In-Place	N/A
438284	3786877	N60W	56SW		Quartz Diorite	Foliation	In-Place	N/A
		N56W	43SW		Quartz Diorite	Foliation	In-Place	N/A
				N21E/63NW/11	Quartz Diorite	Epidote Surface	In-Place	N/A
438278	3786878	N2W	50SW		Quartz Diorite	Foliation	In-Place	N/A

				N50E/79SE/17	Quartz Diorite	Epidote Surface	In-Place	N/A
438264	3786863	N10W	52SW		Quartz Diorite	Foliation	In-Place	N/A
		N15W	49SW		Quartz Diorite	Foliation	In-Place	N/A
		N19W	56SW		Quartz Diorite	Foliation	In-Place	N/A
		N89W	68NE		Quartz Diorite	Joint	In-Place	N/A
438251	3786869	N41W	42SW		Felsic Gneiss/Quartz Diorite	Foliation	In-Place	N/A
		N25E	15NW		Felsic Gneiss/Quartz Diorite	Foliation	In-Place	N/A
		N80E	65NW		Dike (Mafic)		In-Place	N/A
		N79E	68NW		Felsic Gneiss/Quartz Diorite	Joint	In-Place	N/A
		N15E	74NW		Felsic Gneiss/Quartz Diorite	Joint	In-Place	N/A
				N50E/88SE/34	Felsic Gneiss/Quartz Diorite	Epidote Surface	In-Place	N/A
438230	3786867	N63W	39SW		Mafic Gneiss	Foliation	In-Place	N/A
438078	3786895	N21E	37NW		Felsic Gneiss	Foliation	In-Place	N/A
		N25E	63SE		Felsic Gneiss	Joint	In-Place	N/A
438083	3786884	N23E	29NW		Felsic Gneiss	Foliation	In-Place	N/A
438079	3786878	N19E	32NW		Felsic Gneiss	Foliation	In-Place	N/A
438083	3786880	N61W	46NE		Gneiss: Fine grained	Foliation	In-Place	N/A
		N37E	49NW		Gneiss: Fine grained	Foliation	In-Place	N/A
		N54E	38NW		Dike (Mafic)		In-Place	N/A
438099	3786885	N5W	24SW		Felsic Gneiss	Foliation	In-Place	N/A
		N16W	42SW		Felsic Gneiss	Joint	In-Place	N/A
438107	3786888	N40E	49NW		Felsic Gneiss	Foliation	In-Place	N/A
		N43E	58NW		Felsic Gneiss	Foliation	In-Place	N/A
438142	3786895	N37E	38NW		Felsic Gneiss	Foliation	In-Place	N/A
		N31E	37NW		Felsic Gneiss	Foliation	In-Place	N/A
		N21E	69SE		Felsic Gneiss	Joint	In-Place	N/A
438182	3786872	N43E	15NW		Felsic Gneiss	Foliation	In-Place	N/A
		N40E	89SE		Felsic Gneiss	Joint	In-Place	N/A
438184	3786857	N41E	50SW		Felsic Gneiss	Foliation	In-Place	N/A
438205	3786863	N35W	33SW		Felsic Gneiss	Foliation	In-Place	N/A

Appendix B: Hog Back Slide Composite Map

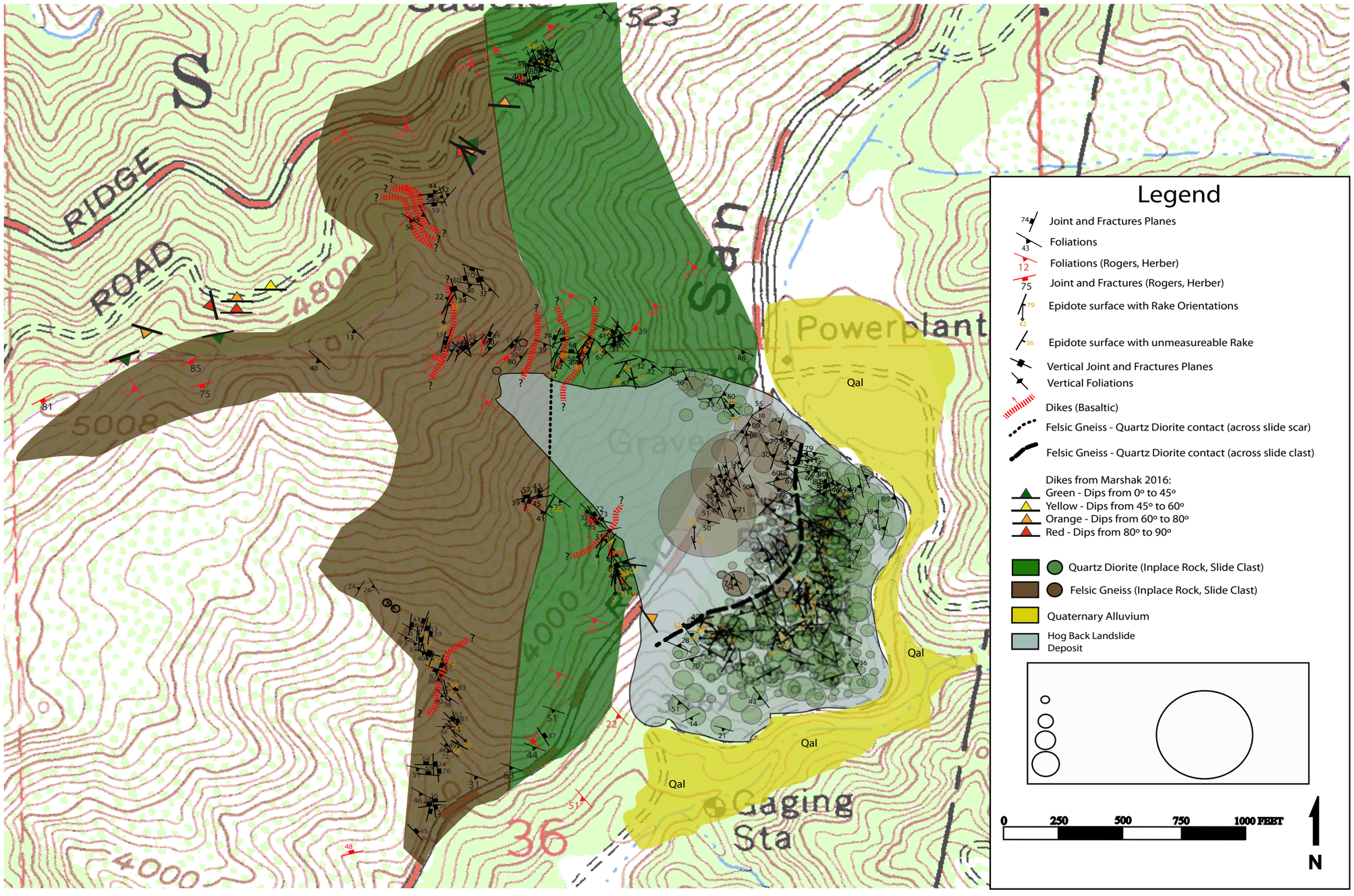

Appendix C: Cross Section Restored “Method of Slices” Volume Calculations

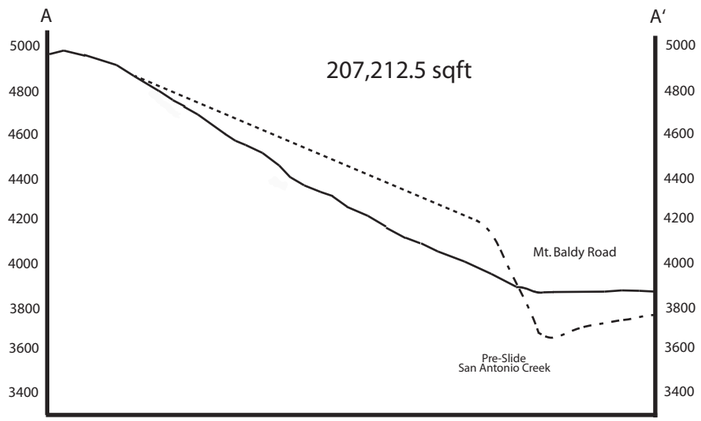

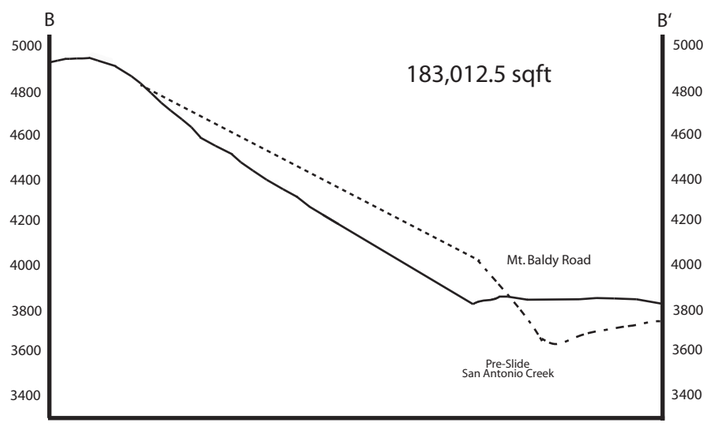

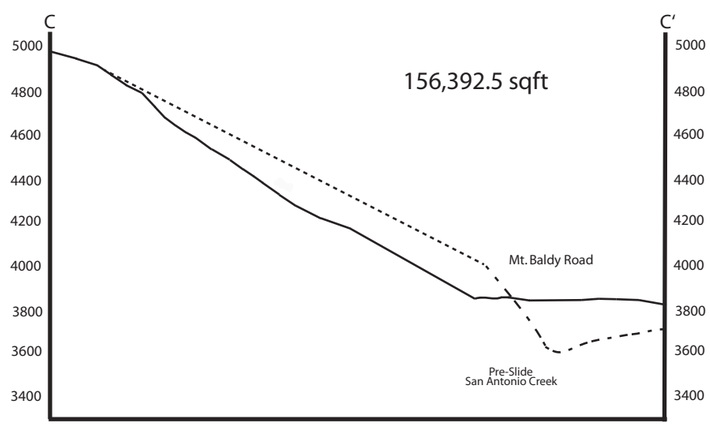

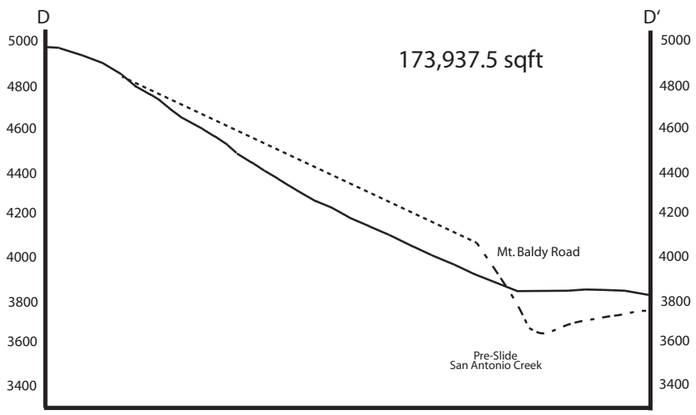

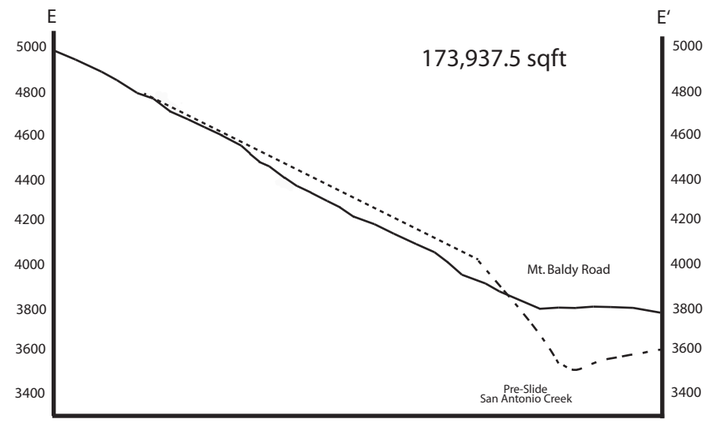

Volume AB:

$$\frac{(207{,}212.5 \text{ sqft} + 183{,}012.5 \text{ sqft})}{2}(260.27 \text{ ft}) = 50{,}729{,}250 \text{ cuft}$$

(50,729,250 cuft) (165 lbs/cuft) = 8,370,326,250 lbs

Volume BC:

$$\frac{(183{,}012.5 \text{ sqft} + 156{,}392.5 \text{ sqft})}{2}(92.73 \text{ ft}) = 15{,}736{,}652 \text{ cuft}$$

(15,736,652 cuft) (165 lbs/cuft) = 2,596,547,567 lbs

Volume CD:

$$\frac{(156{,}392.5 \text{ sqft} + 173{,}937.5 \text{ sqft})}{2}(182.74 \text{ ft}) = 30{,}060{,}030 \text{ cuft}$$

(30,060,030 cuft) (165 lbs/cuft) = 4,959,904,950 lbs

Volume DE:

$$\frac{(173{,}937.5 \text{ sqft} + 173{,}937.5 \text{ sqft})}{2}(200.59 \text{ ft}) = 34{,}787{,}500 \text{ cuft}$$

(34,787,500 cuft) (165 lbs/cuft) = 5,739,937,500 lbs

Total Volume = 131,313,432 cuft
Total Mass = 21,666,716,267 lbs